INVERSE ANALYSIS OF HEAT GENERATING BODY FOR SAFETY APPLICATIONS

by

SANDEEP PATIL

Presented to the Faculty of the Graduate School of
The University of Texas at Arlington in Partial Fulfillment
of the Requirements
for the Degree of

DOCTOR OF PHILOSOPHY

THE UNIVERSITY OF TEXAS AT ARLINGTON

August 2018

To my parents, Pandurang and Lata Patil, without them I'm nothing.

To my brothers, Amit and Ravindra, for their support.

To my gorgeous wife, Minal, for being caring and loving.

To my friends and relatives, who always motivated me in life.

ACKNOWLEDGEMENTS

It has been a long journey started in slums of Mumbai, India and reached today at zenith point in my academic life. When I look back, it is not only me but there are so many people who had helped me to achieve this goal. I would love to extend my thanks to all of them. First, I would like to express my sincere gratitude to my advisors, Dr. Ratan Kumar and Dr. Brian Dennis for their academic advice, constant support, motivation and encouragement for completion of doctorate program. I would like to thank Professors Dr. Hyjein Moon, Dr. Donghyun Shin, Dr. Gautam Das, Dr. Dereje Agonafer for serving on my committee and providing valuable insights. I am thankful to Dr. Pranesh Aswath for guiding me in personal and academic development.

I would like to acknowledge my friends from CFD lab, specifically Dr. Siddarth Chintamani, Dr. Alok Rege, Dr. James Grisham, Dr. Aditya Raman, Dr. Ashkan Akbariyeah, Manoj Kanduri, Oscar Fabela, Anirudh Rajagopal, Dr. Rajeev Kumar, Dr. Pawarat (Fern) Bootpakdeetam, Saiedeh for all the support. Special thanks to Dr. Siddarth Chintamani for helping me in every aspects of code development and his constant thought provoking questions, helped me to complete my thesis with new dynamics and perspective. Another special thanks to Oscar Fabela, who has helped me in carrying out experiments and collecting data amidst his busy schedule. I am also thankful to MAE Department staff, Debi Barton, Lanie Gordon, Sally Thompson, Janet Gober, Kathy Priester, Ayesha Fatima, Flora Pinegar, Wendy Ryan for

always being cheerful and helpful.

Furthermore, I would like to acknowledge the financial support provided by the MAE Department through various fellowships and the computational resources provided by the Texas Advance Computing Center (TACC). I am also thankful to Suresh Ketha, CEO, RISE Inc, for providing guidance, and augmented reality devices for experimentation.

A very special gratitude goes to Dr. Nagaraj Alangi, Scientific Officer, Bhabha Atomic Research Centre, for constant encouragement, financial support and inspiration to pursue doctorate. I would also like to thanks Shankar Jagadale, CEO, eBharat, India, for helping and providing guidance in personal, financial as well as mechanical engineering aspects. I could not forget the way he helped me providing books, stationery during my undergraduate studies.

I would like to extend my thanks to all colleague at Bhabha Atomic Research Centre for providing guidance and support during my tenure- Shri K.K.Prasad, Shri Rajendra Kumar Gupta, Late P.B.S. Sengar, Shri A.K. Singh, Shri K. Jayarajan, Shri Satish Patil, Shri Ramkant, Shri A.K. Mudaiya, Shri Ajay Shirole, Shri Devendra, Shri Shivaji Shendge, Shri S.M. Wavare, Shri Jitendra Sarawat, Shri Santosh Takale, Shri Prasad Karkhanis, Shri Gangadhar Huddar, Shri Navin Dubey, Shri Sanjoy Saha, Shri Chandragupta Potdar, Shri Ambarish Deshmukh, Shri Inderjit Yadav, Shri Tarun Patel, Shri Manoj Korde.

Again support of my childhood friends, relatives is enormous- specially making living arrangements amidst of inhospitable environment and encouraging me to

achieve new heights- Ratish Adsul, Satish Adsul, Dr. Prabhakar Rajbhar, Shrikant Kadam, Ganesh Mani, Pramod Mali, Balaji Mudliyar, Rajan Sable, Deepak Lomte, Yogesh Borghare, Mahesh Parab, Sandesh Parab, Vishal Tambewagh, Sandeep Jagadale, Navin Singh, Atul Singh, Anup Singh, Anuj Singh, Pravin Singh, Pravin Nikam, Sachin Nikam, Pradeep Nikam, Bhavu Kurale, Ajit Kurale, Sandep Kurale, Shashi Kurale, Manoj Kamble, Smita Harle, Vanita Harle, Rupali Jadhav, Dipali Jadhav, Vinod Harle, Vijay Harle, Ajay Harle, Amruta Padave, Vikram Palkar, Akshay Bhatkar, Praveen Parab, Pratik Parab.

I will forever be thankful to all my roommates in Arlington- Ajit Modi, Shubham Bajpai, Sambhav Garhwal, Sarthak Joshi, Dheeral Bhole, Kaustubh Shinde, Nachiket Deshpande for constant support and motivating me during doctorate stint.

I am thankful to my friends from Arlington for helping me in every possible ways - Ravindra Javadekar, Ameya Godbole, Pradeep Raghuwanshi, Bhushan Patil, Yogesh Patekari, Vignesh Balasubramanian, Ajit Desai, Vivek Vishwakarma, Patanjali Joshi, Ateen Chaughule, Chinmay Bhat, Keerti Bansod, Manthan Seth, Aaron Pinto, Ravindra Soni, Dhruv Deshpande, Ami Shah, Parita Patel, Neha Shigrekar, Snigdha Rashinkar, Liwanshi Raheja, Debanjana Roy, Krishana Desai, Divya Bharti, Meghana Anoop, Zankar Bapat, Prashant Savant, Tejesh Bagul, Mitali Khadilkar, Rinika Punjabi, Rohan Nilawar, Kaustubh Gosavi, Ajit Chorage, Swaroop Sawant, Amey Barve, Rohan Shroff, Nikhil Asawadekar, Swapnil Shrishrimal, Swapnil Tambadkar, Tejas Patil, Abhijit Satam, Vikram Mohrir, Kunal Tiwari, Avdhut Mankavale, Abhijit Namjoshi, Ajinkya Bandbe, Rushikesh Ganne, Swathi Ganne, Aniket Kalambe, Shrikant Yadav, Himanshu Prasad, Palash Nemade, Pavan Raj-

mane, Manpreet(Shaina) Kaur, Manimala Tripathi, Praveen Tripathi.

I would like to convey my sincere thanks to Shri Madhukar Palkar & family, Shri Gopal Dhone & family, Shri Shamrao and Ananda Harle & family, Shri Ramchandra Vanzare & family, Shri Sambhaji Yadav & family, Shri Nagaraj Alangi & family, Shri Yogesh Borghare & family, Shri Jayratan Singh & family, Shri Mukunda Dawane & family, Shri Bhikaji Padvae & family, Shri Baliram Jadhav & family, Shri Nair & family, Shri Appa Kurale & family, Shri Keshav Kurale & family, Shri Rajendra Shinde & family, Smt Suvarna Nikam & family, Shri Prakash Savant & family, Smt Meena Wadkar & family, Shri Santosh Salavi & family for extending all possible and sincere help since childhood. I want to thank , my in-laws family Shri Satish Solaskar, Smt Pushpa Solaskar, Shri Prashant Solaskar, Smt Pallavi Kakade as being supportive and keeping trust during my doctoral studies. I am thankful towards my brothers and sisters for their constant love and support - Nikhil Patil, Vinayak Patil, Sadhana Patil, Aishwarya Patil, Pratik Patil, Saurabh Karambalkar. I would like to thank Shri Shivaji Patil and Smt Kalpana Patil for making arrangement of necessary equipment and being supportive during my study days. My sincere thanks to Shri Tanaji Patil and Smt Sunita Patil for helping me financially as well as morally in my arduous journey.

Last but not the least, I would like to thank my father Pandurang Patil, mother Lata Patil, brothers Amit and Ravindra for standing behind me, supporting throughout my education and sail through difficult times of the life. I hope I have made you proud. Finally I like to thank my better half, Minal for everything she has done and accompanying me with constant love and support at United States.

My acknowledgment would be incomplete without mentioning my upcoming baby. He had been always constant source of inspiration for me during final semester of doctorate.

August 09, 2018

ABSTRACT

INVERSE ANALYSIS OF HEAT GENERATING BODY FOR SAFETY APPLICATIONS

SANDEEP PATIL, Ph.D.

The University of Texas at Arlington, 2018

Supervising Professor: Ratan Kumar, Brian Dennis

Inverse thermal analysis and its applications have been applied to numerous fields of science and engineering. Historically during the 1950's and early 1960's, space programs played a significant role in the advancement of solution techniques for Inverse Heat transfer Problems(IHTP). It was applied to measure the surface temperature of thermal shield of a space vehicle during its re-entry into atmosphere. Inverse analysis was also used in the estimation of thermo-physical properties of the shield at high operating temperatures. Besides thermal application, inverse technique was also used in other engineering applications such as estimation of alloy specification, design of a shape for aerodynamic configuration and for determining kinetic rate constant of a chemical process.

One of the application area of inverse thermal analysis has been in providing safety and avoiding overheating of Lithium-ion cells. These cells are widely used in powering up consumer electronics and electric cars. Batteries contain oxidizer (cathode) and fuel (anode) in sealed container. Under normal operation, fuel and oxidizer convert chemical energy to electrical energy. However, during accidental

condition, it may lead to fire failures due to elevated heat. Recent accidents like explosion and fire in Tesla car, Samsung Galaxy Note 7, Boeing 787 Dreamliner are few examples of batteries failure.

Another challenging application area for inverse thermal analysis has been in the thermal and safety analysis of nuclear reactors, where the heat is generated by nuclear fission process of radioactive material. This heat is used to generate a highly pressurized steam, which drives turbines that turn electrical generators. The loss of cooling water is extremely dangerous, as it can lead to catastrophic results such as steam explosion and release of radiation. Fukushima, Three Miles Island, Chernobyl are examples of nuclear accidents that occurred in past with disastrous and long term consequences. One common feature of all these accidents was the failure of the cooling system that led to core meltdown or fire in batteries.

Nuclear accidents or fire in batteries can be prevented if the cylindrical rod temperatures are kept within a safe limit. Conventional measuring devices, such as thermocouples or pyrometers, are difficult to install inside nuclear fuel rod or batteries to determine the interior temperature. However instruments can be used to determine the temperature at measurable locations. From these temperature measurement, the temperature distribution of cylindrical rod can be estimated using inverse technique. Such analysis can generate data that provides insight into thermal behavior of fuel rod or batteries in the event of loss in coolant level or improper cooling. This aids in initializing corrective action to avoid increase of temperature above a critical point in and on a rod.

This study is presented in 3 sections. In section 1, a simplified transient numerical model is developed to understand thermal behavior of heat generating cylindrical rod. Parametric studies were performed by changing heat generation rate and coolant height. The numerical model shows temperature changes with the variation in coolant

height. The location and value of the temperature in cylindrical rod at different points is computed, to find critical location that leads to melting.

In section 2, to demonstrate the application of inverse thermal analysis, a single cylindrical rod with Neumann boundary conditions and heat generation is modeled. Temperature obtained from this modeling, along with Gaussian noise, was used as an input to the inverse analysis for estimating heat generation and temperature distribution inside the rod. Sensitivity analysis was carried out to indicate best sensor locations and good response times. The numerical model of cylindrical rod for temperature analysis showed excellent agreement with published results. Moreover results obtained from inverse analysis were in close agreement within 0.59% of input values of direct measurements.

Although inverse analysis is an excellent method to determine temperature under physically challenging situations, it requires a large computation time for a safety analysis,which may be impractical for real time application. To circumvent this, a neural network model was utilized for predicting maximum temperature inside the system, which is described in section 3. Data was generated through simulation using OPENFOAM for axi-symmetric model. This data was used as the basis for training neurons for maximum temperature prediction. To validate the proposed idea, an experiment was setup with cartridge heater as a representation of heat generating rod. The coolant height and temperature measured in fluid region was given as input to trained neural network model to predict surface temperature and inside temperature of the heat generating rod. Temperature obtained from this model was used to display in real time to an augmented reality device, which assist field workers to gauge situation and take preventive measures.

Inverse techniques were also applied to develop general framework for predicting anisotropic properties of materials. In this work, temperature measured at different

locations on the surface was utilized for predicting thermal conductivity of heat generating rod. Results obtained from this analysis was validated with the published results. Moreover this technique was extended to estimate thermal conductivity of porous material.

TABLE OF CONTENTS

LIST OF FIGURES

LIST OF TABLES

CHAPTER 1

INTRODUCTION

1.1 Inverse Analysis

Inverse analysis (IA) is the process of calculating the causal factors from set of observations or results. Inverse problems are typically carried out through numerical modeling and simulation of a different phenomena. To predict or infer knowledge about either physical states or underlying quantities, observations are taken from such phenomena. Schematic of Inverse thermal analysis is shown in Fig.(1.1)

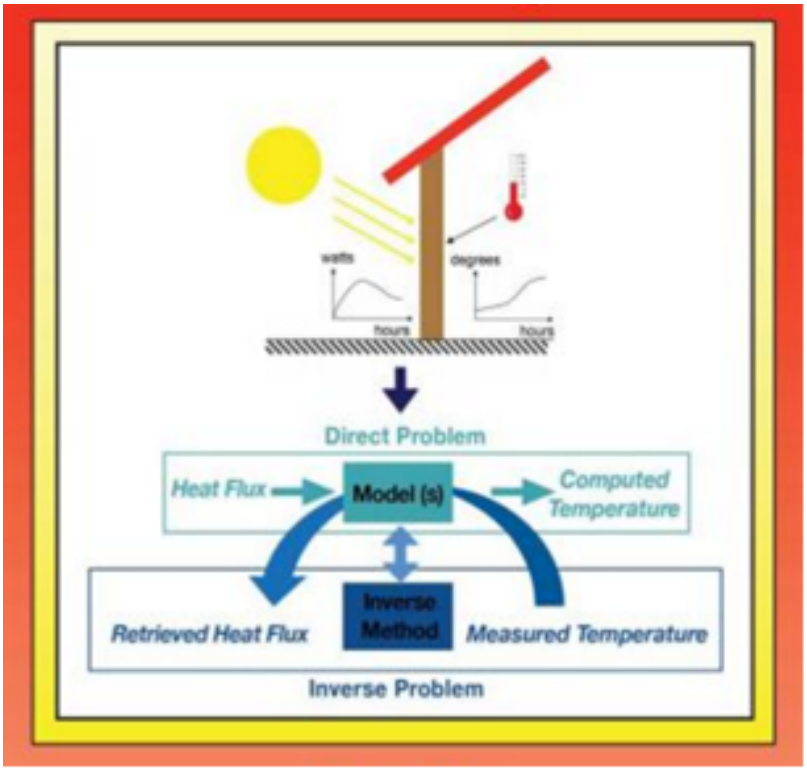

Figure 1.1. Schematic of Inverse thermal analysis [1].

IA is important in the fields, where direct measurement of physical quantities is difficult or inconvenient. In such cases, IA provides insight of causal factors from the observed results. With different problems, there are different causal factors and observed results. For example, in thermal problems, temperature is measured and it is used to predict heat flux or properties (Causal factors). Similarly for structural problems, reaction forces, moments are measured to predict elastic modulus of material. In chemical problems, product concentration is measured to determine reaction rate. One such application of estimation of elastic modulus is shown in Fig. (1.2)

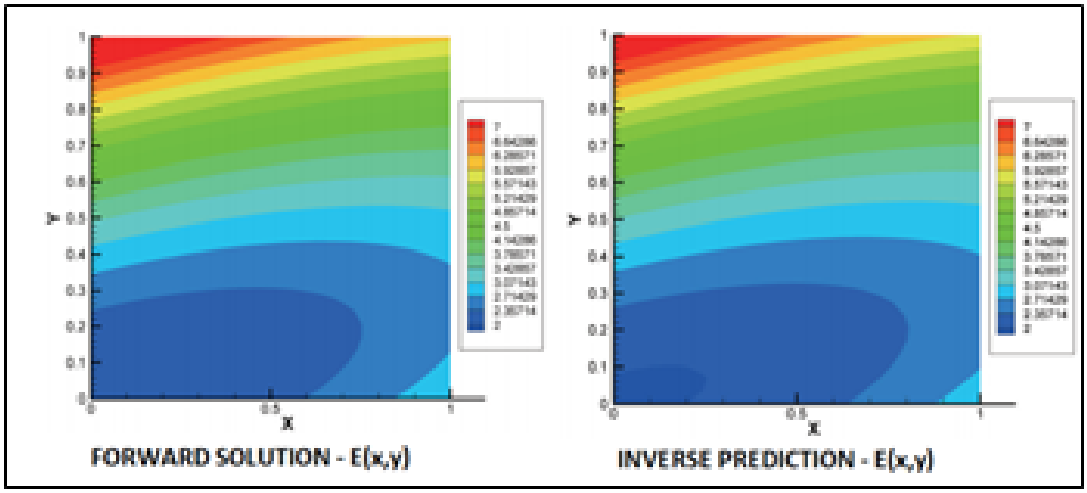

Figure 1.2. Young's Modulus Estimation [2].

In this study, IA was used to estimate the surface temperature of cylindrical heat generating rod by measuring the coolant temperature at a sensitive location. History of inverse analysis (IA) is really interesting considering its inception and development. Inverse Analysis was first introduced by Astronomer Viktor Ambarstsumian in 1929 for relation between oscillation frequencies and homogeneous string in vibration [10]. For over 15 years this work largely remained in obscurity. After 1944, many outstanding mathematicians succeeded in obtaining interesting results [11]. One such

result was published by G. Borg, who worked on inverse of Sturm-Liouville Equation in 1946 [12]. Significant developments in mathematics of inverse problem has taken place since then. While I. Frank [13] developed least square method for inverse problem, A. Tikhonov [14, 15] was well-known for introducing regularization methods. D. Specht [16] introduced general regression neural network for inverse problems. Another recent break-through research work was carried out by K.Deb and group in developing elitist multi-objective genetic algorithm [17].

As mentioned, IA has been widely used for many areas such as safety analysis, structural optimization, alloy composition estimation, thermo-physical properties estimation, chemical process kinetic rate determination, weather prediction, oceanography. First such application of IA for thermal system can be found in one of the earliest paper published by W. Giedt [18], where he predicted heat transfer of inner chamber of gun barrel. Some selected applications of inverse analysis have been presented in table (1.1)

Table 1.1. Applications of Inverse Analysis

Author	Application
W. Giedt (1955)	Heat transfer of inner chamber of gun barrel [18]
G. Stolz (1960)	Estimating surface temperature of quenched body [19]
S.R. Arridge(1999)	Optical tomography in medical imaging(Cited by 2228) [20]
H. Li, M. Ozisik(1992)	Inverse Radiation Problem [21]
G. Dulikravich (2012)	Inverse Design of Alloys for specified properties [2]

There have been a number of industrial problems which involve inverse determination of material properties or thermal behavior using measurements taken at outer surface of the body. Many authors have developed methods to determine properties

such as thermal conductivity, Young's Modulus, heat flux by surface temperature measurement. However there are challenges to place temperature probes or heat flux probes on certain parts of a surface of a solid body as it is difficult or even impossible. This difficulty could be due its small size, geometric inaccessibility or exposure to a harsh environment. Nevertheless, knowledge of the temperature at these positions is important. For example,the center-line temperature of heat generating cylinders (e.g. nuclear fuel rod, battery) may reach its melting point in accidental condition but cannot be directly measured. Hence it is necessary to utilize IA technique to estimate the temperature at center-line for the heat generating cylinder.

Appropriate inverse method can estimate temperature from the boundaries where the temperature can be measured directly. The problem of inverse determination of unknown temperature distribution in solid subjected to different boundary conditions has been solved by a variety of methods [22–27].

1.2 Motivation

Advanced technology with enhanced safety is utilized in nuclear and battery industry applications (airplane, automotive). Still it is prone to accidents, which has long-term and dangerous consequences. Active and continuous monitoring of fuel or battery during fabrication,operation or storage, is required. Direct measurement or temperature is not possible due to radiation hazard or inability to have embedded sensors. Inverse analysis (IA) can address these issue by measuring temperature in coolant temperature and predicting temperature at critical location. This forms the basis and motivation for the current work.

1.3 Battery accidents

In 1991 Sony launched first commercial lithium ion batteries [28]. Since then it has become prominent energy storage in most consumer electronics and electrical vehicles (notebooks,cell phones, cars-Tesla,BMWi3,Renault etc) [29].Many battery standards and regulations have been specifically developed to facilitate and regulate battery use in EVs [30]. In spite of this, fires, explosions have been reported for lithium ion battery during the past years (Table 1.2 and Fig 1.3 shows some of the accidents). In addition, many incidents have been reported for mobile phones and laptops also. It can be seen that fires are caused by overheating of batteries and triggering of thermal runaway.

Thermal runaway is one of the most common features during accidents of lithium ion battery. Generally, when an exothermic reaction inside battery goes out of control, thermal runaway occurs. This reaction rate increases with increasing temperature, which results in explosion [31, 32]. It is proposed that thermal runaway can occur spontaneously above 80 °C due to fire or explosion [33]. For the lithium ion battery runaway, it is caused by the exothermic reactions between the electrolyte, anode and cathode, with the temperature and pressure increasing in the battery, the battery will rupture at last [34].

Table 1.2. Some lithium ion battery accidents

Date	Accident replay
2016	An EV police cat caught fire - Italy [35]
2016	Tesla model S caught fire while fast charging at supercharger-Norway
2013	APU battery pack caught fire inside Boeing 787 Dreamliner-Boston USA
2011	A Chevy Volt caught fire after side-pole impact-USA [36]
2011	EV bus, Taxi catch fire- China [37]
2010	A Boeing B747-400F cargo plane catch fire, Dubai
2010	Acer recalled laptop. Same thing was done by Dell,Apple,Toshiba, Lenovo in 2006
2010	Two ipad Nano music player catches fires-Japan
2009	Cargo plane catch fire- China

(a)

(b)

Figure 1.3. Battery Accidents (a) Aeroplane [3] (b) Car-Tesla S Model [4] .

1.4 Nuclear Accidents

Nuclear reactors use advanced engineering methods and radioactive materials for generating heat with high power density. Heat generated in the radioactive fuel boils water leading generation of pressurized steam, which drives turbine that turn electrical generators. Radioactive fuel assemblies are made up of cluster of fuel rods, which contains pellets of uranium oxide which is encapsulated in thin cladding. Heat generated in the fuel is transferred to the coolant through cladding. Schematic of a nuclear power-plant and fuel rod assembly is given in Fig 1.4(a), 1.4(b) respectively.

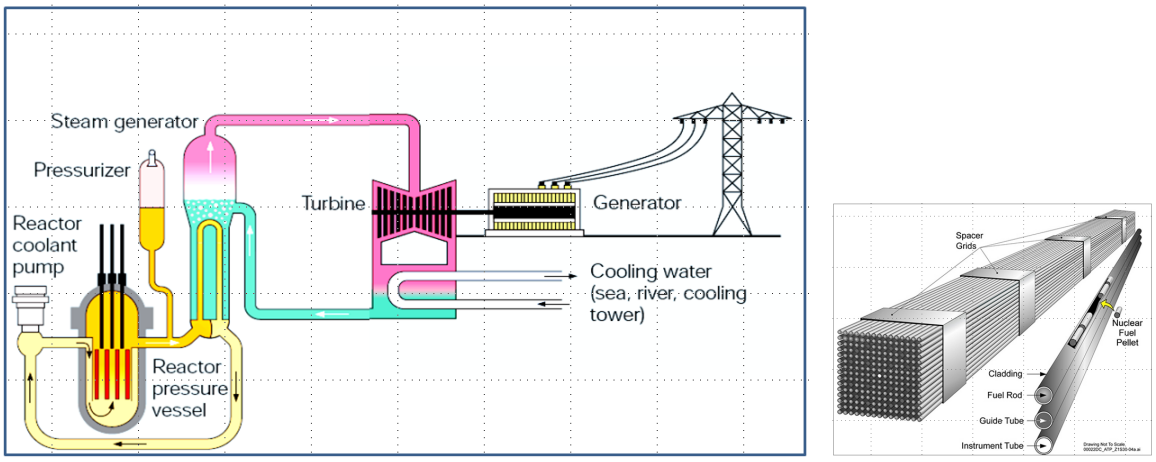

(a) (b)

Figure 1.4. Schematic of nuclear power plant and fuel rod configuration.

Fuel used in nuclear power plants pose radiation hazard, hence it is inherently dangerous and difficult to handle at all stages of its life-cycle. The fuel assembly after the designated residual period in the reactors is removed and is termed as spent fuel. Safe management of spent fuel assemblies is a major challenge due to difficulty of finalizing permanent repository for high level nuclear waste. All nuclear power plants in USA, store their spent fuel rod assemblies in on-site cooling ponds. The spent fuel rods remain in cooling ponds for five to ten years under at least 20 feet

circulating water. Loss of cooling water to cooling pool is extremely dangerous, as it can lead to explosion and catastrophic release or radiation. Nuclear accidents of this nature (Fukushima, Three Miles Island, Chernobyl) occurred in past with disastrous long term consequence. One Common Feature of all these accident was failure of the cooling system [38–45].

Fukushima disaster has been the most significant nuclear accident since 1986, initiated primarily by a tsunami on March 11,2011. Though there were no fatalities linked to radiation due to the accident, the eventual number of cancer deaths, according to the linear no-threshold theory of radiation safety is expected to be around 130 to 640 people in the years and decades ahead [46, 47].

The Fukushima Daiichi nuclear power plant consisted of six numbers of General Electric (GE) made boiling water reactors (BWRs). Combined power capacity of these plants were of the magnitude 4.7 gigawatts, which is one of the world's 25 largest nuclear power stations. It was the first GE-designed nuclear plant to be constructed and run entirely by the Tokyo Electric Power Company (TEPCO). Reactor 1 was a 439 MWe type (BWR-3) reactor and commenced its operation on 26 March 1971 [48]. Reactors 2 and 3 were both 784 MWe type BWR-4s and commenced their operation in July 1974, and March 1976 respectively. Design of these reactors were carried out to withstand an earthquake with a peak ground acceleration of 0.18 g (1.74 m/s^2) and a response spectrum based on the 1952 Kern County earthquake [49]. The earthquake design basis for all units ranged from 0.42 g (4.12 m/s^2) to 0.46 g (4.52 m/s^2) [50, 51]. Schematic representation of Fukushima power plant is given in Fig (1.5) .

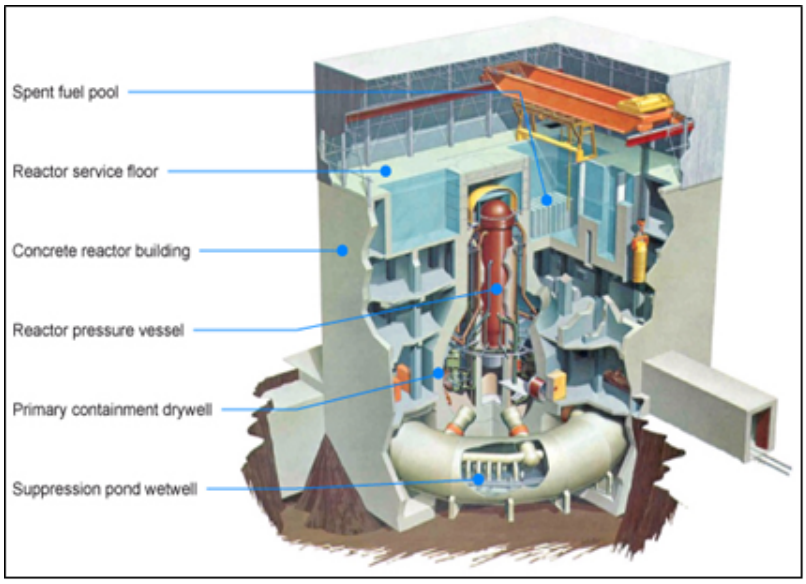

Figure 1.5. Fukushima Nuclear power plant schematic.

Reactors 4, 5, and 6 were shut down for preparation of re-fueling, at the time of the Thoku earthquake on 11 March 2011 [52, 53]. However, their spent fuel pools still required cooling to take away generated decay heat [53, 54].

The largest tsunami wave reported on unfortunate day was 13 meters high and hit 50 minutes after the initial earthquake, surpassing the plant's seawall, which was only of 10 m high [55]. The moment of impact was recorded by a camera [56]. Low-lying area such as emergency generator house was flooded with water [57] and diesel generators failed to start. It resulted in a loss of power to the critical coolant water pumps. These pumps continuously circulates water through reactors to remove decay heat from fuel rods to avoid melting. Decay heat is sufficient to melt fuel rod, if adequate heat sink and sufficient cooling is not available. One day after the tsunami, back up emergency pumps (running on electrical batteries) ran out, which started overheating of reactors [58]. Workers were struggling to supply power to coolant

system of the reactor and restore power in the control rooms during this period, a number of hydrogen-air chemical explosions occurred in Unit 1 and Unit 4 [56,58,59].

Loss of coolant accident eventually led to core meltdowns in Reactors 1, 2, and 3. The full extent of the movement of the resulting corium (lava like mixture of fissile material at meltdown) is unknown. However it is now considered to be residing somewhere between reactor pressure vessel(RPV) and the water-table below each reactor. Sequence of events is depicted in Fig. (1.6).

	Unit 1	Unit 2	Unit 3
Loss of AC power	+ 51 min	+ 54 min	+ 52 min
Loss of cooling	+ 1 hour	+ 70 hours	+ 36 hours
Water level down to top of fuel*	+ 3 hours	+ 74 hours	+ 42 hours
Core damage starts*	+ 4 hours	+ 77 hours	+ 44 hours
Reactor pressure vessel damage*	+11 hours	uncertain	uncertain

Figure 1.6. Sequence of Events.

1.5 Heat Transport in Battery

The mechanism of li-ion battery is given in Fig. 1.7, Lithium ions moves from negative electrode (cathode) to positive electrode (anode) via seperator diaphragm to make discharging cycle and vice versa when charging. The cathode is generally made of carbon (most commercially graphite). The anode is lithium containing com-

pound (generally one of three materials: lithium iron phosphate - $LiFePO_4$, lithium magnesium oxide- $LiMn_2O-4$, lithium cobalt oxide - $LiCoO_2$. The electrolyte is a solution of lithium salt in a non-aqueous solvent such as ethylene carbonate or diethyl carbonate. The current collector for negative electrode is made of copper (cu) while positive electrode is made of aluminium (Al) [5].

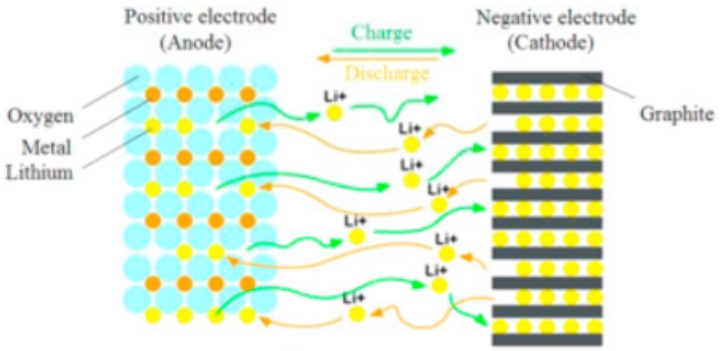

Figure 1.7. Mechanism of Li-ion battery during discharge and charge [5] .

Performance of Lithium ion cell is linked to temperature. The temperature of lithium ion cell is governed by heat generation and heat dissipation by the cell. The heat generation is described by exponential function whereas heat dissipation by linear function. When a cell is heated above certain temperature (above 130-150 °C), exothermic chemical reactions will increase internal temperature. If heat generated is more than dissipation, then rising temperature will accelerate reactions, resulting in thermal runaway [60–64].

Newman and his colleagues carried out comprehensive electrochemical modeling using various mathematical approaches to understand physics of the battery system [65–68]. Existing model can be classified into three different physical mechanism: electro thermal model [69–74], electrochemical model [75–80], thermal runaway

model [81,82]. According to dimensions, the model can be categorized as lumped parameter model [69], two dimensional model [78], three dimensional model [83], mixed dimensional model [84].

Bernardi et al. [65] developed a general energy balanced battery thermal model for estimating the heat generation rate of single cell and a simplified form was written as the following equation.

$$\phi = I(E_{oc} - E) - IT_{bat}\frac{dE_{oc}}{dT_{bat}} \tag{1.1}$$

The heat generation rate comprises two heat source terms caused by overpotential resistance and electrical resistance (the first term), and entropy change (the second term). The first term represents the irreversible heat and the second term the reversible heat. The term $(E_{oc} - E)$ can be replaced by IR, where R denotes overall resistance [85]. This model has been widely used by many researchers.

However, the modeling results need to be validated with experimental data to compare results. In recent years, researchers are increasingly focusing on thermal issues of battery at high C-rates due to the popularity of electric cars. The main experimental methods for heat generation rate measurement are accelerating rate calorimeter (ARC) [86–88] and isothermal battery calorimeter (IBC) [89–91]. The ARC method measures the heat rejected from the battery and allows the surface temperature of battery to rise adiabatically during operation. hence, it is mostly used in thermal runaway testing [92]. However, in order to accurately measure the heat generation rate of battery under normal operation, the temperature variation should be eliminated since the battery performance is temperature sensitive. Pesaran and his coworkers from NREL has designed a series of Isothermal Battery Calorimeters [89]. According to NREL site, the instruments can measure heat generation rates

as low as 15 mW and up to 4000 W with measuring accuracy within 1% and the test samples can be cell, module or pack. However, it needs to emphasize that IBC method can only maintain the battery surface at isothermal condition. For a transient process of large-scale power cell, the measuring accuracy of IBC method may be greatly reduced. It should be noted that there have been some discrepancies between different experimental researches on heat generation rate measurement of single cell and the gap usually cannot be validated due to lack of data. To facilitate a gap analysis, it is suggested that the heat generation rate measuring is carried out at several standard temperatures in a wide operation temperature range (20+50 °C), and at several typical C-rates (e.g., 0.5C, 1C, 5C, etc.). The chemistry, geometry, density, specific heat capacity of battery should be given or measured. The temperature gradient in a cell should always be given a special attention and it results in the difficulty of measuring transient heat generation rate of battery at high C-rates [85].

In this work, lithium-ion battery will be treated as one of the heat generating cylinder. Inverse analysis techniques has been applied to estimate anisotropic thermal properties of batteries and validated with published results. Framework developed in this thesis, can be extended to safety analysis of battery.

1.6 Heat Transport in Nuclear Reactor

Concerns regarding heat removal discussed in earlier section of nuclear accidents, have attracted considerable research focus. Nuclear power plant consists of fuel rod assembly, In the current study single nuclear fuel rod is considered for thermal analysis. Typically for a Boiling water reactor, one cluster consists of an array of 17x17 rods, which include fuel rods, guide rods, control rods and instrumentation rods etc. Each fuel rod is 4 m long. Figure (1.8) shows a single fuel rod which was in this work.

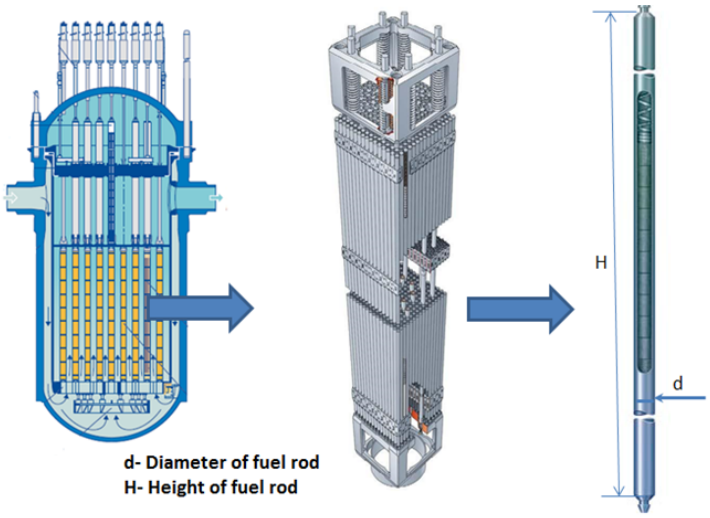

Figure 1.8. Nuclear fuel rod.

Classic assembly of nuclear fuel rod is depicted in Fig. (1.9). There are different fuel constructions used in plants like collapsible fuel pin, Helium bounded, Sodium bounded fuel pin. In this work, only helium bounded fuel pins is considered. It can be observed that heat generated inside UO_2 pellets is transferred to Helium and cladding by conduction. Though heat transfer in helium is through convection, due to small gap, heat transfer inside He gap is assumed as conduction. Coolant extracts heat from cladding surface through convection. Loss of coolant has significant role in increasing temperature of fuel rod. Hence, thermal analysis of this fuel rod at different coolant height will be evaluated in this thesis.

Different researchers have evaluated thermal phenomena inside fuel rods. Nijsing came up with analytical model for calculation of temperature distribution. He also analyzed performance of nuclear fuel rod in normal operation and burnt out condition [93].

Ye et al. carried out design and simulation of spent fuel passive cooling system [94]. A passive cooling system based on a heat pipe, was designed and applied to re-

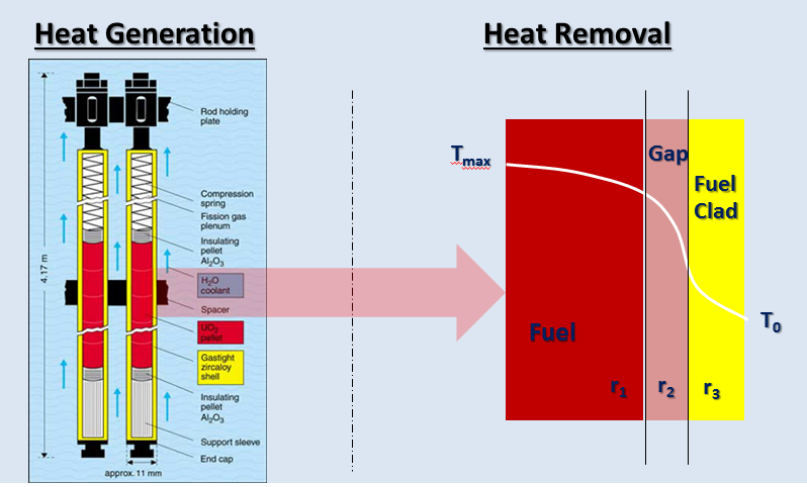

Figure 1.9. Reactor thermal issues.

move the decay heat of the spent fuel pool when the electric power fails. With all the conservative assumptions, it predicted that a spent fuel pool equipped with a completely passive cooling system will operate safely even with biggest decay heat. High heat transfer efficiency is of great interest for its application in spent fuel natural convection cooling. Hung et al [95] developed three-dimensional two-phase CFD model to simulate the thermalhydraulic behavior of the spent-fuel pool for the Kuoshen power station.

Lee et al. carried out thermal-fluid flow analysis of spent fuel storage system using commercial computational fluid dynamics (CFD) code, FLUENT [96]. Effective thermal conductivities of a spent fuel assembly and a fuel basket were derived to optimize a thermal analysis model. Also, a porous model was used in the thermal analysis to simulate the characteristics of a thermal-fluid flow for a fuel assembly. Thermal test and analysis were carried out to verify the thermal analysis method and procedure using a half scaled-down model.

Gomez et al performed two dimensional simulation of natural convection and radiation heat transfer of Pressurized Water Reactor (PWR) fuel assembly within a

square basket tube of a typical transport package using a commercial computational fluid dynamics package [97]. Heat transfer simulations were performed to predict the maximum cladding temperature for assembly heat generation rates between 250 W and 1000 W, uniform basket wall temperatures of 25C and 400C, and with helium and nitrogen back fill gases.

Laursen et al and Wang et al analyzed cooling of spent fuel in large water pool and crud formation on fuel pin clad surfaces respectively, where the simulation was implemented with the worst case situation, in which fuels under full-core discharge are assumed to be moved into Spent Fuel Pool (SFP), and the external cool system was assumed failed. The effective convective coefficient on the pool surface was also modeled based on the empirical correlations. The pressure drop of the coolant flowing through the fuel region in the pool was modeled as a porous-medium [98, 99].

Agabez carried out spent fuel heat transfer analysis as an academic exercise for steel as material, with constant coolant level using finite difference approach and validated his results with finite element software package [100].

Pedro Pupo Sa da Costa has analyzed Loss of coolant accident (LOCA) condition with steady state simulation and validated with laboratory scale experiments. However problem of partially cooled heat generating cylinder was not addressed [101].

1.7 Research Objectives

Most of the previous work on thermal analysis was attributed towards carrying out temperature distribution and impact of coolant loss. In this work, different methods for thermal analysis will be evaluated for their limitations to choose efficient method for capturing thermal phenomena of heat generating bodies. Temperature data obtained from this thermal analysis forms the basis for developing inverse analysis. General framework for inverse analysis (IA) will be developed for safety appli-

cations in nuclear power plant and battery management applications. Furthermore, for rapid prediction of temperature to gauge real time situation, neural network was modeled. This research will address the following areas:

1. Temperature distribution of partially cooled heat generating rod through analytical and numerical method.
2. Inverse analysis to determine center-line and surface temperature of cylindrical rod at different coolant level, which will be helpful in predicting alarm level, below which temperature of cylindrical rod may reach melting point.
3. Rapid prediction of temperature at critical locations for real-time application with the use of neural networks.
4. Displaying real-time data on augmented reality device, which aids in field work for carrying out inspection,maintenance.
5. Anisotropic thermal property estimation through IA will be implemented to predict thermal conductivity of materials.

CHAPTER 2

ANALYTICAL ANALYSIS

Heat transfer analysis and formulation for heat generating cylinder is presented here. To limit scope of the work, a single heat generating rod and its heat transfer with surrounding fluid is analyzed. It is carried out with two methods - Analytical and Numerical method. In Analytical method, heat transfer phenomena within fluid was not considered and the heat transfer coefficient was assumed constant for calculation. While analyzing numerical method the heat transfer coefficients and heat transfer within the fluid were considered. Both approaches have been discussed in details in following sections.

2.1 Governing Equation

Consider a cylindrical body of radius R and Height L as schematically shown in Fig.2.1. Heat rate Q is assumed to be generated inside the cylinder. It is also assumed that cylinder exchanges heat with surrounding by convective heat transfer.

General form of the governing energy equation for the cylinder is given in Eqn.(5.14), It is assumed that heat generation is constant through out the cylinder. Due to rotational symmetry, variation with respect to θ-coordinate is ignored. Considering axial and rotational symmetries, the model is solved as rectangular slice of the cylinder taken from its center to its outer radius. The governing equation in Eqn.(5.14) subjected to boundary condition, is solved using Analytical and finite volume formulation.:

$$\left(\frac{1}{r}\frac{\partial T}{\partial r}\left(k_r\frac{\partial T}{\partial r}\right)+k_z\frac{\partial^2 T}{\partial z^2}\right)+Q=\rho\, C_p\frac{\partial T}{\partial t} \tag{2.1}$$

Where k = Thermal Conductivity, r =radius in m, z = length in m, T = temperature, Q = Volumetric heat generation ρ = Density of cylinder, C_p = Specific Heat of cylinder

The boundary conditions are assumed as follows :

$$k(T)\frac{\partial T}{\partial r}=h_1[T-T_\infty]\ at\ r=R_1\ z\in[L/2,L] \tag{2.2}$$

$$T=T_\infty\ at\ r=R_1\ z\in[0,L/2] \tag{2.3}$$

$$T=T_\infty\ at\ z=0\ r\in[0,R_1] \tag{2.4}$$

$$k(T)\frac{\partial T}{\partial z}=h_2[T-T_\infty]\ at\ z=L\ r\in[0,R_1] \tag{2.5}$$

$$k(T)\frac{\partial T}{\partial r}=0\ at\ r=0\ z\in[0,L] \tag{2.6}$$

$$T=T_\infty\ at\ t=0 \tag{2.7}$$

Where h_1 and h_2 =Heat transfer coefficient of coolant and air respectively, T_∞ =300 K, t =time.

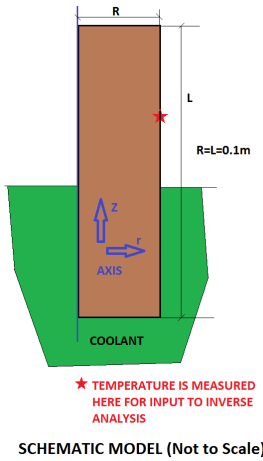

Figure 2.1. Schematic model of partially cooled cylindrical rod.

2.2 Analytical Formulation

Following assumptions are made while deriving analytical formulation for partially cooled heat generating cylinder

1. Solid Cylindrical heat generating cylinder
2. Axi-Symmetric Model
3. Steady State thermal analysis
4. Isotropic Thermal conductivity
5. Ambient temperature = 300 K

Temperature distribution through steady state equation can be obtained through separation of variable methods. Solution of equation is divided into homogenous (f) and non-homogenous (s) part as follows:

$$\theta = s(z) + f(r, z) \tag{2.8}$$

$$s(z) = \frac{-Qz^2}{2K_z} + C_1 z + C_2 z \tag{2.9}$$

Where,

$$C_1 = \frac{h_1 C_2}{K_z} \tag{2.10a}$$

$$C_2 = \frac{QHC_3}{C_4 C_5 C_6} \tag{2.10b}$$

$$C_3 = \frac{C_7 + 2}{2K_z} \tag{2.10c}$$

$$C_4 = \frac{h_1 h_2 H}{K_z K_z} \tag{2.10d}$$

$$C_5 = \frac{h_2}{K_z} \tag{2.10e}$$

$$C_6 = \frac{h_1}{K_z} \tag{2.10f}$$

$$C_7 = \frac{h_2 H}{K_z} \tag{2.10g}$$

Homogeneous part of the equation (2.8) can be written as follows:

$$f(r,z) = \sum_{n=1}^{n=\infty} A_n I_0(\alpha_n r)\phi_n(z) \tag{2.11a}$$

$$\phi_n(z) = (\beta_n H cos(\beta_n z) + \frac{h_1 H}{K_z} sin(\beta_n z)) \tag{2.11b}$$

Where I_0 is modified bessel function. α_n, β_n is eigenvalues which are calculated in following equation

$$(tan(\beta_n)(\beta_n^2 - (\frac{h_1 H}{K_z})^2)) - (2\beta_n(\frac{h_1 H}{K_z})) = 0 \tag{2.12a}$$

$$\alpha_n = \beta_n \sqrt{\frac{K_z}{K_r}} \tag{2.12b}$$

Now using convective boundary condition as mentioned in equation (5.17),(5.18)

$$K_r \frac{\partial f}{\partial r} = -h(z)(f(r,z) + s) \tag{2.13}$$

$$\sum_{n=1}^{n=\infty} I_0^{'}(\alpha_n r)\phi_n(z) = \sum_{n=1}^{n=\infty} -h(z) I_0(\alpha_n r)\phi_n(z) - h(z)s(z) \tag{2.14}$$

Above given equation (2.14) is multiplied by $cos(n\theta)$ and integrated from $\theta = 0$ to $\theta = 2\pi$. Following linear equation is obtained which need to be solved for obtaining temperature distribution.

$$A_m C_m + \sum_{n=1}^{n=\infty} A_n d_{m,n} = P_m \qquad (m = 1, 2, 3...) \tag{2.15a}$$

$$d_{m,n} = \int_0^H -h(z) I_0(\alpha_m r) \phi_m(z) \phi_n(z)\ dz \tag{2.15b}$$

$$P_m = \int_0^H -h(z) s(z) \phi_m(z)\ dz \tag{2.15c}$$

$$C_m = \int_0^H I_0^{'}(\alpha_m r) (\phi_m(z))^2\ dz \tag{2.15d}$$

2.3 Modeling and Results from Analytical Formulation

Temperature distribution are obtained from solving linear equations mentioned in (2.15). To validate the analytical formulation ,data from Comanche Peak Nuclear Power Plant operation manual were used. These results are compared with finite element solution (ANSYS). Two different cases were considered for simulation. One with fully submerged fuel rod in coolant and other one partially cooled. Data is tabulted in table (2.1). Exactly similar model is simulated using commercially available FEM softwares (ANSYS).

Table 2.1. Model parameters

Properties	Cylinder
Radius of cylinder (m)	0.0041
Length of cylinder (m)	4
Thermal Conductivity(W/mK)	4
Heat Generation rate(W/m^3)	1.3 x 10^7
Heat Transfer Coefficient(W/m^2K)	$h1 = 100, h2 = 10\ or\ 100$

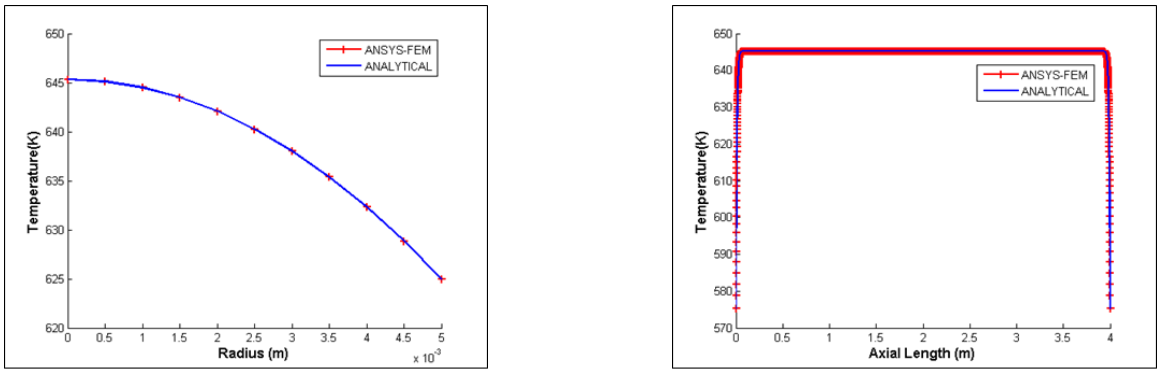

(a) (b)

Figure 2.2. Comparison of Analytical formulation and FEM solution (ANSYS) , when coolant level=length of cylinder, h1=h2=100 (a) Temperature plot along radial direction at H=2m , (b) Temperature plot along axial direction at r=0m .

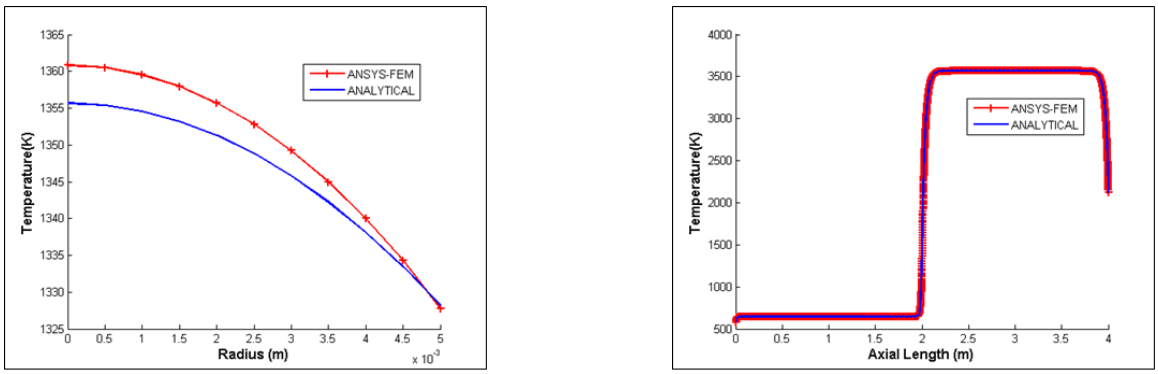

(a) (b)

Figure 2.3. Comparison of Analytical formulation and FEM solution (ANSYS) , coolant level = half-length of fuel rod ,h1=100,h2=10 (a) Temperature plot along radial direction at H=2m , (b) Temperature plot along axial direction at r=0m .

2.4 Observation and limitation of Analytical Formulation

Analytical formulation shows good results for fuel rod of cylindrical shape without any composite layers. Results obtained in previous section, shows good agreement between analytical formulation and FEM solution (ANSYS). However the following limitations makes it difficult to proceed with the analytical model in this thesis.

1. Large number of eigenvalues are required to compute accurate thermal behavior over fuel rod length. This case becomes worse while modeling partially cooled cylinder due to discontinuity at boundary and higher (L/r) ratio.

2. Incorporating temperature dependent thermal properties is a challenging task in analytical formulation.

3. Modeling an actual fuel rod with cladding i.e. composite rod formulation is a difficult task in analytical formulation.

To illustrate error, a case is considered for actual comparison between analytical formulation with non-composite cylindrical rod and numerical formulation with composite cylindrical rod. Composite fuel rod consists of fuel rod, helium gap, cladding. Here, fuel rod is assumed to be fully submerged in coolant (i.e. $h_1 = h_2 = 100$)

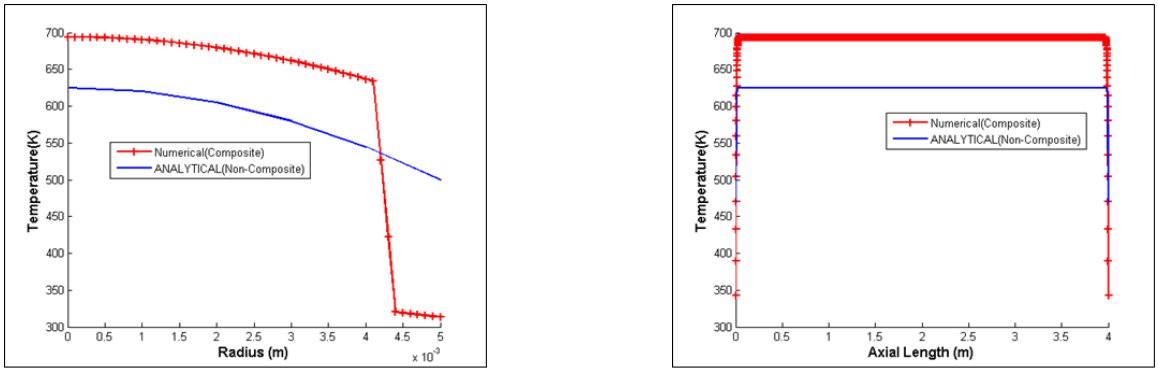

(a) (b)

Figure 2.4. Comparison of Analytical formulation and FEM solution (ANSYS) , coolant level = half-length of fuel rod ,h1=100,h2=10 (a) Temperature plot along radial direction at H=2m , (b) Temperature plot along axial direction at r=0m .

CHAPTER 3

NUMERICAL METHOD (FINITE VOLUME METHOD)

In earlier discussion, it has observed that analytical formulation has its own limitation when working under real practical conditions. As a result, we take recourse of numerical modeling. Numerical method using finite volume method is presented in this chapter. An in-house code was developed using Python and MATLAB for solving governing energy equation assuming constant heat transfer coefficient. Procedure and method are discussed here.

3.1 Finite Volume Formulation

Finite Volume Method (FVM) is well-known among researchers for solving governing energy equations as well as Navier-Stokes Equation. This method is chosen over FEM, FDM as it has shown several advantages, when Navier Stoke's equations is being solved. In this section,a heat transfer coefficient value was assumed and no equation was solved for fluid domain.

Following assumptions are made while deriving finite volume formulation for partially cooled heat generating cylinder

1. Transient thermal analysis
2. Axi-Symmetric Model
3. Temperature dependent Thermal conductivity
4. Cladding and He-gap is considered for analysis
5. Ambient temperature = 300 K

A finite volume code was developed in MATLAB in order to get the temperature distribution in the cylinder with internal heat generation subjected to given boundary conditions. The governing equation given in Eqn.(5.14) was solved using finite volume discretization. The cylinder is discretized by a Cartesian grid of finite volumes and described in Appendix C.

This formulation leads to a set of algebraic equations that need to be solved in a coupled manner with implicit formulation. The matrices obtained from the described formulation are sparse and diagonal dominant. Inbuilt sparse matrix functions in MATLAB are used to obtain the solution.

Temperature distribution obtained from the finite volume code was validated using the commercial software ANSYS APDL. Steady state formulation validation has been demonstrated in earlier papers [102–104]. The variation of the maximum temperature with steady state and time as predicted by both the methods are in close agreement within 0.1%.

To validate code further for fuel rod with clad and Helium gap, temperature distribution obtained is compared with results from published paper [105] and shown in figure (3.1) .

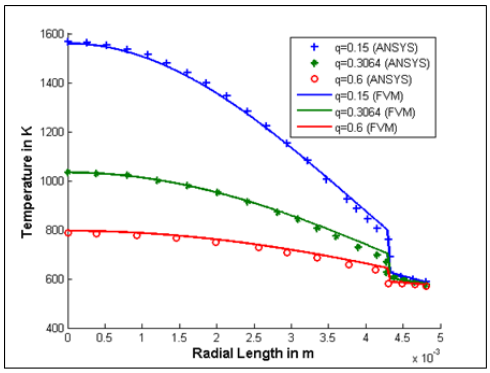

(a)

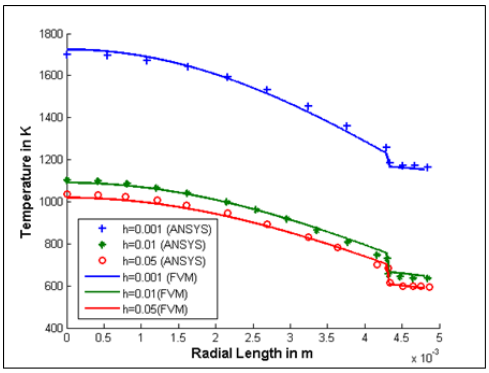

(b)

Figure 3.1. Validation of FVM code with results from published paper (a) Temperature plot with different Heat generation values (W/mm^3) *at* ($h = 0.1W/mm^2k$), (b) Temperature plot with different Heat transfer Coefficients (W/mm^2k) *at* ($q = 0.3064W/mm^3$) .

3.2 Chapter Summary

Heat transfer analysis for partially cooled cylinder was carried out using numerical approach using Finite Volume Method (FVM). As compared to analytical approach, numerical methods has shown easier approach for calculating temperature distribution across partially cooled heat generating fuel rod. Temperature data obtained from numerical method were validated against published results.However, heat transfer phenomena in fluid is not considered in this chapter. To carry out further thermal analysis, tools and libraries of OpenFOAM will be used in next chapter.

CHAPTER 4

NUMERICAL MODELLING (OPENFOAM) AND EXPERIMENTS

In the numerical study conducted in previous section, heat transfer in fluid medium was not analyzed. With reference to different coolant height, fluid and its heat exchange with cylinder is need to be considered. Therefore, heat transfer through a heat generating cylinder that is immersed in partially cooled water is numerically simulated using OpenFOAM. The numerical solution is validated by comparing the temperature data that is obtained from experimental setup representing the numerical simulation.

4.1 Governing Equations

Navier Stokes Equation with Mass, momentum, energy equation were used for carrying out numerical analysis. It consist of components like pre-processor, solver and post-processor. Navier Stokes Equation used in this work is described in Appendix B.

Pre-processor is generally used to specify computational domain, generating the mesh, apply boundary conditions and defining physical properties of the system. Here pre-processor transforms user input data into the form which can be used by solver.

After proper definition of the problem in pre-processor, the solver uses different numerical algorithm to compute solutions. Generally finite volume method (FVM) is used in most commercial CFD solvers. Solver generally consist of following steps:

1. Integrating governing equations over all control volumes in computational domain which was defined in pre-processor. While integration of governing equations, properties (velocity,temperature) are conserved for each control volume in the computational domain.
2. Transforming the integral equations into set of algebraic equations. Various numerical schemes are available for discretizing this equation.
3. Solve algebraic equations by iterative methods like Gauss Siedel, Jacobi Method

The results obtained from solvers can be visualized in the post-processor. There are several data visualization techniques available,Contour plot, vector plot, plot of different variable over time and space

4.2 OPENFOAM

To carry out solid-fluid thermal analysis OPENFOAM (Open Source Field Operation and Manipulation) code is used. OpenFOAM is a open source CFD software written with computer language of C++ and runs on Linux based operating system. It gives flexibility to change and customize functions to match requirement of the case. OpenFOAM structure is built upon libraries which is used by different solvers and utilities. Solvers are made to solve a specific type of problems in continuum mechanics, while utilities are designed to perform data manipulation. [6]

User can also create their custom solvers and utilities with understanding of underlying physics and programming skills. Openfoam does not have graphical user interface (GUI),here input are provided through text files. Results in post-processing can be visualized in Paraview.

For each case, three different folders is used: 0,constant, system. 0 folder contains

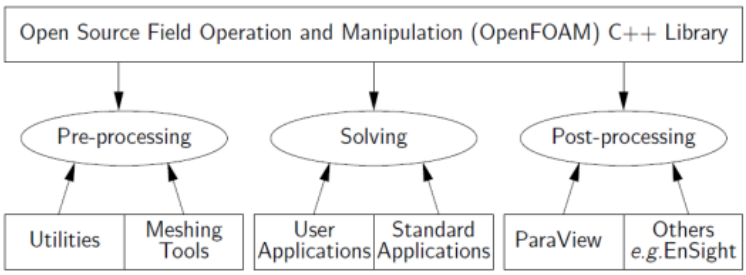

Figure 4.1. Overview of Openfoam Structure [6].

initial conditions for variables as pressure, velocity, temperature.

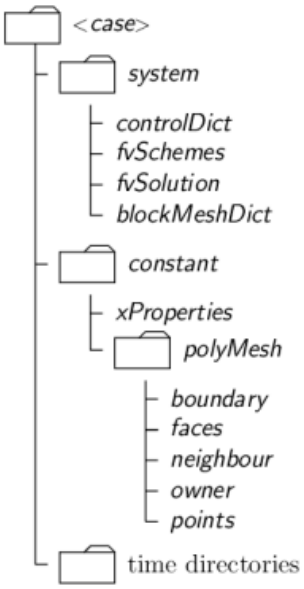

Figure 4.2. Case Directory Structure [6].

Constant folder contains fluid/solid properties and polymesh (information about mesh). System folder consists of solver and solution settings of each field. It contains 3 files : controlDict where run control parameters are set including start/end time, time step and parameters for data output; fvSchemes where discretization schemes

used in the solution may be selected at run-time; and, fvSolution where the equation solvers, tolerances and other algorithm controls are set for the run. Time directories contains individual files of data for fields like initial values.In addition, it is also useful for fixing boundary conditions.

In this thesis, chtMultiRegionFoam solver is used for evaluating thermal phenomena of partially cooled heat generating rod. It is a transient, compressible solver for conjugate heat transfer problems, supporting multiple fluid and solid regions. The solver is a combination of heatConductionFoam for the solid region, and buoyantFoam for the fluid region.

4.3 Experimental Setup

To validate data obtained from numerical analysis, various set of experiments have been carried out. The experiments are performed on a cartridge heater that is immersed in water at several different heights. The temperature measurements are obtained using thermocouple at specified locations within the cylinder for different values of heat generation rates. A model problem representing the experimental setup is formulated for numerical analysis and the resulting conjugate heat transfer problem is solved using the OpenFOAM solvers. The experimental setup consist of tank and heater. To locate heaters at center position, temporary arrangement was made with stand and card board as shown in figure. Thermocouples are attached to heater to measure surface temperature of heater. These thermocouples were equidistant of 15 mm on Heater. Total 4 number of thermocouples were used for measuring surface temperature of heater. Location 2 to Location 5 in Fig. 4.3(b) shows surface temperature measurement points. On other hand, fluid temperature is measured with three thermocouples, which were attached to wooden sticks so that their locations

remain unchanged for achieving consistency in results. However, temperature data obtained at location 6 shown in Fig. 4.3(b), will be used for inverse analysis. For experiments, cartridge heater is used as heat generating cylinder. These heaters are generally made up of Nichrome wire, steel casing and ceramics. Steel casing is covered around ceramic material . This heater has facility to measure internal temperature. Location of internal temperature is near bottom corner of the rod. K type thermocouple were used for temperature measurement in experiment. Their arrangement at different locations is shown in figure (4.3(a)). Electrical resistance of heater is measured to evaluate power supplied to heater. Temperature data was recorded using NI-DAQ and Labview.

Experiments were carried out for three cases: (i) Heater fully submerged in water, (ii) Heater half submerged in water and (iii) No water around the heater. For each case of the water level, the heater was heated at three different rates of heat generation. In total, 9 trials were carried out. However, each trial was repeated 3 times and average temperature data were used for further analysis. For each trial, the experiment was initiated with the heater and water at room temperature and continued till steady state temperature readings from thermocouples was obtained. Time to reach the steady state varied from 500s to 1800s based on the water level and the heat generation rate. Temperature on the cylinder surface and internal was measured using the thermocouples. For surface temperature measurement, 4 equidistant thermocouples were attached to the heater. Figure (4.3(b)) shows points 2 to 5 as locations used for surface temperature measurement. In addition, a thermocouple was placed in the fluid (water or air) to measure fluid temperature (Location 6).

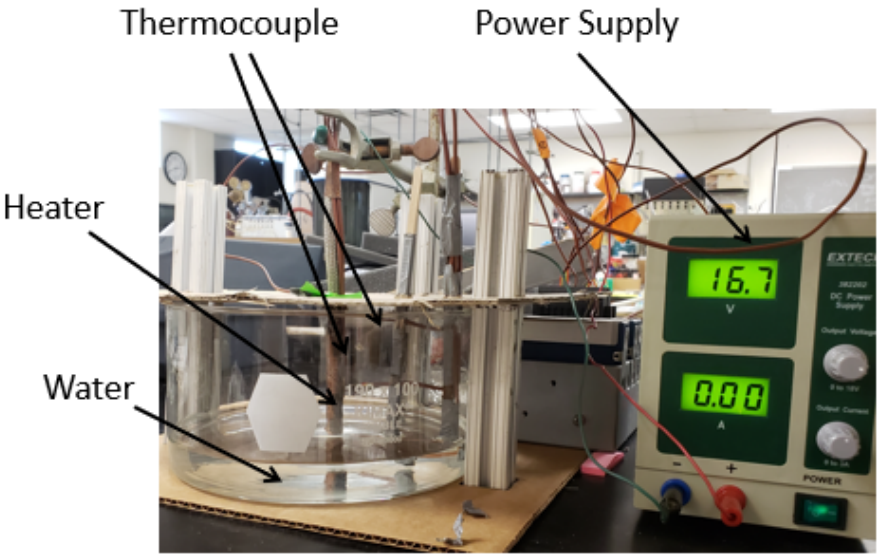

(a)

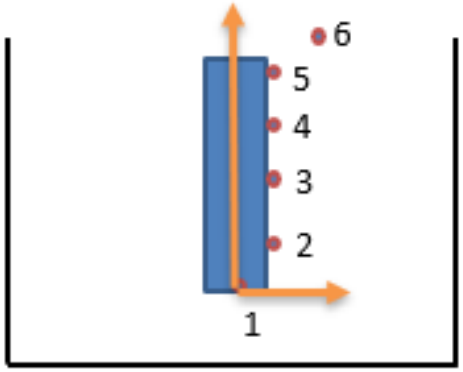

(b)

Figure 4.3. (a) Experimental Setup (b) Model of Heater .

4.4 Modeling

A heat generating cylinder that is partially cooled in water has been modeled using OPENFOAM. Computational simulations were set up for cartridge heater with tank. Heaters are generally made up of Nichrome wire, steel casing and ceramics. Nichrome wire is embedded inside ceramics and it is covered by steel casing.

For modeling, composite material and their properties are taken into consideration. Heater with composite material is shown in Figure (4.4).

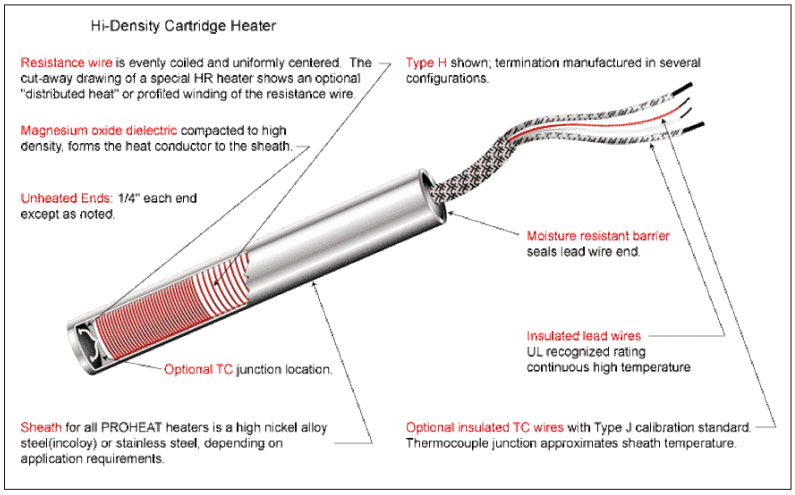

(a)

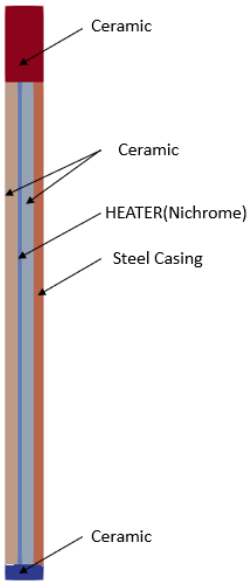

(b)

Figure 4.4. (a) Heater construction (b) Model of Heater .

Thermal properties of composite material inside cartridge heater is given in Table 4.2 The computational domain includes the cylindrical rod that is partially

Table 4.1. Thermal properties

Material	Thermal Conductivity(W/mK)	Specific Heat (J/KgK)	Density (kg/m^3)
Nichrome	13.5	450	4500
Steel	11	250	8000
Ceramic	1.25	1050	3500
Air	0.025	1046	1.25
Water	0.6	4186	1000

immersed in water with air surrounding it. Figure (4.5) shows schematic representation computational domain and the mesh used to discretize the domain. The physical domain consist of cylinder of 9.5 mm diameter and 75 mm length that is partially immersed in a pool of water tank which is made up of diameter of 190 mm and length 100 mm was assumed as pool of water or air. Axi-symmetric model was considered for simulating heat transfer of partially cooled heater.

Experimental setup mimics the partially cooled cylinder condition during nuclear accident. Summary of these conditions, which is used for modeling is given below :

1. This is coupled heat transfer problem as it contains fluid and solid domain
2. Heater specifically nichrome material is modeled as uniform heat source.
3. Heat transfer between fluid and heater is considered as natural convection
4. Fluid flow developed over heater is assumed to be laminar
5. Transients simulation was carried out for validation.
6. Radiation effects are neglected
7. Fluid is considered as Air and water according to different conditions assumed in experiments.

The mesh was generated using BlockMesh utility. The blockMeshDict file is a text file which tells the blockMesh utility how to generate mesh. It is structured as a

list of vertices, list of blocks, number of cells and biasing in each direction, boundary patches. Cell expansion ratios for each direction in the block allows grading. The ratio is the width of the end cell δ_e along one edge of a block to the width of the start cell δ_s along that edge.

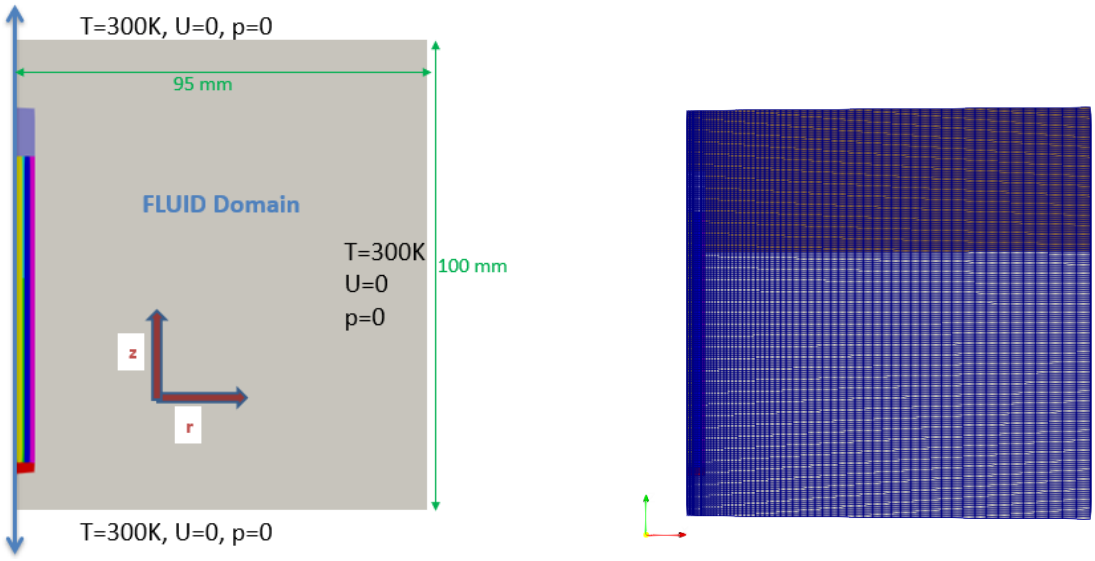

(a) (b)

Figure 4.5. (a) Computational Domain (b) Mesh .

The domain was arbitrarily defined to have 200 cells in z direction. However for r direction, biased meshing was carried out. Grid independence study was conducted using meshes with three different levels of refinement. This study is for evaluating if mesh points are correct enough. A coarse mesh of 9797, a medium mesh of 25257 and fine mesh of 77397 were considered. Simulation was carried out at no coolant condition, which provides maximum temperature gradient. Temperature data was obtained at different time were analyzed for three different meshes. Fig shows the numerical solution obtained on the considered meshes. It is observed that the

maximum error in the solution between medium and fine meshes is less than 2%. As a result, the numerical simulations were run on medium mesh.

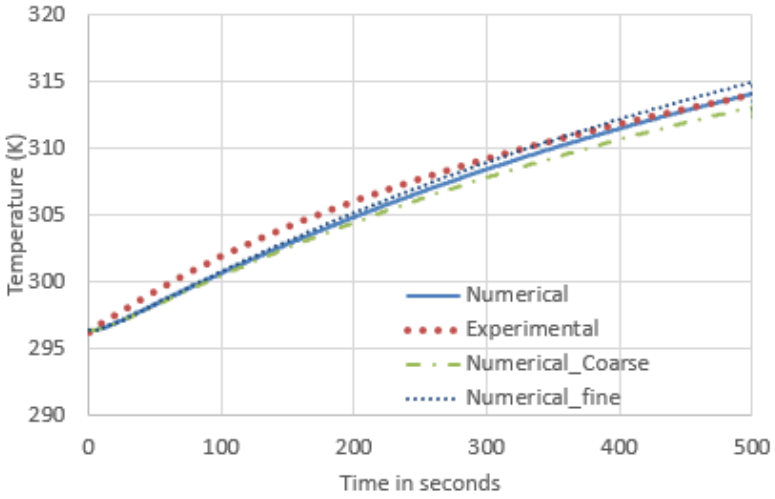

Figure 4.6. Temperature data for three different grid points at location 1.

Boundary conditions are summarized in table.

Table 4.2. Boundary condition

Boundary	Thermal	Velocity	Pressure
Boundary1	300 K	0 m/s	0
Boundary2	300 K	0 m/s	0
Boundary3	300 K	0 m/s	0
Boundary4	$\partial(T)/\partial(n) = 0$	$\partial(T)/\partial(n) = 0$	0

OpenFOAM employs finite volume method for solving incompressible Navier-Stokes Equations and the transport equation representing the heat transfer. The convection terms in the Navier-Stokes Equations was discretized using a second order upwind scheme and second order difference scheme was used for diffusion terms. The

unsteady simulations were carried out using P.I.S.O. Algorithm. To achieve proper convergence time step was chosen as $0.003s$. The residuals in the energy and the momentum equations reached $10^{-}4$ to $10^{-}7$ within each time step. All simulation were carried out using Texas Advanced Computing Centre (TACC) skylake node [106]. Computation time varies from 12 hours for no coolant case to 45 hours for partially cooled cylinder case. Residual for velocity and enthalpy field is shown in Fig. (4.7).

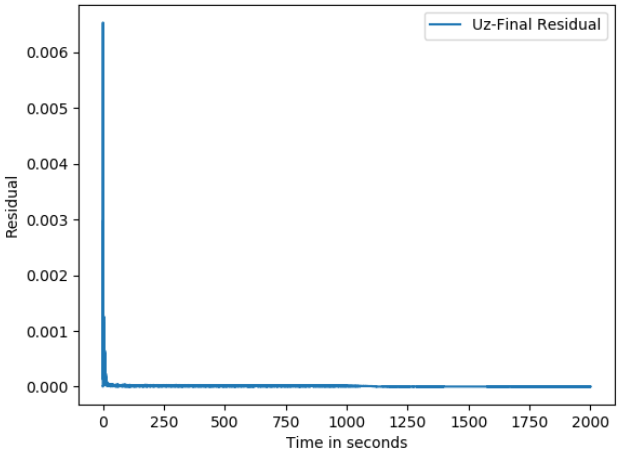

(a)

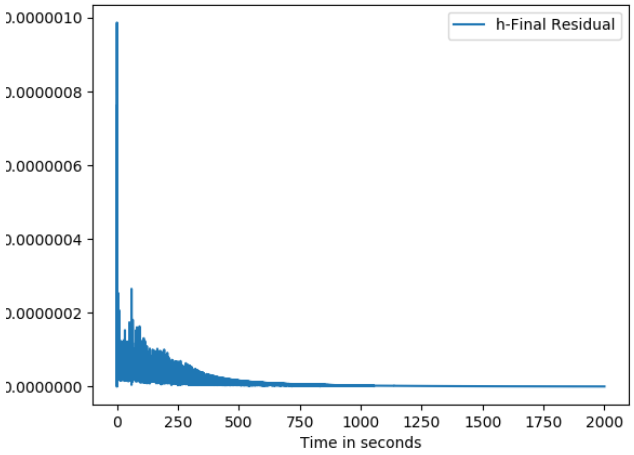

(b)

Figure 4.7. (a) Velocity Residual (b) Enthalpy residual .

4.5 Validation of OpenFOAM code

The temperature data obtained from numerical analysis is validated with conducted experiments.The results obtained from the numerical simulations were compared with the measurements obtained from the experiments at different levels of water and heat generation rates provided to the heater.Temperature obtained at 3 locations were compared: one location at the surface of solid region, one location

within the interior of the solid region and one location in the fluid region.

4.5.1 Coolant level =0

Experiments were carried out when there are no coolant (water). This case corresponds to natural convection. Three different experiments with 1,2,3 Watts of heat generation rates were carried out. Temperature data obtained from these experiments are plotted and compared with data obtained from the numerical simulations as shown in the Fig. 4.8(a) 4.8(b) 4.9(a) 4.9(b)

4.5.2 Coolant level =0.45L

Experiment are carried out with water level filled with 0.45L, where L is length of heater. This case corresponds to partially cooled heat generating cylinder. Again three different experiments were carried out. However another experiments with 4 W were carried out to capture higher temperature transients in partially cooled case. In this experiment, steady state is reached within $500s$. Temperature data obtained from these experiments are plotted and compared with numerical simulation.

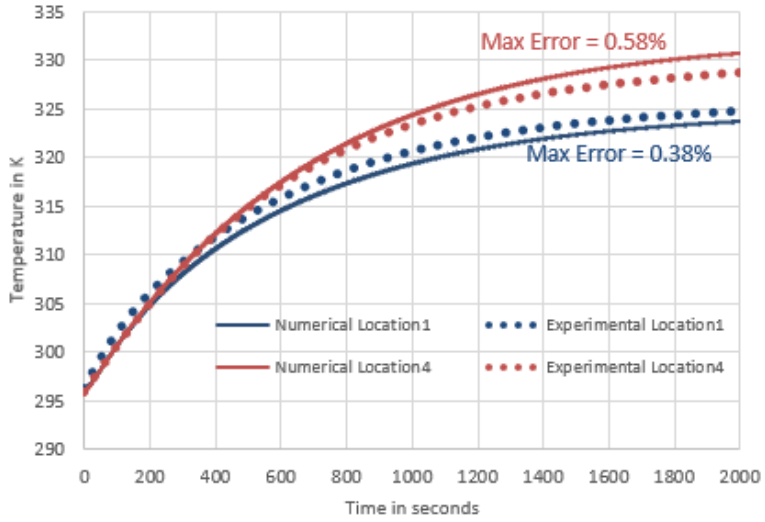

(a)

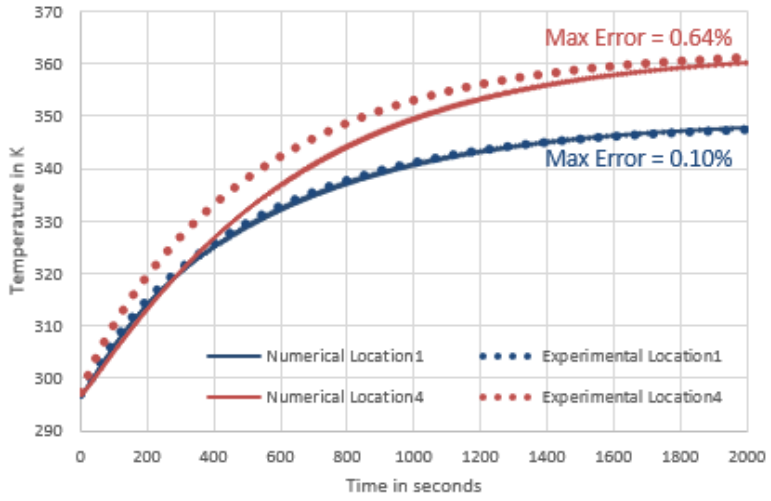

(b)

Figure 4.8. (a) Temperature plot (1W) (b) Temperature plot (2W) .

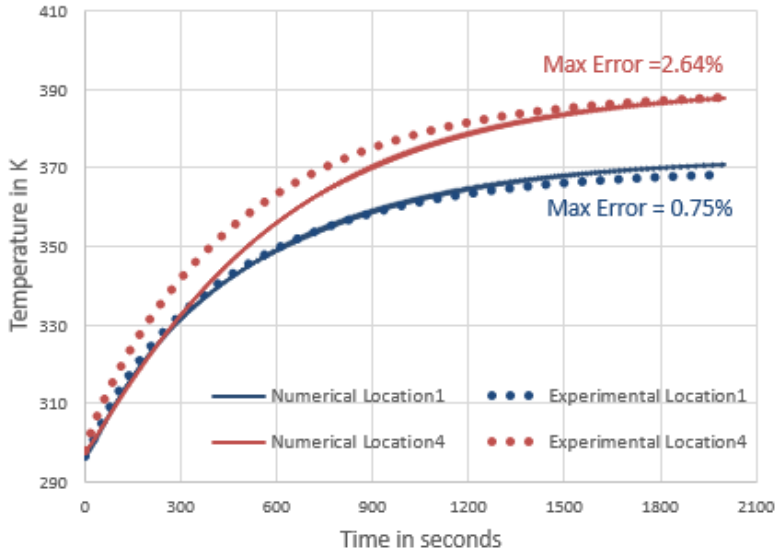

(a)

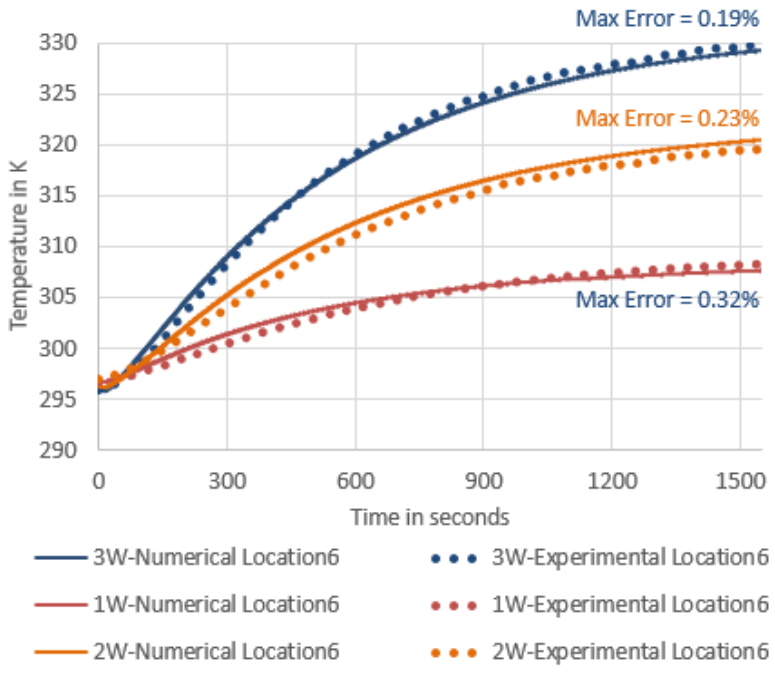

(b)

Figure 4.9. (a) Temperature plot (3W) (b) Temperature plot at Location6 .

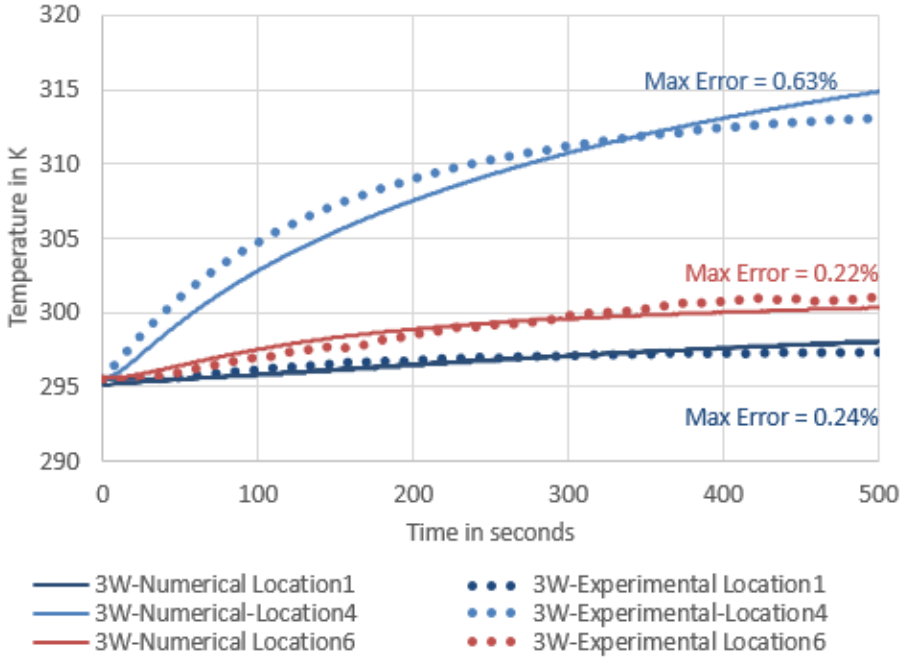

(a)

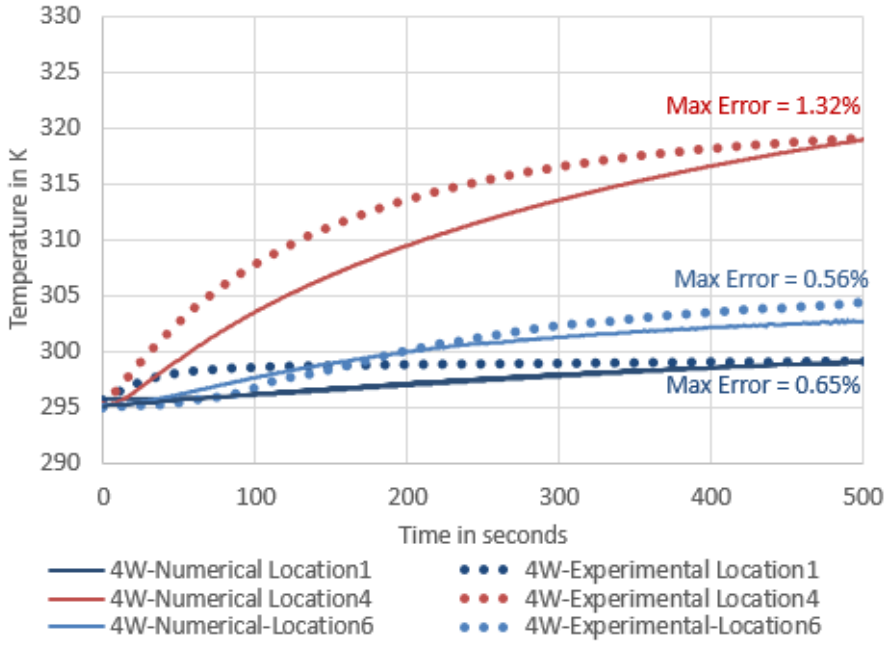

(b)

Figure 4.10. Partially cooled rod at Coolant level= 0.45L (a) Temperature plot (3W) (b) Temperature plot (4W) .

4.6 Chapter Summary

In this chapter, procedure and results for numerical analysis were discussed. An axi-symmetric model and coupled solid-fluid thermal analysis was carried out to evaluate temperature on surface and internal temperature of heat generating body. Different coolant levels were used for simulating partially cooled heat generating body. The results obtained from numerical analysis was validated with experiments. Experiment was setup using cartridge heater and tank to represent a heat generating body and coolant pond. Maximum error between experimental and numerical temperature data was 2.6 %

CHAPTER 5

INVERSE ANALYSIS

Inverse analysis (IA) is the process of calculating the causal factors from set of observations or results. In this study, inverse analysis is carried out to predict temperature distribution of partially cooled heat generating cylinder using two different methods. In first method, temperature measured at rod surface is used as input for predicting center-line temperature.The second method center-line and cylinder surface temperature is predicted by using the fluid temperature measurement around rod as input. Amongst different methods for optimization tools available for inverse techniques, conjugate gradient method or simplex method is used in this study. For computing sensitivity, complex variable semi analytical method (CVSAM) is used in first method whereas temperature gradient of fluid temperature is utilized for second method.

5.1 Inverse formulation

The inverse problem for determining temperature profile can be formulated as an optimization problem by defining suitable objective function and constraints. Unknown coefficients like heat generation rate is a design variable in the optimization problem. This design variable is used as input to the finite volume (FVM) code that predicts temperature distribution over time. Error between temperature obtained from FVM and measurement is minimized by taking norm of the error as given in Eqn.(5.1)

$$objective function \;=\; S \;=\; \sum_{i=1}^{n}(T_i - Tm_i)^2 \tag{5.1}$$

Where, n =number of measurement points, T_i = computed temperature from FVM code, Tm_i = measured temperature, S = Objective function.

The objective function described in Eqn.(5.1) is minimized using Conjugate Gradient Method (CGM). Gradient of objective function to the design variable (i.e. thermal conductivity) is typically required for such type of algorithm. The optimal location of temperature measurements is obtained from CVSAM. The flow chart of the inverse procedure is shown in Fig. 5.1.

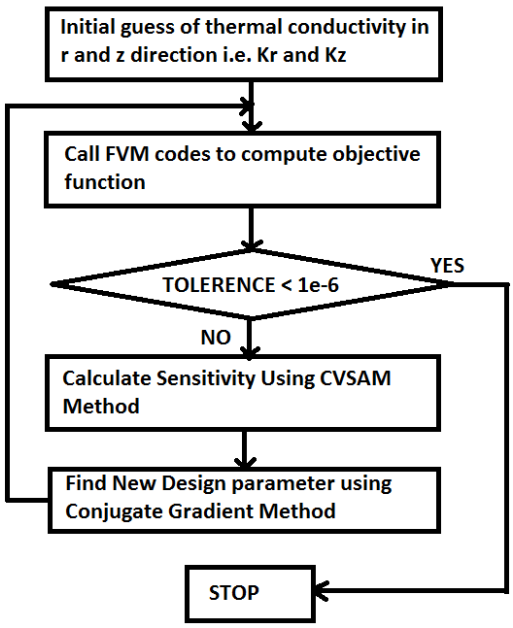

Figure 5.1. Flow chart of inverse analysis.

Noise is also added to measured values of temperature. The iterations are stopped if the change in the value of objective function between successive iterations is less than 10^{-6}.

$$criteria\ for\ stopping\ <=\ (S^{n+1} - S^{n}) \tag{5.2}$$

5.2 Center-line Temperature prediction from cylinder surface temperature measurement

Inverse analysis is performed to predict temperature distribution of partially cooled heat generating cylinder using temperature measured at surface. Here conjugate gradient method is used for optimization. Sensitivity is computed using complex variable semi analytical method (CVSAM).

5.2.1 Sensitivity Analysis

Sensitivity analysis is performed using automatic differentiation and adjoint variable approach. Semi Analytical Method is advantageous due to its generality and computational efficiency. However, it can lead to inaccurate sensitivity analysis if perturbation size is not chosen carefully. An alternative approach is semi analytical complex variable method (CVSAM), which is used to formulate sensitivity in this paper. This method can compute sensitivity with respect to design variable with high accuracy and efficiency [107].

Finite volume global equilibrium equation is

$$[K]\{T\} = \{f\} \tag{5.3}$$

Where $[K]$ is stiffness matrix, $\{T\}$ is the temperature and $\{f\}$ is load vector. Input design variables are considered as $\{X\} = \{X_1, X_2...X_n\}$

Differentiating Finite Volume equation with respect to design variables on both sides, following equations is obtained

$$\frac{\partial[K]}{\partial\{X\}}\{T\} + \frac{\partial\{T\}}{\partial\{X\}}[K] = \frac{\partial\{f\}}{\partial\{X\}} \tag{5.4}$$

Derivative of Temperature with respect design variable $\{X\}$ can be written as follows

$$\frac{\partial\{T\}}{\partial\{X\}} = \frac{\{\Delta T\}}{\{\Delta X\}} = [K]^{-1}\left(\frac{\{\Delta f\}}{\{\Delta X\}} - \frac{[\Delta K]}{\{\Delta X\}}\{T\}\right) \tag{5.5}$$

In this equation same stiffness matrix is used for calculating temperature and sensitivity. SAM programming is convenient and computationally efficient as same stiffness matrix used in equation Eqn.(5.3) and equation Eqn.(5.6). However finite difference is used for calculation of $\frac{[\Delta K]}{\{\Delta X\}}$ and $\frac{\{\Delta f\}}{\{\Delta X\}}$. Choice of perturbation size is important to calculate accurate sensitivity. It is difficult to find optimal perturbation size with respect to multiple design variable. This issue of determining optimal perturbation size is addressed considering finite difference in complex plane. Taylor series expansion with perturbation size in imaginary dimension is calculated as follows

$$f(x + i\Delta x) = f(x) + i\Delta x\Delta f'(x) - \frac{\Delta x^2 f''(x)}{2!} - \frac{i\Delta x^3 f'''(x)}{3!} + ... \tag{5.6}$$

Real and imaginary parts of above equation are separated and grouped together. First order term can be obtained as follows

$$f'(x) = \frac{Imag(f(x + i\Delta x))}{\Delta x} + O(\Delta x^2) \tag{5.7}$$

It can observed from above equation Eqn.(5.7) that subtractive cancellation error has been eliminated. By combining equations, CVSAM is obtained. Sensitivity of the response to design variable is given in following equation.

$$\frac{\partial\{T\}}{\partial\{X\}} \approx [K]^{-1}\left(\frac{Imag\{f(X_i+i\Delta X_i)\}}{\{\Delta X_i\}} - \frac{Imag\,[K(X_i+i\Delta X_i)]}{\{\Delta X_i\}}\{T\}\right) \tag{5.8a}$$

5.2.2 Conjugate Gradient Method

Conjugate Gradient Method is used in this study due to its robustness and high rate of convergence. In this method, design variable for each iteration is calculated using minimizing objective function by searching along direction of descent $D^{(n)}$ and search step size β^n. For orthotropic material, thermal conductivity in r and z direction is calculated using following equation.

$$k_r^{n+1} = k_r^n - \beta_r^{(n)}\ D_r^{(n)} \tag{5.9a}$$

$$k_z^{n+1} = k_z^n - \beta_z^{(n)}\ D_z^{(n)} \tag{5.9b}$$

Where, $D_r\&D_z$ = direction of descent in r and z coordinates respectively, $\beta_r\&\beta_z$ = step size in r and z coordinates, n = Iteration number.

The direction of descent for the current iteration is calculated using linear combination of direction of descent of previous iteration and gradient direction as given below:

$$D_r^{(n)} = \frac{dS}{dk_r}^{(n)} + \gamma_r^{(n)} D_r^{(n-1)} \tag{5.10a}$$

$$D_z^{(n)} = \frac{dS}{dk_z}^{(n)} + \gamma_z^{(n)} D_z^{(n-1)} \tag{5.10b}$$

Where, $\gamma^{(n)}$ = Conjugation Coefficient

$$\gamma_r^{(n)} = \frac{\frac{dS}{dk_r}^{(n)} \frac{dS}{dk_r}^{(n)}}{\frac{dS}{dk_r}^{(n-1)} \frac{dS}{dk_r}^{(n-1)}} \tag{5.11a}$$

$$\gamma_z^{(n)} = \frac{\frac{dS}{dk_z}^{(n)} \frac{dS}{dk_z}^{(n)}}{\frac{dS}{dk_z}^{(n-1)} \frac{dS}{dk_z}^{(n-1)}} \tag{5.11b}$$

Step size can be obtained by minimizing objective function S with respect to step size $\beta^{(n)}$ as follows

$$\beta_r^{(n)} = \frac{\frac{dT}{dk_r}^{n}(T_i - Tm_i)}{(\frac{dT}{dk_r}^{n})^T \frac{dT}{dk_r}^{n}} \tag{5.12a}$$

$$\beta_z^{(n)} = \frac{\frac{dT}{dk_z}^{n}(T_i - Tm_i)}{(\frac{dT}{dk_z}^{n})^T \frac{dT}{dk_z}^{n}} \tag{5.12b}$$

5.2.3 Modeling and results

To validate the inverse analysis procedure, model is used from table (2.1).Using finite volume code, developed in earlier chapter, temperature distribution on surface of the rod was obtained. Assumptions made during this study are as follows.

- Axisymmetric Modeling
- Transient thermal Analysis
- Ambient temperature is assumed as 300 K

Temperature data at 5 points as shown in Fig.5.2 are used as input to inverse analysis. Moreover, dimensions and thermal properties of the fuel rod are also used as input to inverse analysis. Aim of this study is to centre-line temperature from given input.

Algorithm depicted in earlier section is used for predicting heat generation rate. The model assumes a constant internal heat generation rate. Simulated temperature data is generated by running the forward problem using finite volume method. The temperature at the location shown in fig (5.2) at different time steps with added noise

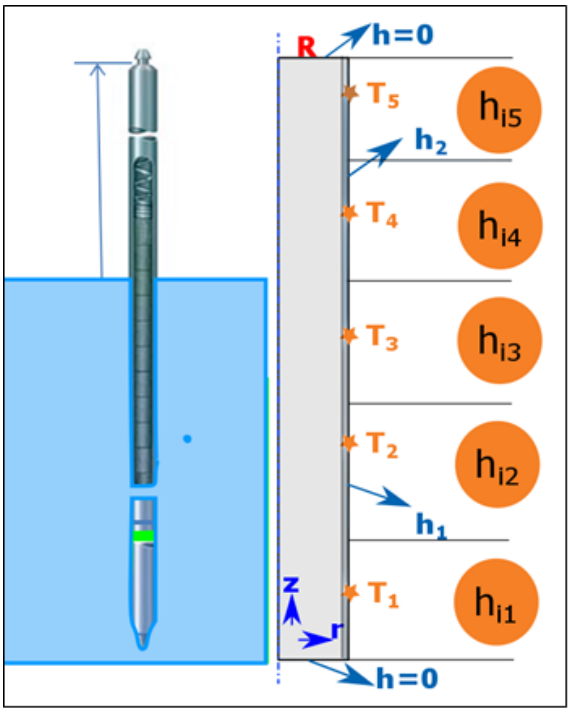

Figure 5.2. Schematic model of partially cooled cylindrical rod for inverse analysis.

was given as input to inverse analysis formulation. Noise was added according to the Eqn.(5.19).

$$T_{noise} = \pm\sqrt{-2\sigma^2 \ \ln R} \tag{5.13}$$

Where R = Random number between 0 and 1. σ =Standard deviation

Table. 5.1 shows the result from the inverse analysis for noise with different normal distribution profiles. It is observed that inverse analysis formulation provides good results even with added noise in the measurement.

Table 5.1. Results from Inverse analysis

Properties	Actual Value	Predicted Value			
		$\sigma = 0$	$\sigma = 0.01$	$\sigma = 0.05$	$\sigma = 0.1$
Heat Generation rate(W/m^3)	8 x 10^7	7.999 x 10^7	8.004 x 10^7	7.9984 x 10^7	
Heat Transfer Coefficient(W/m^2K)					
h_{i1}	1000	999.9991	999.934	999.89	1001
h_{i2}	1000	999.9991	1000.0004	1002.82	999.8
h_{i3}	1000	999.9991	999.993	999.68	999.1
h_{i4}	10	9.9998	9.9635	10.48	9.9
h_{i5}	10	9.9997	9.9917	10.28	9.3

5.3 Thermal conductivity prediction from rod surface temperature

In this section, numerical inverse analysis is used to predict thermal properties of heat generating material (thermal conductivity) by measuring temperature at surface. Accuracy and efficiency of the method is enhanced by using accurate sensitivity information by use of Semi-Analytical Complex Variable Method(CVSAM). Steady state heat transfer analysis with an axi-symmetric model was carried out using finite volume method. Temperature obtained from this analysis, is used as input for the inverse method. Objective function for the optimization is difference between computed and measured temperature. This function was minimized with Conjugate Gradient Method (CGM). Coefficients obtained from CVSAM were used in gradient based optimization method. The robustness of developed approach was evaluated by adding Gaussian noise these temperature values. Material properties predicted from this method show close agreement with published values.

5.3.1 Earlier Work and overview

Over the past decades, the inverse analysis has been carried out for estimation of material properties as thermal conductivity, specific heat etc. [21, 27, 108–118] using measurement taken at surface. In previous works, temperature measurements at multiple locations had to be provided as input to get accurate estimate of the material thermal properties.

The formulation for inverse determination of temperature distribution inside a heat generating cylinder subjected to homogeneous boundary condition, has been presented for estimating thermal conductivity of the cylinder. A finite volume code is developed and optimization is carried out with conjugate gradient method. A test involving a heat generating cylinder with orthotropic thermal properties exposed to air, is used to demonstrate the developed method. The convection boundary conditions on the surfaces were determined using heat transfer coefficients that are available in the literature. With the given value of heat generation, the temperature distribution in the interior of the cylinder is obtained using the finite volume code. The temperature distribution if the cylinder obtained from finite volume code was given as input to the developed inverse analysis formulation. In order to simulate the measurement error, noise with normal distribution was added to the temperature distribution which given as input to the inverse analysis and the robustness of the developed approach is evaluated. The sensitivity of the inverse formulation to the location of temperature measurement was analyzed using Semi Analytical Complex Variable Sensitivity Analysis Method (CVSAM). The orthotropic thermal properties were obtained from inverse analysis. The calculations showed consistent results.

It should be emphasized that the developed approaches are general and may be applied to other heat transfer problems as well. In the present work, the material properties have been determined using measured temperature distribution along only

one surface. This method is advantageous as it can be easily automated along with single thermal imaging system to predict properties.

5.3.2 Problem Definition

A cylindrical body of radius R and height L as shown schematically in Fig.5.3 is considered. Heat Generation rate Q is assumed to be constant inside the cylinder. It is also assumed that cylinder exchanges heat with surrounding by convective heat transfer. Heat transfer coefficient of h_r and h_z are considered for outer surfaces along the radial and longitudinal directions respectively. For present paper, both heat transfer coefficients are taken to be (10 W/m^2K) [119]. Considering rotational symmetry, variation with respect to θ-coordinate is ignored.

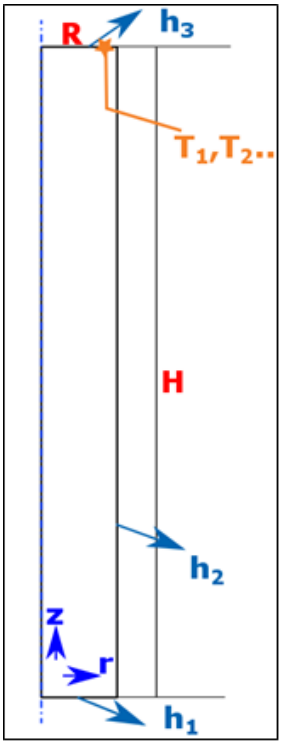

Figure 5.3. Schematic model of axisymmetric heat generating cylindrical rod.

General form of the governing energy equation for the cylinder is given by Eqn.(5.14). It is assumed that heat generation is constant through out the cylinder:

$$\left(\frac{1}{r}\frac{\partial T}{\partial r}\left(k_r\frac{\partial T}{\partial r}\right)+k_z\frac{\partial^2 T}{\partial z^2}\right)+Q=0 \tag{5.14}$$

Where k = Thermal Conductivity, r =radius in m, z = length in m, T = temperature, Q = Volumetric heat generation

The governing equation in Eqn.(5.14) subjected to boundary condition (explained in earlier section) is solved using finite volume formulation.

$$k_r\frac{\partial T}{\partial r}=h_r[T-T_\infty]\ at\ r=R_1\ z\in[0,L] \tag{5.15}$$

$$k_z\frac{\partial T}{\partial z}=h_z[T-T_\infty]\ \ at\ z=0\ r\in[0,R] \tag{5.16}$$

$$k_z\frac{\partial T}{\partial z}=h_z[T-T_\infty]\ at\ z=L\ r\in[0,R_1] \tag{5.17}$$

$$k_r\frac{\partial T}{\partial r}=0\ at\ r=0\ z\in[0,L] \tag{5.18}$$

Where r, z = directions, $hz = hr$ =Heat transfer coefficient, T_∞ =300 K, L = Length of cylinder, $R1$ = Radius of cylinder, K_z, K_r = Thermal conductivity in z and r direction.

5.3.3 Algorithm

To find thermal conductivity of heat generating cylinder in r and z direction following algorithm is used:

1. Specify physical domain, governing equation,boundary conditions and surface temperature of the cylinder. For given case, with the known value of thermal conductivity forward problem is solved to get surface temperature value of the cylinder.

2. Solve entire problem with initial guess of thermal conductivity. (thermal conductivity will be updated after each iteration)

3. Compute objective function as given in Eqn (5.1).

4. Check for the stopping criteria for given objective function. If it is less than 10^{-6} then stop calculation otherwise follow step 5.

5. Calculate sensitivity matrix using equation (5.8a).

6. Calculate gradient direction using equation (5.10a).

7. Calculate Conjugation Coefficient using equation (5.11a).

8. Calculate the direction of descend from equation (5.10a).

9. Calculate step size from equation (5.12a).

10. Calculate new thermal conductivity k_r and k_z and go to next iteration i.e. (n+1)

11. Go to step 2.

5.3.4 Test Case

A cylindrical rod of radius 0.013 m and length 0.066 m, as shown in Fig. C.1 is considered as model problem to test developed method for inverse analysis. It can be considered as battery as referred in [120]. Convective heat transfer occurs with air, having film coefficient h (10 W/m^2) K and ambient temperature 300 K. Material is assumed to be linearly orthotropic for the analysis. Thermal conductivity in r and z direction are considered to be differ in values $K_r = 0.15\ W/m^2K$, $K_z = 32\ W/m^2K$. Heat generation value is assumed as constant over time for calculation.

Convective heat transfer boundary conditions are applied on outer edge of cylinder, which is exposed to air as shown in Fig. (C.1). Simulation is initiated with heat generation and applying boundary condition. Temperature distribution obtained from this simulation at surface are used as input to the inverse analysis.

However sensitivity with reference to orthotropic thermal conductivity is calculated and shown in figure. This data gives valuable information for selection of thermal measurement points. Hence only two points and five points at surface $z = L$ is taken for measurement and inverse analysis. Temperature measurement on one surface gives advantage of using thermal camera and automate the program for thermal conductivity measurement.

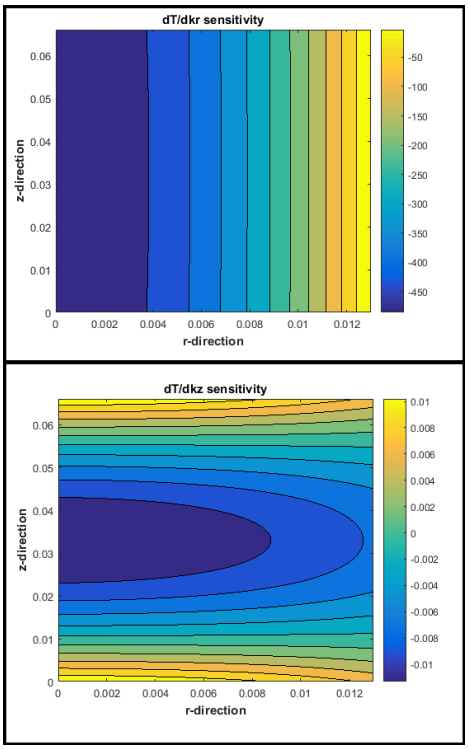

Figure 5.4. Sensitivity plot - dT/dk_r and dT/dk_z .

Considering real scenario, there is always noise in terms of measurement error. To show robustness of the method, noise in form of Gaussian distribution has been added to temperature data, which was obtained from numerical solution of the problem. The results for different values of standard deviation of profile of noise is shown in Fig 5.5.

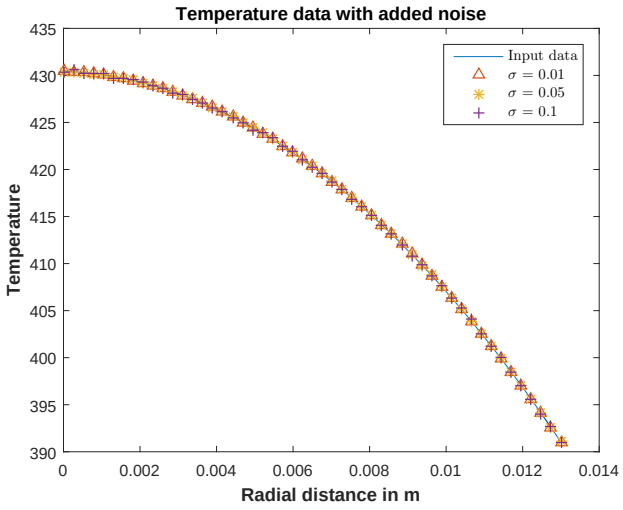

Figure 5.5. Temperature data in r direction at $z = 0.066m$ direction with addition of different simulated noise.

The model is subjected to constant internal heat generation rate of 6 W. Simulated data is generated by running the forward problem using finite volume method.The temperature at the location $z = L$ with added noise was given as input to inverse analysis formulation. Noise was added according to the Eqn.(5.19).

$$T_{noise} = \pm\sqrt{-2\sigma^2 \ \ln R} \tag{5.19}$$

Where $R =$ Random number between 0 and 1. σ =Standard deviation

5.3.5 Results

Case 1: Two measurement points

The temperature at the location $r = 0.013\ m$, $r = 0.01274\ m$ with added noise was given as input to inverse analysis as this location has least sensitivity along radial surface. Percentage error between predicted thermal conductivity with that of obtained from literature [120] is shown in Fig.(5.6)

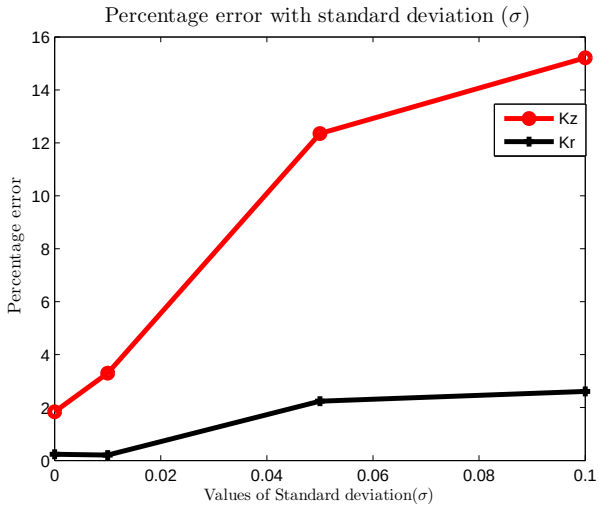

Figure 5.6. Percentage error at different standard deviation - Two Measurement Points.

Case 2: Five measurement points

In this case, five measurement points at surface $z = 0.013\ m$ are used for inverse analysis for estimation of thermal conductivity. Error between estimated and literature value is shown in Fig.(5.7). It has been seen that error reduces with more measuring points at surface.

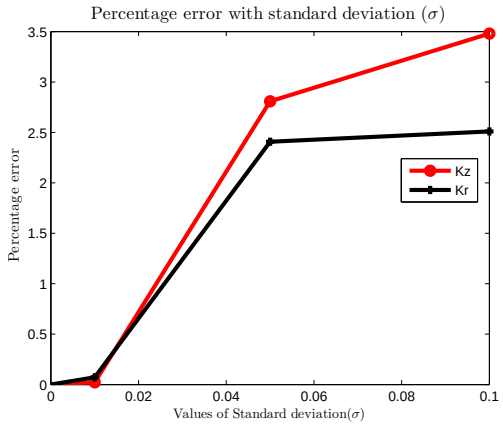

Figure 5.7. Percentage error at different standard deviation- Five Measurement Points.

Case 3: Five measurement points and different ratio of orthotropy

In this case different ratio of anisotropy (i.e. K_z/K_r) was considered for the model, where K_r is kept constant and value of k_z is changed.This model was used for inverse analysis for prediction of thermal conductivity. For consistency of results, same five measurement points are used as input to inverse method. Moreover 20 simulations were carried out with same initial guess for specific standard deviation and degree of orthorpic value. Average error is calculated as difference between these estimated values with actual values (i.e. K_z/K_r) and plotted for different orthotropy ratio and standard deviation as shown in Fig.(5.8).

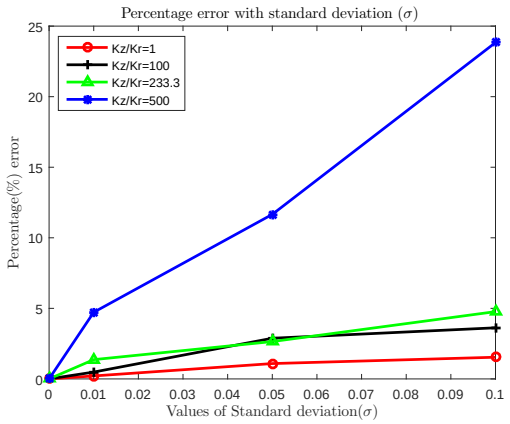

Figure 5.8. Percentage error at different standard deviation and orthotropy ratio.

5.4 Inverse Analysis using fluid temperature

In this section, inverse analysis approach was used for predicting temperature over heat generating body from fluid temperature measurement. In earlier discussion, it has been observed that measurement need to taken on the surface of heat generating cylinder. Here,the inverse problem for determining temperature profile can be formulated as an optimization problem by defining suitable objective function. Unknown

coefficients like heat generation rate is design variable , which is used as input to finite volume (FVM) code that predicts temperature distribution over time. Libraries of OpenFOAM is utilized for numerical analysis to determine temperature distribution in solid and fluid. Error between temperature obtained from FVM and measurement at fluid location is minimized by taking norm of the error as given in Eqn.(5.1).

Objective function described in Eqn.(5.1) is minimized using Simplex Method, which is derivative free method. In absence of sensitivity, location with higher temperature change is selected as input to inverse analysis. Schematic representation of inverse analysis setup is shown in Fig. 5.9. Temperature measured at location 6 is used as input to inverse analysis model. The flow chart of the inverse procedure is shown in Fig. 5.1.

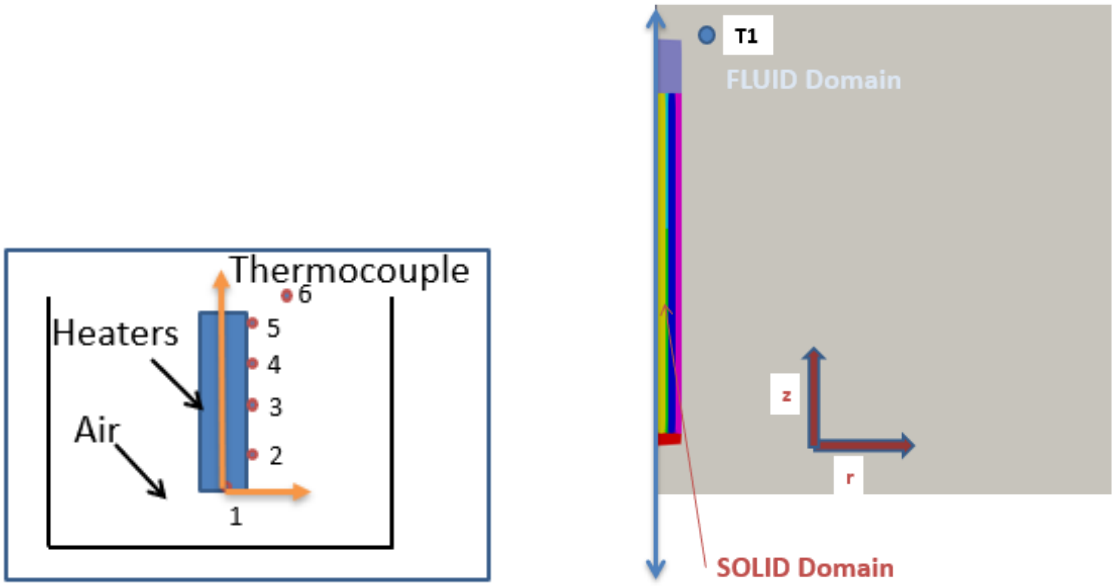

(a) (b)

Figure 5.9. (a) Schematic Inverse Analysis Model (b) Numerical Analysis Model .

5.4.1 Sensitivity Analysis

For inverse analysis, location of point 6 is really important as higher changes in temperature aids in predicting heat generation rate and temperature at critical locations over heat generating body. In fluid domain, three different locations in z and r direction was chosen. Temperature change was observed at these six locations and plotted in Fig. 5.10. It is evident from graph that temperature at location 6 which is at $r = 10\ mm,\ z = 85\ mm$, shows more changes for particular heat generation rate. Hence for inverse analysis, temperature at location 6 is considered as input to the model. Temperature obtained at this location is validated with experimental data also.

5.4.2 Modeling and results

For carrying out inverse analysis simplex method was used. Code was developed in Python where Simplex library was utilized to predict temperature on centre point as well as surface temperature. Simulation was carried out on TACC. Optimized results were obtained after 40 hours of simulation. Temperature from numerical analysis was compared with predicted temperature from inverse analysis. It shows really good agreement with maximum error of 1.09% and shown in Fig. 5.11.

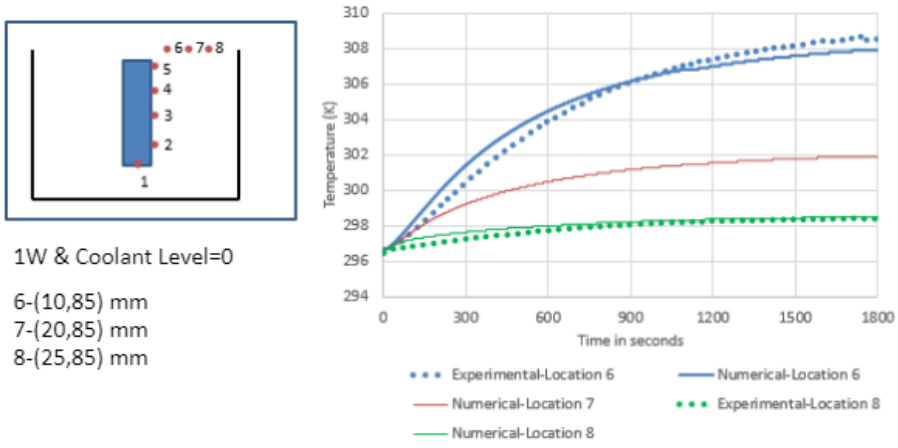

(a)

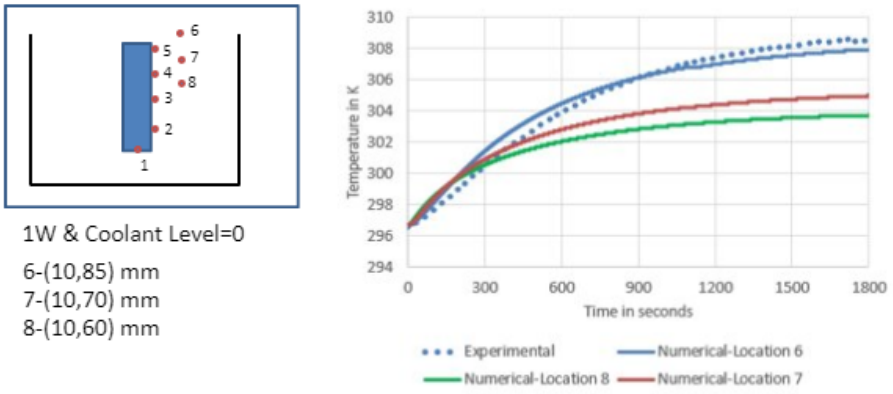

(b)

Figure 5.10. Temperature in fluid domain (a) Three locations in r direction (b) Three locations in z direction .

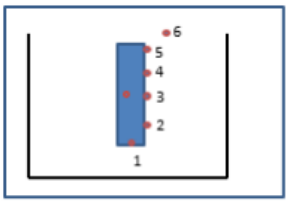

Input

- Temperature at Location 6 – calculated from OpenFoam
- Domain Dimension
- Thermal property (k,Cp,ρ)

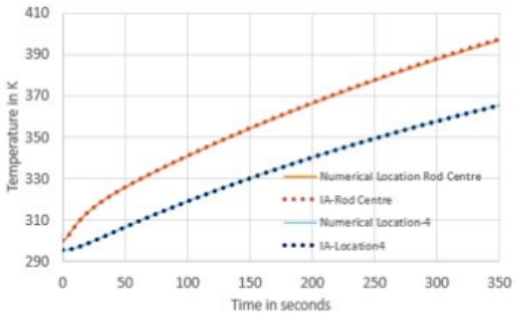

Results

- Predicted(q) = 10880.389 kW/m^3 (Actual q = 10873.259)
- Temperature chart is shown above
- Calculation Time = 40 hours

(a)

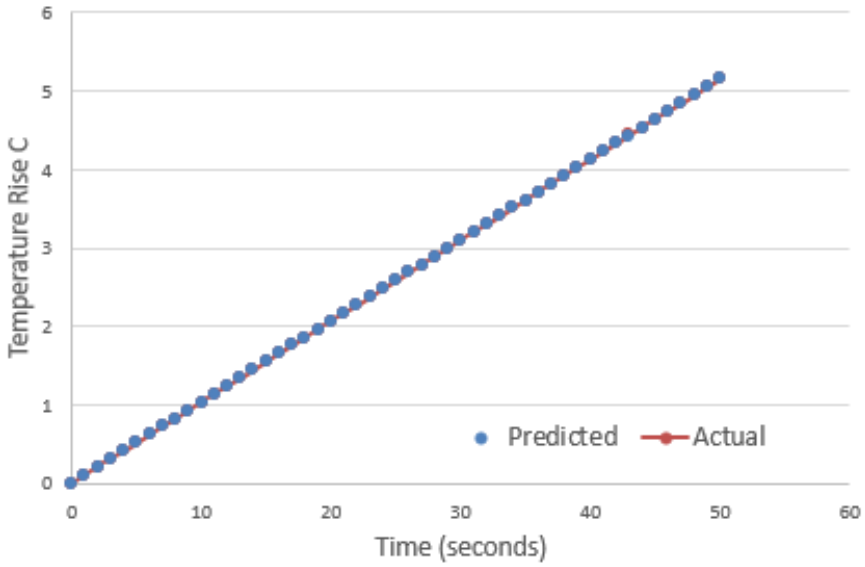

(b)

Figure 5.11. Predicted temperature from inverse analysis (a) Heat generation rate of 5W (b) Heat generation rate of 1W .

5.5 Observation and Limitation

Inverse analysis for determination of spatially varying temperature distribution for partially cooled heat generating cylinder, is developed. This formulation can predict critical temperature of the cylinder. In first method, sensitivity analysis was carried out using complex variable semi-analytical method, while for second method, temperature gradient were used for sensitivity analysis . This procedure is analyzed and validated using simulated measurements. Applicability of this method to realistic scenario with measurement error has been tested by adding noise to input data to inverse formulation. Analysis has been carried out with noise following Gaussian distribution with different standard deviation values. This method predicted accurate temperature and heat generation values in the cylinder even with this added noise (Maximum error of 0.59%). However, this approach of inverse analysis has its own limitation, are depicted below.

- Time required to predict heat generation value is approx 40 hours. It will be really impractical in real-time application where temperature may reach to high value within seconds.
- In present study only axi-symmetric model is considered, which needs lot of computational power.

CHAPTER 6

MACHINE LEARNING

The limitation of inverse analysis by numerical computation has been reported in earlier chapter. Searching optimized value in space, takes a long time for simple problem of two dimensional axi-symmetric model. This problem gets more costlier for three dimensional models. Keeping this in mind, such IA techniques can not be useful for real-time prediction. Machine learning technique is analyzed for predicting causal factor from measured temperature. In this chapter a general overview of machine learning and its application to heat transfer analysis will be discussed.

6.1 Machine Learning

Machine learning is a method of data analysis that automates analytical model building. It is a subset of artificial intelligence based on the idea that machines has ability to learn and adapt through different experience. Machine learning can be defined as a field of computer science that provides computers the ability to learn without being explicitly programmed. The name of machine learning was coined in 1959 by Arthur Samuel. [121].

Machine learning and artificial intelligence began in 1950 when Alan Turing developed 'Turing Test' to determine real intelligence of computer. Arthur Samuel published the first computer learning algorithm in 1952 for checkers game. In 1957, Frank Rosenblatt designed the first neural network to simulate processing of human brain. The nearest neighbor algorithm was developed in 1967 where some basic patterns recognized by computer. In 1990, approach of machine learning changed

from knowledge driven to data driven. Of late big corporation like Google, IBM, Facebook, Amazon, Microsoft have contributed largely towards machine learning. With research in machine learning reaching advanced stages, Elon Musk and Steve Wozniak have signed an open letter describing of danger of autonomous computation.

Machine learning utilizes computational statistics, that focuses on prediction-making. It has strong ties to mathematical optimization, which delivers methods, theory and application domains to the field [122]. Machine learning can be unsupervised and be used to learn and establish baseline behavioral profiles for various entities [123, 124] and then used to find meaningful anomalies [122].

Within the field of data analytic, machine learning is a method used to devise complex models and algorithms that lend themselves to prediction; in commercial use, this is known as predictive analytic. These analytical models allow researchers, data scientists, engineers, and analysts to "produce reliable, repeatable decisions and results" as well as uncover "hidden insights" through learning from historical relationships and trends in the data [125].

6.2 Artificial Neural Network

Artificial neural networks (ANNs), a form of connectionism, are computing systems inspired by the biological neural networks that constitute animal brains. Such systems learn to do tasks by considering examples, generally without task-specific programming. For example,learning might be carried out to identify numbers from images that have been handwritten in image recognization. These systems have found great use in applications that are difficult to express in a traditional computer algorithm using rule-based programming.

An ANN is based on a collection of connected units called artificial neurons. These neurons are analogous to biological neurons in an animal brain. Each con-

nection (synapse) between neurons can transmit a signal to another neuron. The receiving (postsynaptic) neuron can process the signal(s) and then signal downstream neurons connected to it. Neurons may have a state. This is generally represented by real numbers, typically between 0 and 1. As learning proceeds, neurons and synapses may also have a weight that varies, which can increase or decrease the strength of the signal that it sends downstream. Furthermore, if neurons have a threshold that only aggregates the signal above or below that level, then the downstream signal is sent.

Typically, neurons are organized in layers. Different layers may perform different kinds of transformations on their inputs. Signals travel from the first (input), to the last (output) layer, possibly after traversing the layers multiple times. In artificial networks with multiple hidden layers, the initial layers might detect primitives (e.g. cars, bikes, no vehicle etc) and their output is fed forward to deeper layers who perform more abstract generalizations (e.g. cars, bikes) and so on until the final layers perform the complex object recognition (e.g. cars).

The original goal of the neural network approach was to solve problems in the same way that a human brain would. Over time, attention focused on matching specific mental abilities, leading to deviations from biology such as back-propagation, or passing information in the reverse direction and adjusting the network to reflect that information.

Neural networks have been used for numerous applications, including computer vision, speech recognition, machine translation, social network filtering, playing board and video games, medical diagnosis and in many other domain. Neural networks are universal approximates, and it works best if the system you are using them to model has a high tolerance to error. Some of the areas whether they work well are:

- Capturing pattern and discovering irregularities
- Diversified data and large number of variable

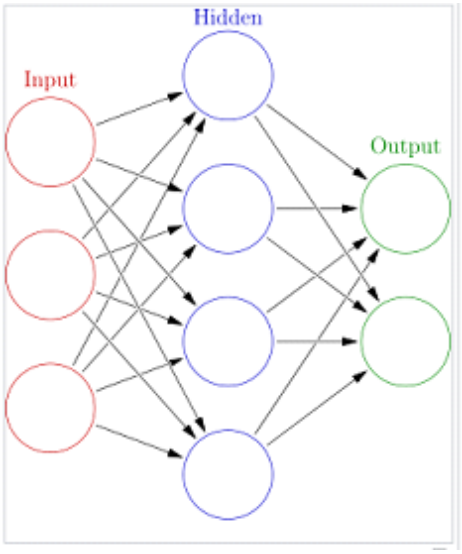

Figure 6.1. Neural network is group of nodes, akin to vast network of neurons in a brain .

- Difficulty in establishing relation between input and output

6.3 Machine Learning for Heat transfer analysis

Many researchers has contributed towards use of machine learning in predicting different variables in heat transfer analysis. L.M.Tam and group [126] have developed heat transfer correlation of transitional flow in a horizontal tube using support vector machines. H.K. Tam and group [127] worked to establish correlation for two phase flow in vertical pipes. Anurag Kumra and team [128] implemented artificial intelligence approach to predict heat transfer rate of wire on tube type heat exchanger. Recently Milani et al has determined tubrbulent diffusivity in film cooling flows through machine learning approach [129]. Zhan and team published in scientifc reports for prediction of thermal boundary resistance by machine learning method [130].

6.4 Training Algorithms

The training of neurons involves updating weight of matrices, and that need to be accurate and fast. For the ANN training, there are several algorithms which could be used viz.

1. Levenberg-Marquardt algorithm
2. Gradient Descent method
3. Bayesian Regularization
4. Scaled Conjugate Gradient method
5. One Step Secant method

There are number of libraries which are used for pattern recognition/ machine learning etc. Most of the popular deep learning libraries have interface for Python, followed by Lua, Java and Matlab. The most popular libraries, to name a few, are Caffe, DeepLearning, TensorFlow, Theano, Torch. For this thesis, Tensorflow will be used for training and learning. Tensorflow is an open source software library for numerical computation. Moreover flexible architecture allows one to deploy computation to one or more CPUs and GPUs in a desktop, server, with a single API. Advantages of Tensorflow are intuitive construct, easy to train on CPU/GPU with distributed computing, flexibility in programming.

6.5 TensorFlow

TensorFlow is open-source software library, which was developed by Google Brain team and released on November 9,2015. It is symbolic math library used for machine learning applications. [7,131,132]. TensorFlow can run on multiple CPUs and GPUS [133].TensorFlow is available on different platforms like 64-bit Linux, macOS,

Windows, Android, IOS. In May 2017, Google announced TensoFlow Lite for Android development [134].

A TensorFlow computation consists of directed graph, which is composed of a set of nodes. The graph represents a dataflow computation, with extensions for allowing some kinds of nodes to maintain and update persistent state and for branching and looping control structures within the graph in a manner similar to Naiad [135]. Computational graph is constructed using one of the supported frontend languages (C++ or Python). An example for construction and execution a TensorFlow graph using the Python front end is shown in Fig. (6.2(a)), and the resulting computation graph in Figure Fig. (6.2(b)).

In a TensorFlow graph, each node has zero or more inputs and zero or more outputs, and represents the instantiation of an operation. Values that flow along normal edges in the graph (from outputs to inputs) are tensors, arbitrary dimensionality arrays where the underlying element type is specified or inferred at graph-construction time. Special edges, called control dependencies, can also exist in the graph: no data flows along such edges, but they indicate that the source node for the control dependence must finish executing before the destination node for the control dependence starts executing. Since TensorFlow model includes mutable state, control dependencies can be used directly to enforce happens before relationships. TensorFlow implementation also sometimes inserts control dependencies to enforce orderings between otherwise independent operations as a way of, for example, controlling the peak memory usage. [7]

An operation has a name, which represents an abstract computation (e.g. add or Matmul-Matrix Multiplication). An operation can have attributes, which need to be provided at the time graph-construction in order to instantiate a node for performing specific operation. One common use of attributes is to make operation polymorphic

```
import tensorflow as tf

b = tf.Variable(tf.zeros([100]))                    # 100-d vector, init to zeroes
W = tf.Variable(tf.random_uniform([784,100],-1,1)) # 784x100 matrix w/rnd vals
x = tf.placeholder(name="x")                        # Placeholder for input
relu = tf.nn.relu(tf.matmul(W, x) + b)              # Relu(Wx+b)
C = [...]                                           # Cost computed as a function
                                                    # of Relu


s = tf.Session()
for step in xrange(0, 10):
  input = ...construct 100-D input array ...        # Create 100-d vector for input
  result = s.run(C, feed_dict={x: input})           # Fetch cost, feeding x=input
  print step, result
```

(a)

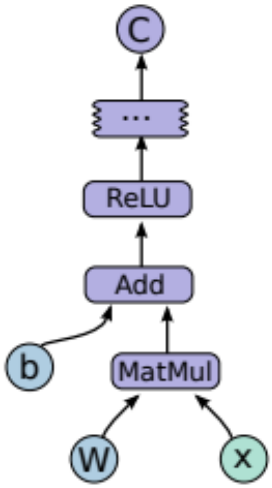

(b)

Figure 6.2. (a) Example TensorFlow Code Snippet (b) Computation Graph [7] .

over different tensor element types. A Kernel is a particular implementation of an operation that can be run on particular type of device (e.g. CPU or GPU). Table 6.1 shows different kind of operations built into TensorFlow Library. [7]

Programs interact with TensorFlow system by creating Session. For creating a computation graph, the Session interface supports an Extend method to augment the current graph managed by the session with additional nodes and edges. The initial graph when a session is created is empty. Run is the other primary operation supported by Session interface, it takes a set of output names ,operational set of

Table 6.1. TensorFlow Operation types [7]

Category	Examples
Mathematical Operations	Add, Sub, Mul, Div, Exp, Log, Greater, Less, Equal,...
Array operation	Concat, Slice, Split, Constant, Rank, Shape, Shuffle,..
Matrix operations	MatMul, MatrixInverse, MatrixDeterminant, ...
Neural-net building blocks	SoftMax, Sigmoid, ReLU, Convolution2D, MaxPool, ...
Checkpointing operations	Save, Restore
Stateful operations	Variable, Assign, AssignAdd, ...

tensors to be fed into graph in place of certain output of nodes. Using the arguments to Run, the TensorFlow implementation can compute the transitive closure of all nodes that must be executed in order to compute the outputs that were requested, and can then arrange to execute the appropriate nodes in an order that respects their dependencies. Most of uses of TensorFlow set up a Session with a graph once, and then execute the full graph or a few distinct subgraphs thousands or millions of times via Run calls.

In most computations a graph is executed multiple times. Most tensors do not survive past a single execution of the graph. However, a Variable is a special kind of operation that returns a handle to a persistent mutable tensor that survives across executions of a graph. Handles to these persistent mutable tensors can be passed to a handful of special operations, such as Assign and AssignAdd (equivalent to +=) that mutate the referenced tensor. For machine learning applications of TensorFlow, the parameters of the model are typically stored in tensors held in variables, and are updated as part of the Run of the training graph for the model.

A tensor in our implementation is a typed, multidimensional array. TensorFlow support a variety of tensor element types, including signed and unsigned integers

ranging in size from 8 bits to 64 bits, IEEE float and double types, a complex number type, and a string type (an arbitrary byte array). Backing store of the appropriate size is managed by an allocator that is specific to the device on which the tensor resides. Tensor backing store buffers are reference counted and are deallocated when no references remain.

The main components in a TensorFlow system are the client, which uses the Session interface to communicate with the master, and one or more worker processes, with each worker process responsible for arbitrating access to one or more computational devices (such as CPU cores or GPU cards) and for executing graph nodes on those devices as instructed by the master.

6.6 ANN Training

Neural network architecture and training is vital in successful temperature prediction on critical location of heat generating cylinder. Training data consist of Input (X) layer and Output (Y) layer. Fig. (6.12) shows fully connected multilayer feed-forward network, where each neuron in one layer is connected to all neurons of subsequent layer. Training is process of finding weights that represents knowledge of system. In other words, it adjusts weight values in order to define relation between input and output data. Learning algorithm is an automatic adaptive method which tried to fit appropriate weights to the neural network system.

The neural network has to be set with data to carry out the learning and testing processes. All models need an input data pattern to be applied in its input neurons in order to learn or test data pattern. The data to be applied to the network must be prepared in a way that the network is able to understand and process it. Typically, each data pattern must be transformed in a vector of values that represent the pattern to be applied. The appropriate transformation of the data in the input

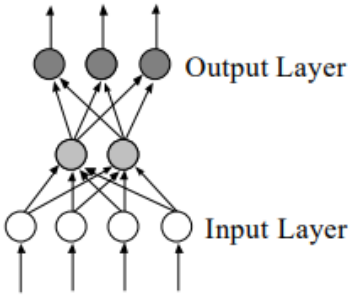

Figure 6.3. Fully Connected Multilayer neural network .

vector is essential to the learning process [136]. Here temperature data at location 6, time and coolant level are used as input data to the neural network, whereas temperature measured/calculated at critical location (Location1, Location4, Cylinder centre location) are used the output of neural network. To make a more robust neural network, Gaussian noise were added to input temperature data. The neural networks that need to have input and output patterns presented during the learning process, the networks based on supervised learning can execute the error correction learning algorithm. The input pattern is applied to the input neurons, then the signal flows over the network producing an output. The produced output is compared with the desired output for the given input pattern. The comparison results in a difference that is used to do the error correction of the network connection weights.

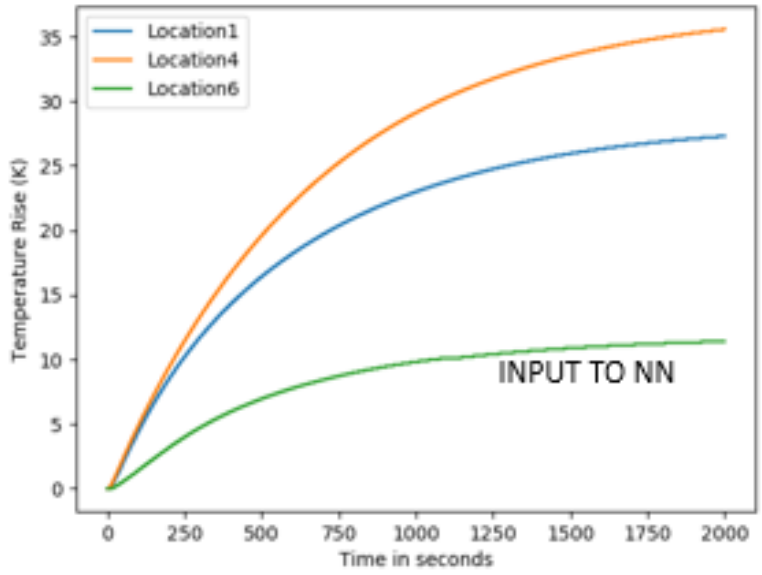

(a)

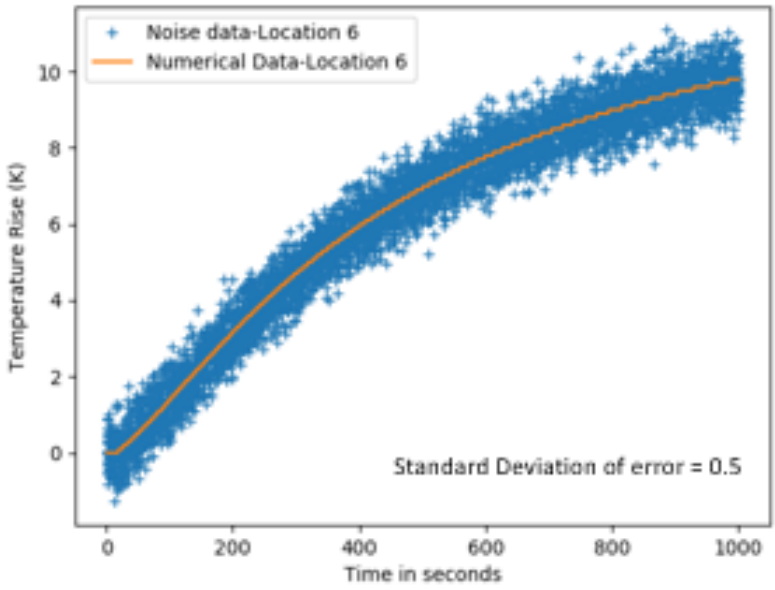

(b)

Figure 6.4. Training data to Neural Network (a) temperature data of 1W showing input and output to neural network (b) Gaussian Noise added to input of neural network .

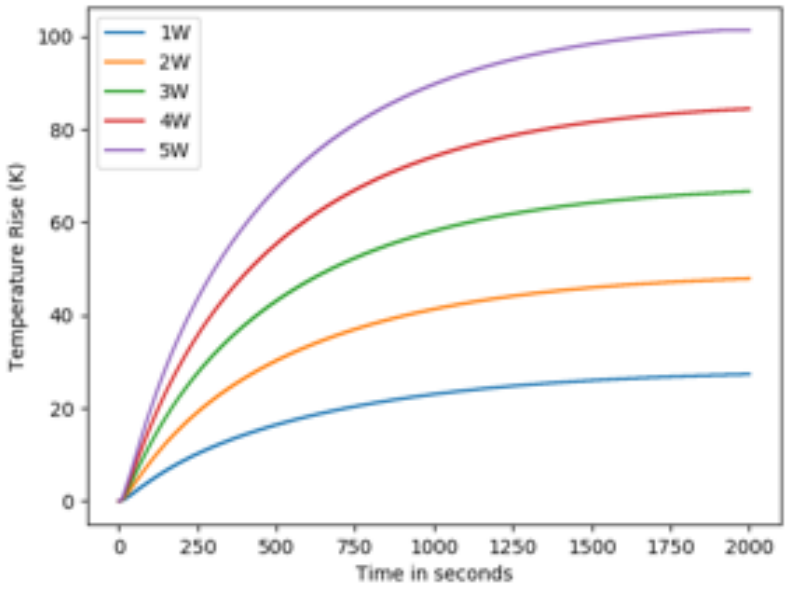

(a)

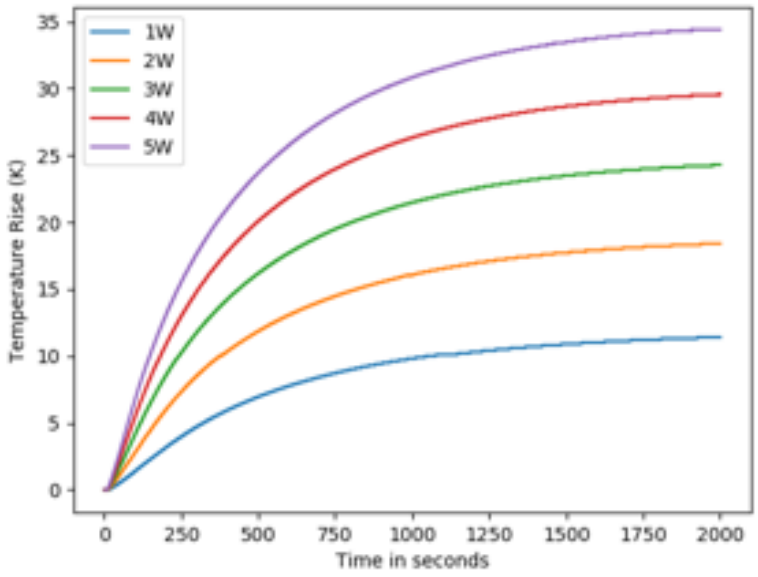

(b)

Figure 6.5. Training data to Neural Network (a) Output data at different power (b) Input data for different power .

6.7 ANN results

Neural Network training with dataset has been carried out using TensorFlow. Function loss was stored at each iteration and plotted in Fig.6.6. It has been observed learning rate of 0.0001 will be advantageous for minimizing the loss.

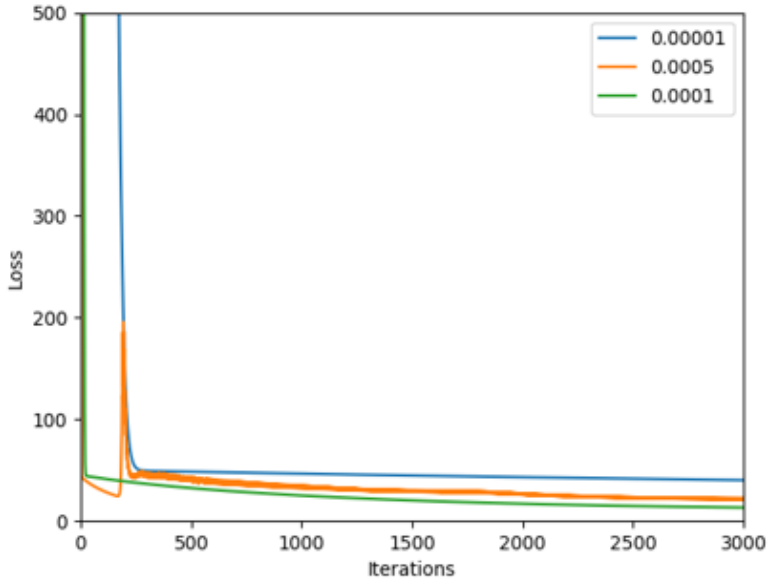

Figure 6.6. Function loss with different learning rate .

After training, neural network was tested for different scenario. Temperature data at location 6 as function of time are provided to neural network for checking its accuracy. Two different scenarios are considered- one with coolant level= 0 and other is at coolant level= 0.45L. Temperature prediction has been carried out for Location1 and Location4. Data obtained from neural network is validated with experimental results.

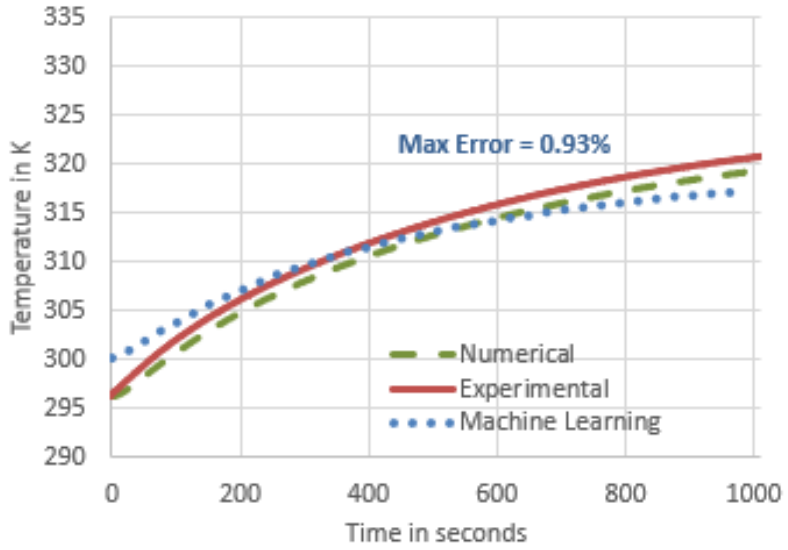

(a)

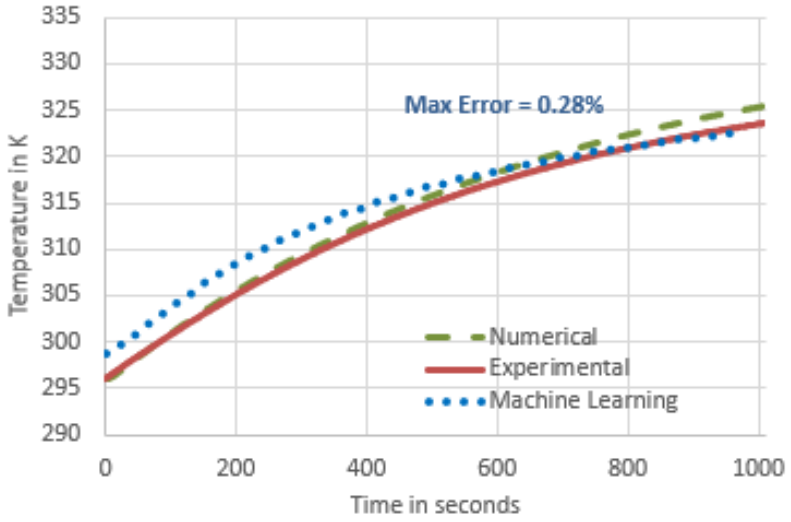

(b)

Figure 6.7. Predicted temperature from Machine learning with heat generation of 1W coolant level=0(a) Location1 (b) Location4 .

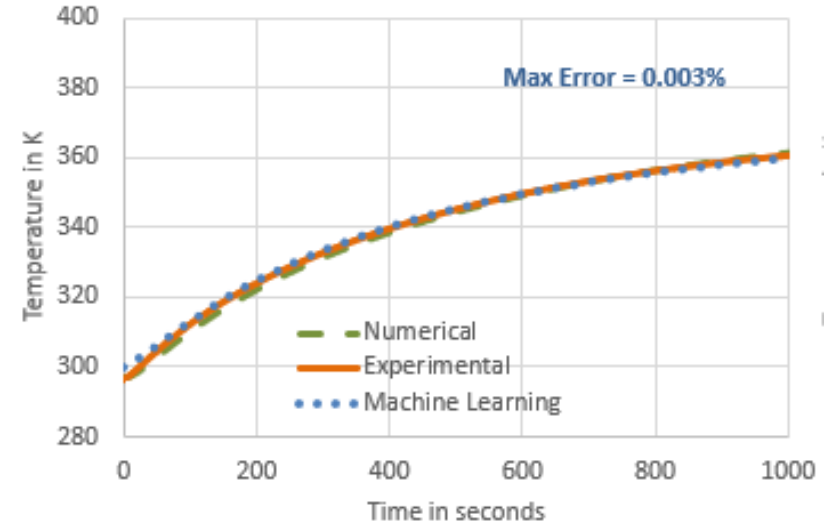

(a)

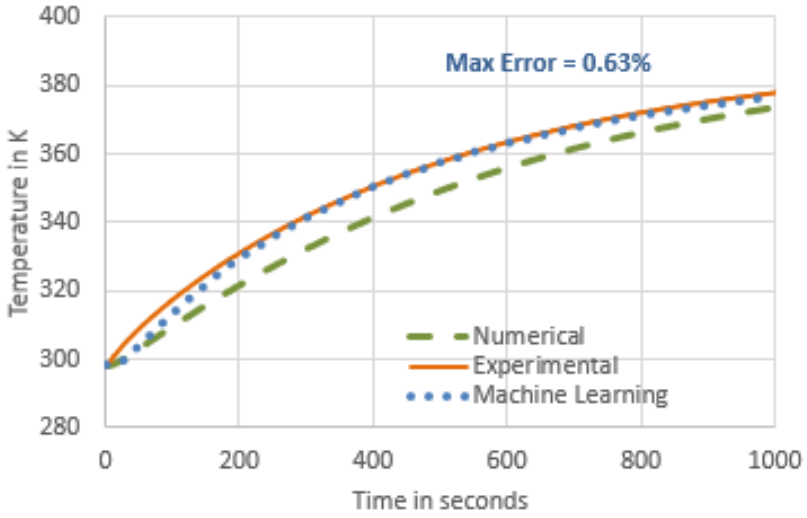

(b)

Figure 6.8. Predicted temperature from Machine learning with heat generation of 3W coolant level=0(a) Location1 (b) Location4 .

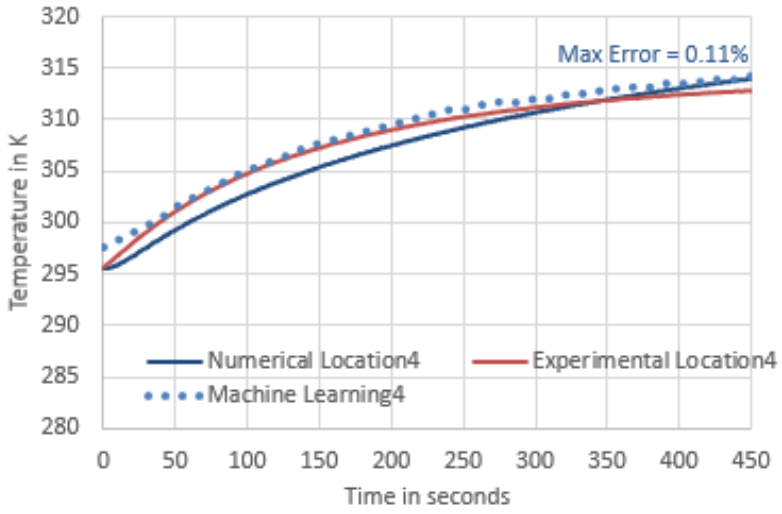

(a)

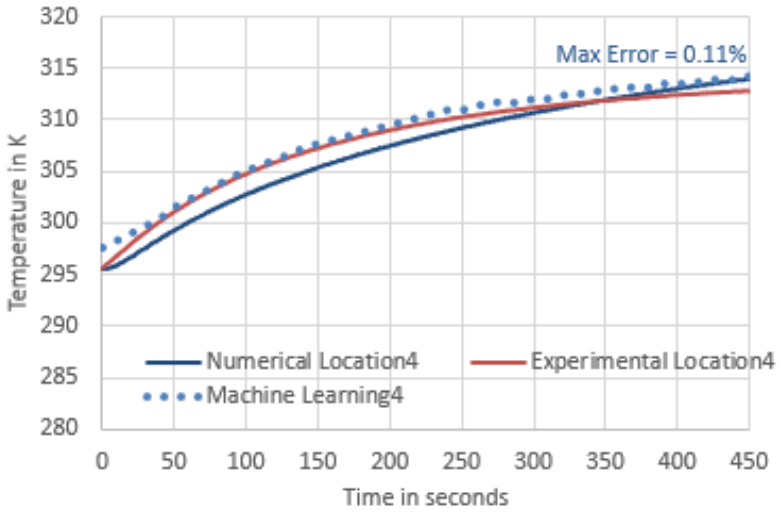

(b)

Figure 6.9. Predicted temperature from Machine learning with heat generation of 3W coolant level= $0.45L$(a) Location1 (b) Location4 .

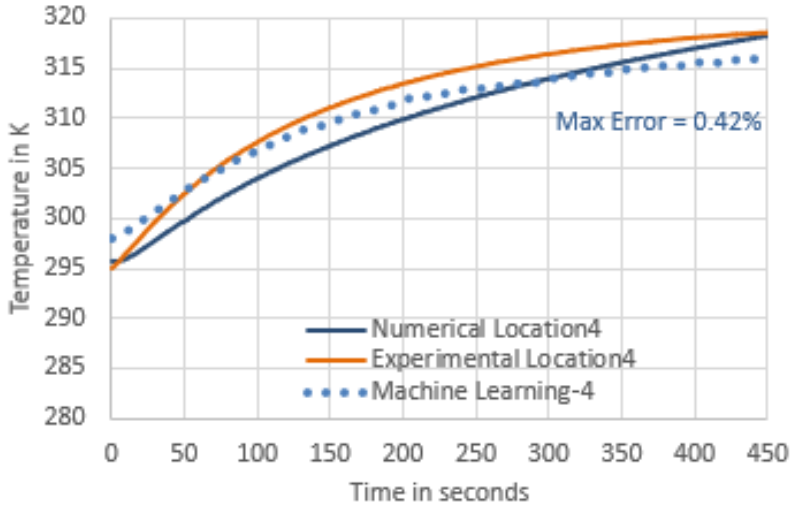

(a)

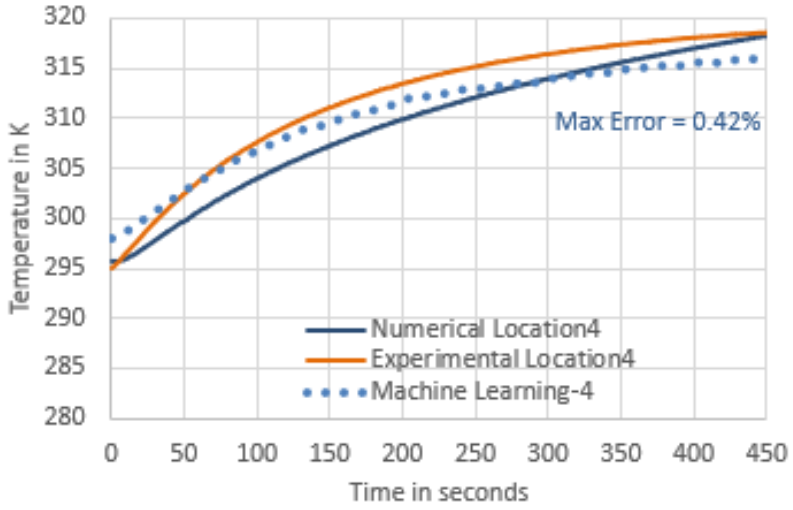

(b)

Figure 6.10. Predicted temperature from Machine learning with heat generation of 4W coolant level= $0.45L$(a) Location1 (b) Location4 .

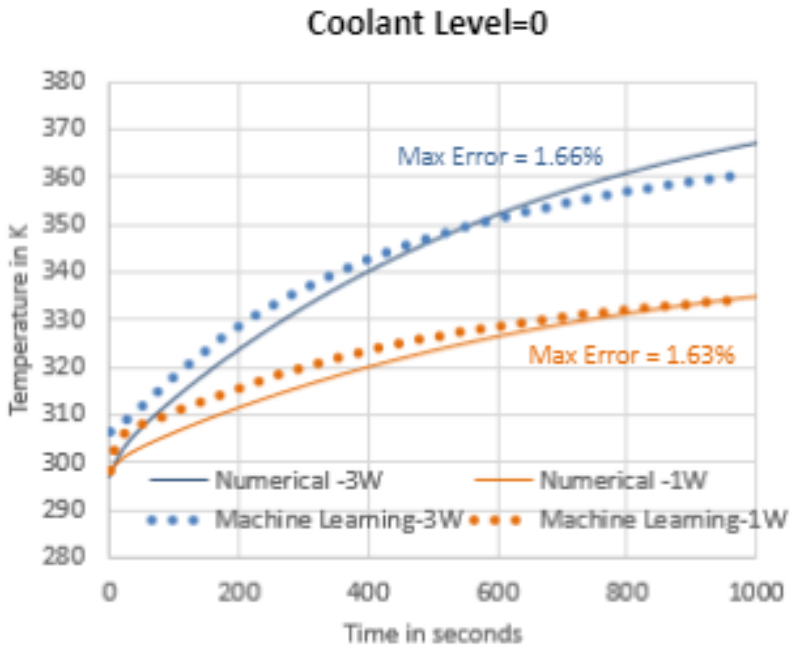

(a)

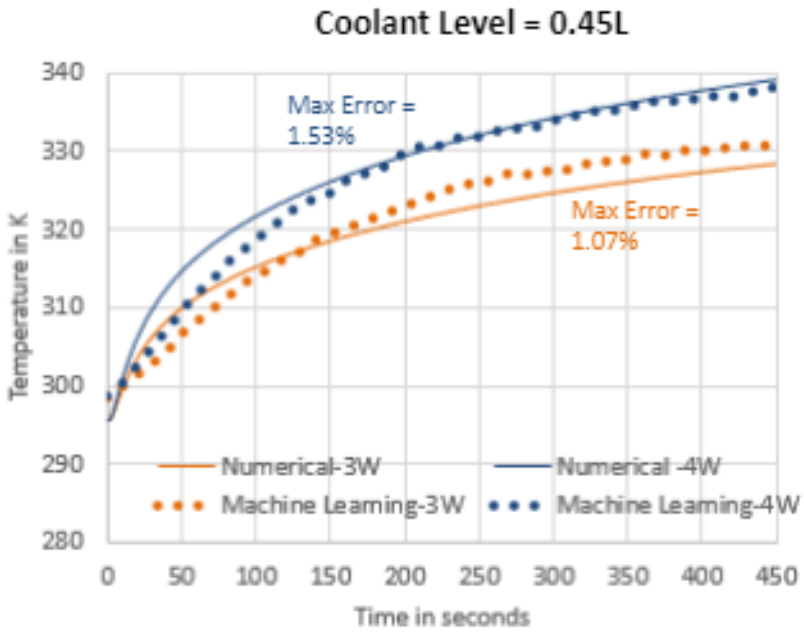

(b)

Figure 6.11. Predicted temperature from Machine learning at center rod (a) Level= $0L$ (b) Level= $0.45L$.

6.8 Augmented Reality

Augmented Reality (AR) is an experience of interacting with real world environment whose different elements are -so called- "'augmented"' by various computer generated perceptual information. This overlaid information can be added to natural environment or masked over natural environment and interwoven seamlessly with physical world as it is perceived as an immersive aspect of real environment.

Augmented reality provides value as it brings digital world components into real world. It doesn't only display data but also provides experience through integration of immersive sensation. The first functional AR systems that provided immersive mixed reality experiences for users were invented in the early 1990s, starting with the Virtual Fixtures system developed at the U.S. Air Force's Armstrong Laboratory in 1992. [137–139]

Augmented reality combines real world content with virtual world. It also provides facility to user to interact with virtual world environment. Milgram and Kishino [8] published reality-virtuality continuum that defines link between real and virtual world.AR is just one possible representation of Mixed Reality (MR), which brings together real and virtual within a single display. AR is mostly grounded in the real world, with a limited set of virtual objects mixed in. The inverse concept, Augmented Virtuality (AV), is conceived as a virtual Environment with some real aspects - a recurring example for AV are video-textured avatars (showing a live video feed of real people) within a Virtual Environment. The boundary between AR and AV is not strictly defined [140]. However, we will use Augmented Reality (AR) in the study.

AR device hardware components are processors, displays,input devices (microphone,touch, gestures), sensors. Modern mobile devices like smartphones/tablet computers contain camera,acceleromenter,GPS,compass which make them suitable

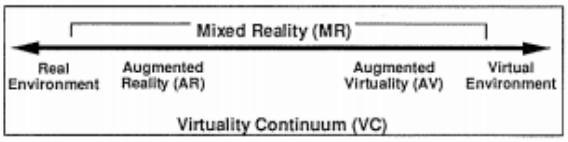

Figure 6.12. Reality-Virtuality Continuum [8].

for AR Environment [141]. A head mounted display (HMD) is a display worn on the forehead,such as helmet. HMDs shows images of both real world and virtual objects in the range of user's field of view. On February 17, 2016, Meta announced the product Meta 2,head-mounted display headset uses a sensory array for hand interactions and positional tracking, visual field view of 90 degrees (diagonal), and resolution display of 2560 x 1440 (20 pixels per degree), which is considered the largest field of view (FOV) [**?**,142–144]. Another well-known head mounted device- Realwear, which is widely used in industry. Their product HMT-1 is completely hands free, voice controlled user interface, allowing workers to operate tools and equipment needed for the field job. This device runs on android 6.0 platform, which makes it useful for deploying custom applications. It is water-proof, dust tight, drop-proof [145]

For current thesis, components of augmented reality were used to display three dimensional model of cartridge heater with real-time temperature data. It provides valuable information to field-workers to understand the system in better way. To build this demonstration, different software with AR devices were tied together. Three dimensional model of catridge heater and experimental setup is prepared using SOLIDWORKS [146]. This model is exported in OBJ format. For setting up AR enviroment in UNITY, VUFORIA sdk libraries were used. [147, 148]. Unity provides integrated development platform for importing and setting up with virtual environment. Three dimensional model of experimental setup, is imported in Unity. Then Vuforia SDK is useful in providing relation between QR code (specifically generated for the exper-

iment) and three dimensional model. It aids in recognizing QR code and overlaying virtual object on top of that. Unity provides support in building this overall code, which can be used for different cross-platform operating systems like android, ios, windows. In addition to AR environment, project was further developed to provide real temperature data. It is achieved through Firebase real-time database - provides client libraries to integrate into different applications [149]. One such database was created and links for the same was integrated inside Unity using C# script. Firebase database is used for displaying ans storing realtime temperature. Temperature data measured at fluid region (Location 6) using Ni DAQ and Labview is parsed inside Python scripts. This data is given as input to trained neural network model. Output of this model is stored on firebase database. Now it can be displayed in AR environment. Fig. 6.13(a), 6.13(b) shows complete architecture and demonstration of AR Field. Following is overview of software utilized to setup augmented reality.

1. C++- Language to setup case in OpenFOAM and getting results
2. OpenFOAM- Carry out Numerical Analysis and get temperature data to train Neural network Model
3. LabView Temperature Measurement while carrying out experiments
4. TensorFlow Trained Neural network model
5. Python Scripting for taking input from LabView and Sending to Firebase Database
6. Firebase- It is real-time database to store and display data.
7. SOLIDWORKS Three Dimensional Model
8. Vuforia Vuforia engine is required to QR Code recognition
9. UNITY Importing three dimensional model , embedding Vuforia Engine, building application cross platform (Android)
10. C# Language is needed to compile and scripting UNITY libraries
11. Android Install built library

12. Java Carry out programming in Android

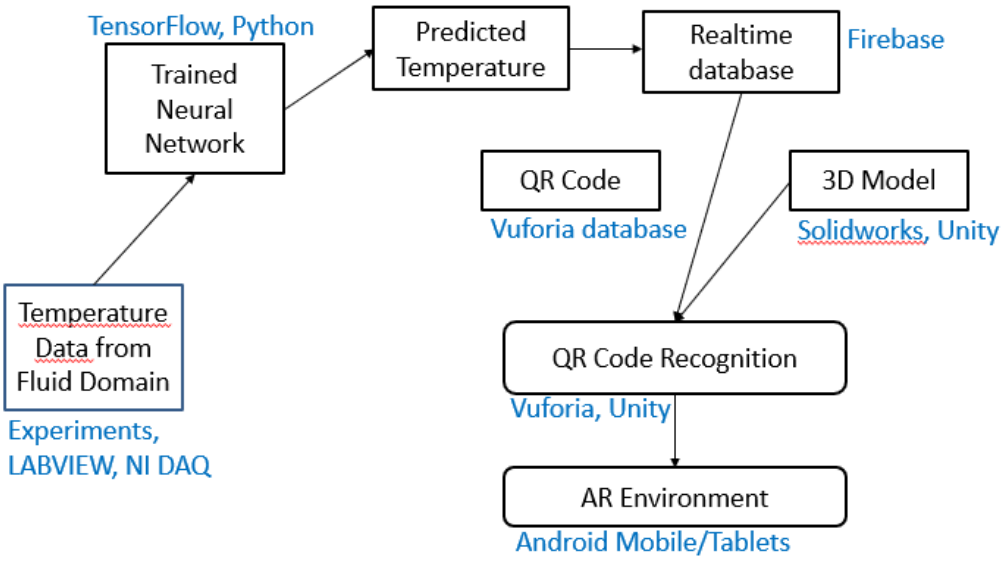

(a)

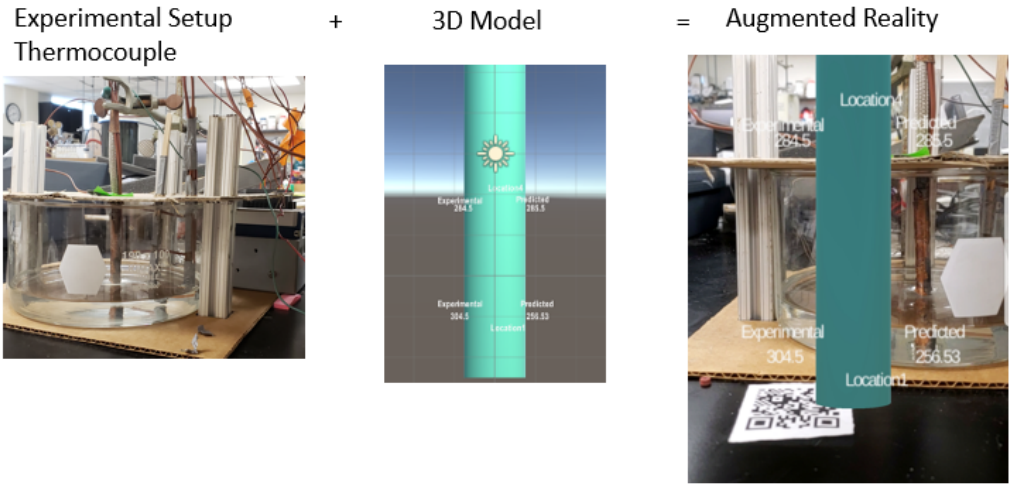

(b)

Figure 6.13. Augmented Reality demonstration on Android mobile phone (a) Software architecture (b) Real-time pictures on Android mobile .

6.9 Chapter Summary

In this chapter, machine learning and neural networks were discussed. Their ability to learn by example makes them very flexible and powerful. Furthermore there is no need to devise an algorithm in order to perform a specific task; i.e. there is no need to understand the internal mechanisms of that task. They are also very well suited for real time systems because of their fast response and computational times. TensorFlow, widely used, open-source was implemented for predicting center-line or surface temperature of the cylindrical body by temperature measurement at fluids. It is observed that neural network model predicts temperature with maximum error of 0.93 % and 1.66% for surface and center-line temperature prediction respectively. After providing input to neural network, it takes 0.098 seconds for prediction. This trained neural network study further extended to augmented reality,where field worker can gauge real time condition and take corrective action through hands-free AR devices.

CHAPTER 7

CONCLUDING REMARKS

7.1 Summary

The objective of this thesis is to utilize inverse techniques for predicting maximum temperature inside a partially cooled heat generating solid rod by measuring temperature at fluid region. The study was motivated in providing thermal safety analysis of spent fuel rods for nuclear power plant and battery management.

Analytical formulation was carried out to study temperature distribution in heat generating rod. This formulation has limitations in handling discontinuous boundary and composite material, was also taking lot of time while computation of simple axi-symmetric model. Hence temperature distribution was analyzed using finite volume numerical method. For robust study, finite volume control method was extended to simulate natural convection for two dimensional axi-symmetric model using OpenFOAM.

While performing inverse analysis techniques, a code was developed using finite volume code and conjugate gradient method. However, such approach takes a large computation time. So, neural network (NN) model was adopted for performing inverse analysis. This model was trained with different simulated data from numerical analysis. Predicted values from NN model was in close agreement to maximum temperature rise in rod. For code validation, experiments were conducted to simulate heat generating rods. This machine learning method was extended to attach augmented reality environment. This facilitates field worker to gauge real time condition and take corrective action.

In addition, a framework was developed for predicting anisotropic properties of material. For this, temperature was measured at different location of surface as input for predicting thermal conductivity of heat generating rod. Results obtained from this analysis was validated with published results. This framework is also utilized for estimating equivalent thermal conductivity of pellets.

7.2 Future work

The analysis proposed in this thesis can be extended to study rod bundles, that represent actual scenario. This method will allow one to predict maximum temperature inside a rod in nuclear plants. Operating data from the plant can be used as basis for training neural network model.

Neural network model with ReLU method is used in this thesis. A much more comprehensive study is needed using different model like Convolution Neural Network (CNN), Support Vector.

The current study uses temperature data of one location as input to NN model. However, NN model should be trained with various locations. This will be advantageous for power plants, where temperature measured at any location can be used as input data to predict maximum temperature inside the system.

Augmented reality shows how technology can be employed to aid field worker. Current scenario, real time interaction of worker is not deployed in software. For future project, this can be extended through developing advanced software techniques.

In the current research, boiling phenomena is not considered during numerical analysis and coolant level is used as input data to neural network model. In future work, boiling can be introduced in the numerical study to predict critical coolant level inside plant.

Moreover, in this thesis coolant level is assumed as constant for study. Considering real-time scenario, where the level changes , will require the code modification. This will allow incorporating changing level at certain rate and predicting critical temperature inside heat generating body.

APPENDIX A

Appnedix A-Thermal Conductivity Prediction of pellets

In this appendix section, numerical inverse analysis is used to predict thermal properties of porous material by measuring temperature at surface. Accuracy and efficiency of the method is enhanced by using accurate sensitivity information by use of Semi-Analytical Complex Variable Method(CVSAM). Steady state heat transfer analysis with an axi-symmetric model was carried out using finite volume method. Temperature obtained from this analysis, is used as input for the inverse method. Objective function for the optimization is difference between computed and measured temperature. This function was minimized with Conjugate Gradient Method (CGM). Coefficients obtained from CVSAM were used in gradient based optimization method. The robustness of developed approach was evaluated by adding Gaussian noise these temperature values. This work is extension of earlier work carried out, where results were validated with published results [150].

A.1 Experimentation [151, 152]

In order to obtain the proper boundary conditions for the Inverse Analysis method, a series of experiments were carried out in a closed plastic 2x1x1 ft. plastic box to allow natural convection. In this box a copper tube of length 0.1905 m, 0.0148 m outer radius, and a wall thickness of 0.0008 m was placed in a horizontal configuration. Inside this tube, a Tutco 750 W electrical cartridge heater with diameter of 0.0128 m was placed in the center. In order to ensure that the heater was centered inside the copper tube, special fixtures were manufactured, this will create an annular gap where the porous media will be placed. The top and bottom of the copper tube are insulated with Asbestos to force radial heat transfer [151].

A set of K-type thermocouples are placed at the surfaces of the cartridge heater and another set was placed in copper tube surface. The sensors output was measured by National Instruments NI-9211-channel thermocouple input module which

was placed inside a NI-cDAQ 9174 4-slot USB. The channels were configured to write data in the micro voltage range. This equipment was used alongside with a NI LabVIEW for data acquisition from the thermocouple readings, program can be seen in Fig A.1.

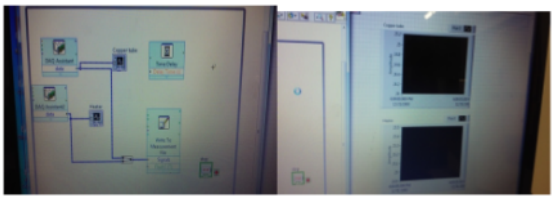

Figure A.1. LabView Program.

Temperature measurements were taken at every second until steady state heat transfer was reached, these measurements were taken at four equidistant points on the surface of the cartridge heater as well as on the copper tube surface. In Fig. A.2 the copper tube and the thermocouples can be seen.

The Tutco cartridge heater was calibrated using a calorimeter as seen on Fig A.3. The heater was outputting the same power as it was supplied, so it was properly set to be used in the experiments. The power to the heater in the experiments was supplied by using a BK Precision, Model VSP12010 programmable PFC DC 120V/10A power supply, shown in Fig A.4.

In order to verify the voltage and the current that was supplied to the experiment, an Extech instruments, model EX330 multimeter was connected in series to measure the current, a Fluke 287 True-RMS multimeter was connected in parallel to measure the voltage. The power supplied to the heater were 1W, 2W and 3W, in order to determine if there is a difference in the conductivities. A K-type thermocouple measures the ambient temperature inside the box at each experiment run.

Figure A.2. Experimental setup.

Table A.1. Different material were used to obtain equivalent thermal conductivity

Number	Material	Dimensions	Type
1	Glass	3 mm diameter	bead
2	Silica Catalyst	2 mm dia and 3 mm long	cylinder
3	Aluminium unpolished	1/4 inch	pellet
4	Aluminium polished finish	3/8 inch	pellet
5	Aluminium unpolished	3/8 inch	pellet

Figure A.3. Catridge heater calibration.

Figure A.4. Power supply.

A.2 Results and discussions

Results obtained from inverse heat transfer analysis code are presented in this table. It is observed that thermal conductivity increases with power supplied to the system.

Table A.2. Mean thermal conductivity at 1 W

Number	K_m (W/mK)	ϵ
1	0.0877	0.5
2	0.0357	0.4968
3	0.1103	0.4057
4	0.1418	0.3868
5	0.1000	0.4528

Table A.3. Mean thermal conductivity at 2 W

Number	K_m(W/mK)	ϵ
1	0.1018	0.5
2	0.0420	0.4968
3	0.1330	0.4057
4	0.1600	0.3868
5	0.1290	0.4528

Table A.4. Mean thermal conductivity at 3 W

Number	K_m (W/mK)	ϵ
1	0.1020	0.5
2	0.0430	0.4968
3	0.1390	0.4057
4	0.1660	0.3868
5	0.1340	0.4528

APPENDIX B

Appendix B- Axi-symmetric Governing Equation

Axi-symmetric Navier Stokes Equation are explained here.

$$\frac{\partial(U)}{\partial t} + \frac{\partial A}{\partial z} + \frac{\partial B}{\partial r} + \frac{C}{r} = 0 \tag{B.1}$$

Where,

$$U = \begin{bmatrix} \rho \\ \rho\ u_z \\ \rho\ u_r \\ \rho\ E \end{bmatrix} \tag{B.2}$$

$$A = \begin{bmatrix} \rho\ u_z \\ \rho\ u_z\ u_z + p - \tau_{zz} \\ \rho\ u_r\ u_r - \tau_{rz} \\ \rho\ u_z\ H + q_z - u_z\ \tau_{zz} - u_r\ \tau_{rz} \end{bmatrix} \tag{B.3}$$

$$B = \begin{bmatrix} \rho\ u_r \\ \rho\ u_r\ u_z + p - \tau_{rz} \\ \rho\ u_r\ u_r - \tau_{rr} \\ \rho\ u_r\ H + q_r - u_z\ \tau_{rz} - u_r\ \tau_{rr} \end{bmatrix} \tag{B.4}$$

$$C = \begin{bmatrix} \rho\ u_r \\ \rho\ u_z\ u_r + p - \tau_{rz} \\ \rho\ u_r\ u_r - \tau_{rr} \\ \rho\ u_r\ H + q_r - u_z\ \tau_{rz} - u_r\ \tau_{rr} \end{bmatrix} \tag{B.5}$$

$$\tau_{zz} = \frac{2\ \mu}{3Re}\ \left[\frac{2\ \partial u_z}{\partial z} - \frac{\partial u_r}{\partial r} - \frac{u_r}{r}\right] \tag{B.6}$$

$$\tau_{rr} = \frac{2\ \mu}{3Re}\ \left[\frac{-\partial u_z}{\partial z} + 2\frac{\partial u_r}{\partial r} - \frac{u_r}{r}\right] \tag{B.7}$$

$$\tau_{rz} = \frac{\mu}{3Re}\ \left[\frac{\partial u_z}{\partial r} + 2\frac{\partial u_r}{\partial z}\right] \tag{B.8}$$

$$q_z = \frac{-\mu}{P_r(\gamma-1)M^2\ Re}\ \frac{\partial T}{\partial z} \tag{B.9}$$

$$q_r = \frac{-\mu}{P_r(\gamma-1)M^2\ Re}\ \frac{\partial T}{\partial r} \tag{B.10}$$

APPENDIX C

Appendix C- Finite Volume Method

A finite volume code was developed in MATLAB in order to get the temperature distribution in the cylinder with internal heat generation subjected to given boundary conditions. The governing equation given in Eqn.(5.14) was solved using finite volume discretization. The cylinder is discretized by a Cartesian grid of finite volumes. The heat conduction operator is defined as

$$L_e(T) = \frac{1}{r}\frac{\partial T}{\partial r}\left(k_r \frac{\partial T}{\partial r}\right) + \frac{\partial T}{\partial z}\left(k_z \frac{\partial T}{\partial z}\right) \tag{C.1}$$

The finite volume formulation is obtained from the following expression

$$\begin{aligned} L_e(T) &= \frac{1}{r_c h_i h_j}\int\int (krT_r)_r + (krT_z)_z dr dz \\ &= \frac{1}{r_c h_i h_j}\int krT.nd\Gamma \end{aligned} \tag{C.2}$$

where r_c is the value of r-coordinate at the cell center, h is grid spacing,n is the normal vector to the boundary of the cell and the subscript indicates the differential with respect to the sub-scripted variable.

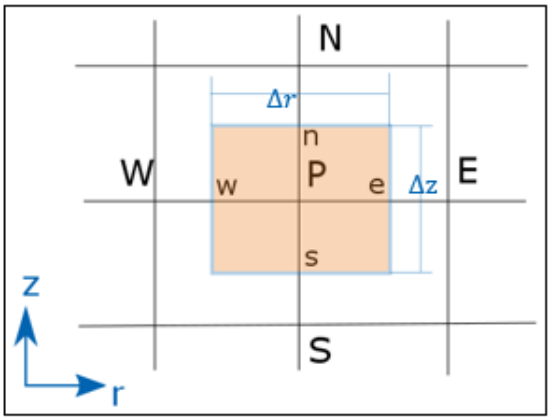

Figure C.1. Schematic control volume (not to scale) [9].

The discrete form of the above expression by using central differencing at cell i is given by

$$L_{e,h,i}(T) = \frac{1}{r_c h_i h_j} \left(\sum_{d=1}^{2} \; F^d_{i+\frac{1}{2}e_d} - F^d_{i+\frac{1}{2}e_d} + F^B_i \right) \tag{C.3}$$

Where fluxes are given by

$$F^1_{i\pm\frac{1}{2},j} = k_{i\pm\frac{1}{2},j} r_{i\pm\frac{1}{2},j} \left(\mp T_{i,j} \pm T_{i\pm1,j} \right) h_j / h_i \tag{C.4}$$

$$F^2_{i,j\pm\frac{1}{2}} = k_{i,j\pm\frac{1}{2}} r_{i,j} \left(\mp T_{i,j} \pm T_{i,j\pm1} \right) h_i / h_j \tag{C.5}$$

The boundary flux is given by $F^B_i \; = \; r_B k_B \left(\frac{\partial T}{\partial n} _B \right) h_j$ which is obtained through boundary conditions.

The time discretization is done using the first order backward Euler scheme. The governing equation can be cast in the form.

$$T^{n+1}_i = \frac{\delta t}{(\rho C)_i} \; L_{e,h,i} \left(T^{n+1} \right) \; + \; S \tag{C.6}$$

where $S = \frac{\delta t Q_i}{(\rho C)_i} + T^n_i$

APPENDIX D

Appnedix D-Video

Video is attached herewith. In this video, experiment has been carried out and temperature at location 1 and location 4 has been measured experimentally as well as through machine learning. It can be seen that whenever mobile camera point towards specific QR code, current temperature value and schematic representation of rod appears. Predicted temperature is calculated using machine learning and temperature at location 6 (fluid temperature around heat generating rod). Predicted values shows good agreement with experimental data.

Link for video - `https://youtu.be/cl_tiWSN68M`

REFERENCES

[1] H. Orlande, O. Fudyam, and R. Mailet, D.and Cotta, *Thermal Measurements and Inverse Techniques*, 2011.

[2] G. Dulikravich and I. Egorov, "Identification of the temperature profile in an absorbing, Emitting and isotropically scattering medium by Inverse analysis," *Computational Methods for Applied Inverse Problems*, pp. 197–220, 2012.

[3] M. Thurber, "Cargo Carriage of Lithium Batteries Suspected in Some Accidents," *AIN online*, 2012. [Online]. Available: https://www.ainonline.com/aviation-news/aviation-international-news/2012-02-01/cargo-carriage-lithium-batteries-suspected-some-accidents

[4] F. Lambert, "Tesla Model S battery caught on fire without accident, says owner Tesla is investigating," *electrek*, 2018. [Online]. Available: https://electrek.co/2018/06/16/tesla-model-s-battery-fire-investigating/

[5] Q. wang, B. Jang, B. Li, and Y. Yan, "A critical review of thermal management models and solutions of lithium-ion batteries for the development of pure electric vehicles," *JRenewable and Sustainable Energy Reviews Volume 64, October 2016, Pages 106-128*, 2016.

[6] O. Foundation, " Openfoam userguide," *Openfoam Org*, 2015.

[7] J. Dean and R. Monga, "TensorFlow Large scale machine learning on heterogeneous distributed systems ," 2015.

[8] P. Milgram and F. Kishino, " A Taxonomy of Mixed reality Visual Displays ," 1994.

[9] S. Patankar, *Numerical Heat transfer and fluid flow Taylor and Franscis journal*, 1970.

[10] V. Ambartsumian, "Theorem that among all strings, the homogeneous string is uniquely determined by the set of its oscillation frequencies," *Zeitschrift fr Physik*, 1929.

[11] R. Ambartsumian, "A life in astrophycis. Selected papers of Viktor A. Ambartsumian," *Astrophysics*, vol. 41, pp. 328–330, 1998.

[12] G. Borg, "A reversal of Storm-Liouville's self-esteem," *Acta Mathematica*, vol. 78, pp. 1–96, 1946.

[13] I. Frank, "An application of least squares Method to the solution of Inverse problem of Heat conduction," *Journal of Heat Transfer*, vol. 85, pp. 378–379, 1963.

[14] A. Tikonov, "Solution of Incorrectly Formulated Problems and the Regularization Method," *Soviet Mathematics Doklady,*, vol. 4(4), pp. 1035–38, 1963.

[15] ——, "Regularization of Incorrectly posed problems," *Soviet Mathematics Doklady,*, vol. 4(6), pp. 1624–27, 1963.

[16] D. Specht, "Probablistic Neural Networks," *Neural Networks*, vol. 3, pp. 109–118, 1990.

[17] K. Deb, A. Pratap, S. Agarwal, and M. T., "A fast and elitist multiobjective genetic algorithm: NSGA-II," *IEEE transactions on evolutionary computation*, vol. 6, pp. 182–197, 2002.

[18] W. Giedt, "The Determination of Transient Temperatures and Heat Transfer at a Gas-Metal Interface Applied to a 40-mm Gun Barrel," *Journal of Jet Propulsion*, vol. 4, pp. 158–162, 1955.

[19] G. Stolz, "Numerical Solutions to an Inverse Problem of Heat Conduction for Simple Shapes," *Journal of Heat Transfer*, vol. 82(1), pp. 20–25, 1960.

[20] S. Arridge, "Optical tomography in medical imaging," *Inverse Problems*, vol. 15, pp. 41–93, 1999.

[21] Y. Li and M. Ozisik, "Identification of the temperature profile in an absorbing, Emitting and isotropically scattering medium by Inverse analysis," *Journal of Heat Transfer*, vol. 118, pp. 1060–1063, 1992.

[22] M. Larsen, "An Inverse Problem: Heat Flux and Temperature Prediction for a High Heat Flux Measurement," *Technical Report, SAND-85-2671*, 1985.

[23] E. Hensel and R. Hills, "Kinematic design of a double wishbone type front suspension mechanism using multi-objective optimization," *Numerical Heat Transfer*, vol. 15, pp. 227–240, 1989.

[24] B. Dennis and G. Dulikravich, "Simultaneous Determination of Temperatures, Heat Fluxes, Deformations adn Tranctions on Inaccesible Boundaries," *ASME Journal of Heat transfer*, vol. 121, pp. 537–545, 1999.

[25] T. Matin and G. Dulikravich, "Invese Determination of Boundary conditions in steady state Heat conduction," *ASME Journal of Heat Transfer*, vol. 3, pp. 546–554, 1999.

[26] B. Dennis, G. Dulikravich, and S. Yoshimura, "A Finite Element formulation for the determination of unknown boundary conditions for three-dimensional steady thermoelastic problems," *Transactions of ASME*, vol. 35, pp. 319–360, 2004.

[27] W. Jin and B. Dennis, "Application of the complex variable semi-analytic method to inverse determination of unknown material properties," *Proceedings of the ASME 2011 international Design Engineering Technical Conferences and Computers and Information in Engineering Conference IDETC/CIE 2011*, vol. 44, pp. 913–920, 2011.

[28] S. Corporation, "Lithium Ion Rechargeable Batteries Technical Handbook," *Technical Handbook*, 2010. [Online]. Available: https://www.4project.co.il/documents/doc_286_2661.pdf

[29] M. Lowe, S. Tokuoka, T. Trigg, and G. Gereffi, "Lithium-ion batteries for electric vehicles: the US value chain," *Centre on Globalization*, 2010.

[30] V. Ruiz, A. Pfrang, A. Kriston, N. Omar, P. Van den Vossache, and L. Boon-Brett, "A review of international abuse testing standards and regulations for lithium ion batteries in electric and hybrid electric vehicles," *Renewable and Sustainable Energy Reviews*, 2018.

[31] R. Spotnitz, J. Weaver, Y. G., D. Doughty, and E. Roth, "Simulation of Abuse Tolerance of Lithium-ion Battery Packs," *Journal of Power Sources*, 2007.

[32] B. Mandal, A. Padhi, Z. Shi, S. Chakraborty, and R. Filler, " Thermal runaway inhibitors for lithium battery electrolytes," *Journal of Power Sources*, 2006.

[33] A. Hammami, N. Raymond, and M. Armand, "Lithium-ion batteries: runaway risk of forming toxic compounds," *Nature*, 2003.

[34] Q. wang, P. Ping, X. Zhao, G. Chu, J. Sun, and C. Chen, "Thermal runaway caused fire and explosion of lithium ion battery," *Journal of Power Sources*, 2012.

[35] X. Feng, M. Ouyang, X. Liu, L. Lu, Y. Xia, and X. He, "Thermal runaway mechanism of lithium ion battery for electric vehicles: A review," *Energy Storage Materials*, 2018.

[36] B. Smith, "Chevrolet volt battery incident overview report,1 ," *U.S. Department of Transportation National Highway Traffic Safety Administration*, 2012.

[37] NTSB, "Aircraft incident report: auxiliary power unit battery fire, Japan airlines Boeing 787, JA 829 J, Boston, Massachusetts, January 7, 2013. ," *National*

Transportation Safety Board, DC, Rep. No. PB2014-108867, Nov. 21, 2014., 2014.

[38] IAEA, *International fact finding expert mission of the Fukushima Dai-ichi NPP accident following the greateast japan earthquake and tsunami*, 2012, /http://www-pub.iaea.org/MTCD/meetings/PDFplus/2011/cn200/documentation/cn200_Final-Fukushima-Mission_Report.pdf.

[39] N. I. S. Agency, *Report of Japanese Government IAEA Ministerial Conference on Nuclear Safety: The Accidental TEPCO's Fukushima Power stations,*, 2011.

[40] TEPCO, *Nuclear Accident Analysis Report (Interim Report)The Tokyo Electric Power Company,Inc*, 2011.

[41] SUZUKI, *Nuclear energy policy in Japan after the 3/11 Fukushima nuclear accident*, 2011.

[42] J. Rees, "Hostages of each other: the transformation of nuclear safety since Three MileIsland,UniversityofChicagoPress,Illinois," *University of Chicago Press, Illinois*, 1996.

[43] R. J, "Lessons from Chernobyl: the event the aftermath Fallout: radio-active, political, social. Thyroid," pp. 189–192, 1997.

[44] R. A. Meserve, "The global nuclear safety regime," pp. 100–111, 2009.

[45] D. Clery, "Current designs address safety problems in Fukushima reactors," *Science 2011*, pp. 100–111, 2011.

[46] D. Normile, "Is Nuclear power good for you?" *Science*, pp. 395–96, 2012.

[47] T. Hoeve and J. Mark, " Worldwide health effects of the Fukushima Daiichi nuclear accident," *Energy and environmental Science*, pp. 1–15, 2012.

[48] A. Brady and E. B., "An Investigation of the Miyagi-ken-oki, Japan, earthquake of June 12, 1978," *United States Department of Commerce, National Bureau of Standards*, 1980.

[49] ICJT, "Fukushima Daichi Information Screen," *ICJT.org*, 2011.

[50] TEPCO, "The record of the earthquake intensity observed at Fukushima Daiichi Nuclear Power Station and Fukushima Daini Nuclear Power Station (Interim Report)," *TEPCO Press Release*, 2014.

[51] wnn, " Fukushima faced 14-metre tsunami," *World Nuclear News*, 2011.

[52] R. Black, "Reactor breach worsens prospects," *BBC Online*, 2011.

[53] Archive, "Japnese Earthquake Update," *IAEA Press release*, 2011.

[54] ——, "Fukushima Accident Progression," *Fukushima Areva*, 2011.

[55] P. Lipscy, K. Kushida, and T. Incerti, "Fukushima Disaster and Japans Nuclear Plant Vulnerability in Comparative Perspective," *Environmental Science and Technology*, pp. 6082–6088, 2013.

[56] W. Maschek, A. Rineiski, M. Flad, V. Kriventsev, F. Gabrielli, and M. K., "Recriticality, a Key Phenomenon to Investigate in Core Disruptive Accident Scenarios of Current and Future Fast Reactor Designs," *IAEA Press release*, 2011.

[57] E. Strickland, "24 Hours at Fukushima A blow-by-blow account of the worst nuclear accident since Chernobyl," *IEEE Spetrum*, 2011.

[58] Archive, "Timeline for the Fukushima Daiichi nuclear power plant accident," *Nuclear Energy Agency*, 2011.

[59] ——, "Hydrogen explosions Fukushima nuclear plant: what happened?" *Hyer Members*, 2011.

[60] R. Spotnitz and J. Franklin, "Abuse behavior of high-power, lithium-ion cells," *Journal of Power Sources*, 2003.

[61] Q. wang and J. Ping, P.and Sun, "Catastrophe analysis of cylindrical lithium ion battery," *Nonlinear Dynamics*, 2010.

[62] K. Kumaresan, G. Sikha, and R. White, "Thermal Model for a Li-Ion Cell," *Journal of the Electrochemical Society*, 2008.

[63] Q. wang, J. Sun, and G. Chu, "Lithium ion battery fire and explosion," *Proceedings of the Eighth International Symposium International Association for Fire Safety Science, Beijing*, 2005.

[64] G. Kim, P. Peasaran, and R. Spotnitz, "A three-dimensional thermal abuse model for lithium-ion cells," *Journal of Power Sources*, 2007.

[65] D. Bernardi, E. Pawlikowski, and J. Newman, "A general energy balance for battery systems," *Journal of Electrochemical society*, vol. 132, pp. 5–12, 1985.

[66] M. Doyle, J. Fuller, and J. Newman, "Modeling of galvanostatic charge and discharge of the lithium/polymer/insertion cellA general energy balance for battery systems," *Journal of Electrochemical society*, vol. 140, pp. 1526–1533, 1993.

[67] K. Thomas and J. Newman, "Thermal modeling of porous insertion electrodes," *Journal of Electrochemical society*, vol. 150, pp. A176–A192, 2003.

[68] W. Tiedemann and J. Newman, "Porous-elecrode theory with battery applications," *AIChE Journal*, vol. 21, pp. 25–41, 1975.

[69] X. Lin, H. Perez, S. Mohan, J. Siegel, A. Stefanopoulou, Y. Ding, and M. Castanier, "A lumped-parameter electro-thermal model for cylindrical batteries," *Journal of Power Sources*, vol. 257, pp. 1–11, 2014.

[70] Y. Ye, S. Shi, and A. Tay, "Electro-thermal cycle life model for lithium iron phosphate battery," *Journal of Power Sources*, vol. 217, pp. 509–518, 2012.

[71] A. Fotouhi, D. Duger, K. Propp, S. Longo, and M. Wild, "A review on electric vehicle battery modelling: from Lithium-ion toward LithiumSulphur," *Renewable Sustainable Energy*, vol. 56, pp. 1008–1021, 2016.

[72] Y. Ye, S. Shi, and A. Tay, "An electro-thermal model and its application on a spiral-wound lithium ion battery with porous current collectors," *Electrochemica Acta*, vol. 121, pp. 143–153, 2014.

[73] D. Jeon and S. Baek, "Thermal modeling of cylindrical lithium ion battery during discharge cycle," *Energy Conversion Management*, vol. 52, pp. 2973–2981, 2011.

[74] L. Saw, K. Somasundarama, and A. Tay, "Electro-thermal analysis of Lithium Iron Phosphate battery for electric vehicles," *Journal of Power sources*, vol. 249, pp. 231–238, 2014.

[75] S. V. and C. Wang, "Analysis of electrochemical and thermal behavior of Li-Ion cells," *Journal of Electrochemical Society*, vol. 150, pp. A98–A106, 2003.

[76] K. Kumaresan, G. Sikha, and R. White, "Thermal model for a Li-Ion cell," *Journal of Electrochemical Society*, vol. 155, pp. A164–A171, 2008.

[77] X. Zhang, "Thermal analysis of a cylindrical lithium-ion battery," *Electrochimica Acta*, vol. 56, pp. 1246–1255, 2011.

[78] S. Al Hallaj, H. Maleki, J. Hong, and J. Selman, "Thermal modeling and design considerations of lithium-ion batteries," *Journal of Power Sources*, vol. 83, pp. 1–8, 1999.

[79] L. Cai and R. White, "An efficient electrochemicalthermal model for a lithium-ion cell by using the proper orthogonal decomposition method," *Journal of Electrochecmical society*, vol. 157, p. A1188, 2010.

[80] F. Jiang, P. Peng, and Y. Sun, "Thermal analyses of LiFePO4/graphite battery discharge processes," *Journal of Power Sources*, vol. 243, pp. 181–194, 2013.

[81] P. Peng and F. Jiang, "Thermal safety of lithium-ion batteries with various cathode materials: a numerical study," *International Journal of Heat and mass transfer*, vol. 103, pp. 1008–1016, 2016.

[82] g. Guo, S. Long, B.and Cheng, S. Zhou, P. Xy, and B. Cao, "Three-dimensional thermal finite element modeling of lithium-ion battery in thermal abuse application," *Journal of Power sources*, vol. 195, pp. 2393–2398, 2010.

[83] N. Baba, H. Yoshida, M. nagoka, C. Okuda, and S. Kawauchi, "Numerical simulation of thermal behavior of lithium-ion secondary batteries using the enhanced single particle model," *Journal of Power sources*, vol. 252, pp. 214–228, 2014.

[84] B. Wu, Y. Yufit, M. Marinescu, G. Offer, R. Martinez-Botas, and N. Brandon, "Coupled thermalelectrochemical modelling of uneven heat generation in lithium-ion battery pack," *Journal of Power sources*, vol. 243, pp. 544–554, 2013.

[85] G. X., L. Cao, and B. Guanglong, "A review on battery thermal management in electric vehicle application," *Journal of Power sources*, vol. 367, pp. 90–105, 2017.

[86] P. Ping, Q. Wang, P. Huang, J. Sun, and C. Chen, "Thermal behaviour analysis of lithium-ion battery at elevated temperature using deconvolution method," *Applied energy*, vol. 129, pp. 261–273, 2014.

[87] X. Feng, M. Fang, X. He, M. Ouyang, L. Lu, and H. Wang, "Thermal runaway features of large format prismatic lithium ion battery using extended volume accelerating rate calorimetry," *Journal of Power Sources*, vol. 255, pp. 294–301, 2014.

[88] X. Feng, J. Sun, M. Ouyang, X. He, L. Lu, and X. Han, "Characterization of large format lithium ion battery exposed to extremely high temperature," *Journal of Power Sources*, vol. 272, pp. 457–467, 2014.

[89] A. Peasaran, M. Keyser, G. Kim, S. Santhanagoplana, and K. Smith, "Tools for designing thermal management of batteries in electric drive vehicles," *Advanced automotive battery conference*, 2013.

[90] W. Lu and J. Prakash, "Situ measurements of heat generation in a Li/Mesocarbon microbead half-cell," *Journal of Electrochemical Society*, vol. 150, pp. A262–A266, 2003.

[91] W. Lu, I. Belharouak, and D. Vissers, "In situ thermal study of Li1+x[Ni1/3Co1/3Mn1/3]1-xO2 using isothermal micro-calorimetric techniques," *Journal of Electrochemical Society*, vol. 153, pp. A2147–A2151, 2006.

[92] J. Selman, S. Al hallaj, I. Uchida, and Y. Hirano, "Cooperative research on safety fundamentals of lithium batteries," *Journal of Power Sources*, vol. 97-98, pp. 726–732, 2001.

[93] R. Nijsing, "Temperature and Heat Flux Distribution in Nuclear Fuel element rods," *Nuclear Engineering and Design 4*, pp. 1–20, 1966.

[94] e. a. Ye, C., "The design and simulation of a new spent fuel pool passive cooling system," *Annals of Nuclear Energy*, vol. 58, pp. 124–131, 2013.

[95] T. Hung, T. Chen, and et al, "The development of three dimensional transient CFD model for predicting cooling ability of spent fuel pools," *Applied Thermal Engineering*, vol. 50, pp. 496–504, 2013.

[96] e. a. Lee, J.C., "Thermal-fluid flow analysis and demonstration test of a spent fuel storage system ," *Nuclear Engineering and Design*, vol. 239, pp. 551–558, 2009.

[97] P. Gomez and M. Griener, "2D Natural Convection and Radiation Heat Transfer Simulations of a PWR Fuel Assembly Within a ConstantTemperature Support Structure ," *ASME Paper No. PVP2006-ICPVT-119332*, 2006.

[98] A. Laursen, F. Moody, and J. Law, "Air Cooling Temperature Analysis of Spent Fuel," *International Conference on Nuclear Engineering 2014, Miami, Florida*, pp. 275–282, 2014.

[99] e. a. Wang, G., "Single Rod Heat Transfer Tests to Study the Effects of Crud Deposition," *International Conference on Nuclear Engineering 2014, Miami, Florida*, pp. 275–282, 2014.

[100] L. Agabez, "Transient Heat Transfer in partially cooled cylindrical rod," *Journal of Heat Transfer*, vol. 131, 2009.

[101] P. Costa, " Validation of a mathematical model for the simulation of loss of coolant accidents in nuclear power plants," *Tecnico Lisboa*, 2016.

[102] S. Patil, S. Chintamani, J. Grisham, R. Kumar, and B. Dennis, "Inverse Determination of Temperature Distribution in Partially Cooled Heat Generating Cylinder," *ASME 2015 International Mechanical Engineering Congress and Exposition*, 2015.

[103] S. Patil, S. Chintamani, R. Kumar, R. Kumar, and B. Dennis, "Numerical Analysis of Transient Temperature Distribution in a Partially Cooled Nuclear Fuel Rod," *ASME 2015 International Mechanical Engineering Congress and Exposition*, 2015.

[104] S. Patil, B. Dennis, and R. Kumar, "Transient Analysis of spent fuel rod using ANSYS," *ANSYS Symposium*, 2014.

[105] Y. Jiang, Y. Cui, Y. Huo, and S. Ding, "Three Dimensional FE Analysis of thermal-Mechanical behaviors in the nuclear fuel rods," *Annals of Nuclear Energy*, vol. 38, pp. 2581–2593, 2011.

[106] U. of Texas Austin, *Texas Advanced Computing Centre, University of Texas Austin*, 2018.

[107] W. Jin, "Semi-Analytical Complex variable based stochastic Finite Element Method," *Theses and Dissertations,UTA Library*, 2012.

[108] E. Artyukhin, "Reconstruction of the thermal conductivity coefficient from the solution of the nonlinear inverse problem," *J. Eng. Phys. Thermophys.*, vol. 41(4), pp. 1054–1058, 1981.

[109] O. Alifnov and A. Tryanin, "Determination of the coefficient of internal heat exchange and the effective thermal conductivity of a porous solid on the basis of a nonstationary experiment," *J. Eng. Phys.*, vol. 48(3), pp. 356–365, 1985.

[110] M. Ozisik and H. Orlande, *Inverse Heat Transfer: Fundamentals and Applications*, 2000.

[111] T. Jurkowski, Y. Jarny, and D. Delaunay, "Estimation of thermal conductivity of thermoplastics under moulding conditions: an apparatus and an inverse algorithm," *Int. J. Heat Mass Transf.*, vol. 40 (17), pp. 4169–4181, 1997.

[112] H. Chen, "Simultaneous estimations of temperaturedependent thermal conductivity and heat capacity," *Int. J. Heat Mass Transfer*, vol. 41(14), pp. 2237–2244, 1998.

[113] N. Ukrainczyk, "Thermal diffusivity estimation using numerical inverse solution for 1D heat conduction," *Int. J. Heat and Mass Transfer*, vol. 52, pp. 5675–5681, 2009.

[114] M. Mierzwiczak and J. Kolodziej, "The determination temperature-dependent thermal conductivity as inverse steady heat conduction problem," *Int. J. Heat and Mass Transfer*, vol. 54, pp. 790–796, 2011.

[115] F. Liu, "A hybrid method for the inverse heat transfer of estimating fluid thermal conductivity and heat capacity," *International Jounal of Thermal Science*, vol. 50, pp. 718–724, 2011.

[116] F. Mohebbi and M. Sellier, "Estimation of thermal conductivity, heat transfer coefficient, and heat flux using a three dimensional inverse analysis," *International Journal of Thermal Sciences*, vol. 99, pp. 258–270, 2016.

[117] P. Rajmane, F. Mirza, and D. Agonafer, "Chip Package Interaction Study to Analyze the Mechanical Integrity of a 3-D TSV Package," *ASME. International Electronic Packaging Technical Conference and Exhibition, Volume 2: Advanced Electronics and Photonics, Packaging Materials and Processing;*, 2015.

[118] P. Rajmane and D. Agonafer, "Failure mechanisms of boards in a thin wafer level chip scale package," *16th IEEE Intersociety Conference on Thermal and Thermomechanical Phenomena in Electronic Systems (ITherm), Orlando, FL, 2017*, 2017.

[119] F. Incropera and D. Dewitt, "Introduction to Heat Transfer," *Wiley Inc*, 2006.

[120] S. Drake, D. Wetz, J. Ostanek, S. Miller, H. J., and A. Jain, "Measurement of anisotropic thermophysical properties of cylindrical Li-ion cells," *Journal of Power Source*, vol. 252, pp. 298–304, 2014.

[121] A. Samuel, "Some Studies in Machine Learning Using the Game of Checkers I," *Computer Games*, pp. 335–365, 1959.

[122] H. Mannila, "Data mining: machine learning, statistics, and databases," *International Conference Scientific and Statistical Database Management*, 1996.

[123] G. Engel, *3 Flavors of Machine Learning: Who, What and Where*, 2016. [Online]. Available: DARKReading(https://www.darkreading.com/threat-intelligence/3-flavors-of-machine-learning--who-what-and-where/a/d-id/1324278)

[124] J. Friedman, "Data Mining and Statistics: What's the connection?" *Computing Science and Statistics*, 1998.

[125] S. SAS, "The evolution of machine learning," 2016.

[126] L. Tam, A. Ghajar, H. Tam, and S. Tam, "Development of a Heat Transfer Correlation for the Transitional Flow in a Horizontal Tube Using Support Vector Machines," *ASME 2008 Heat Transfer Summer Conference collocated with the Fluids Engineering, Energy Sustainability, and 3rd Energy Nanotechnology Conferences*, vol. 1, 2008.

[127] H. Tam, L. Tam, and GhajarA., "Heat Transfer Correlation for Two-Phase Flow in Vertical Pipes Using Support Vector Machines," *Heat Transfer Engineering*, vol. 32, pp. 74–83, 2011.

[128] N. Kumra A., Rawal and P. Samui, "Prediction of Heat Transfer Rate of a Wire-on-Tube Type Heat Exchange- An Artificial Intelligence Approach," *Procedia Engineering*, vol. 64, pp. 74–83, 2013.

[129] P. Milani, J. Liang, G. Mischlich, J. Bodart, and J. Eaton, "A Machine Learning Approach for Determining the Turbulent Diffusivity in Film Cooling Flows," *ASME Turbo Expo 2017: Turbomachinery Technical Conference and Exposition*, vol. 5A, 2017.

[130] T. Zhan, L. Fang, and X. Yibin, "Prediction of thermal boundary resistance by the machine learning method," *Scientific Reports*, vol. 7, 2017.

[131] TensorFlow, *Tensorflow* , 2015.

[132] J. Dean, *It is machine learning software being used for various kinds of perceptual and language understanding tasks* , 2015.

[133] M. Cade, *TensorFlow, Google's Open Source AI, Points to a Fast-Changing Hardware World* , 2010.

[134] J. Vincent, *Googles new machine learning framework is going to put more AI on your phone-The Verge* , 2017.

[135] F. Murray, D.and McSherry, R. Issacs, M. Isard, P. Barham, and M. Abadi, *Naiad:Timely dataflow system- Microsoft Research* , 2017.

[136] F. Beckenkamp, "A COMPONENT ARCHITECTURE FOR ARTIFICIAL NEURAL NETWORK SYSTEMS ," 2002.

[137] L. Rosenberg, "The Use of Virtual Fixtures As Perceptual Overlays to Enhance Operator Performance in Remote Environments," *Technical Report AL-TR-0089, USAF Armstrong Laboratory, Wright-Patterson AFB OH*, 1992.

[138] ——, "Virtual Fixtures: Perceptual Overlays for Telerobotic Manipulation," *Proc. of the IEEE Annual Int. Symposium on Virtual Reality*, pp. 76–82, 1993.

[139] W. Dennis, "The History of Augmented Reality (Infographic)," *Huffington Post*, 2016.

[140] D. Wagner, "Handheld Augmented Reality- Dissertation," *Graz University of Technology*, 2007.

[141] R. Metz, "Augmented Reality is Finally getting Real," *MIT Technology review*, 2012.

[142] J. Wakefield, "Meta augmented reality headset demoed at TED," *BBC*, 2016.

[143] M. Helft, "New Augmented Reality startup Meta dazzles TED Crowd," *Forbes*, 2016.

[144] S. Rosenbaum, "Meron Gribetz wants to build IOS of the mind," *Forbes*, 2016.

[145] H. realwear, *Realwear product catalogue*, 2016. [Online]. Available: https://www.realwear.com/products/hmt-1

[146] D. Systems, "Solidworks Software," 2017. [Online]. Available: https://www.solidworks.com

[147] T. U. Technologies, "UNITY," 2017. [Online]. Available: https://unity3d.com/

[148] I. P. INC, "VUFORIA," 2017. [Online]. Available: https://www.vuforia.com/

[149] C. google com, "Firebase," 2017. [Online]. Available: https://firebase.google.com/

[150] S. Patil, S. Chintamani, B. Dennis, and R. Kumar, "Determination of Orthotropic Thermal Conductivity in heat Generating Cylinder," *ASME 2016 International Mechanical Engineering Congress and Exposition*, 2016.

[151] O. Fabela, S. Patil, S. Chintamnai, and B. Dennis, "Estimation of Effective thermal conductivity of porous media utilizing inverse heat transfer analysis on cylindrical configuration," *ASME 2017 International Mechanical Engineering Congress and Exposition*, 2017.

[152] O. Fabela, "Effective thermal conductivity of porous media by inverse heat transfer analysis," *University of Texas Arlington Master Thesis*, 2017.

BIOGRAPHICAL STATEMENT

Sandeep Patil received his Doctorate degree from University of Texas at Arlington (UTA) majoring in Mechanical Engineering. He received his Bachelors' degree with distinction in Mechanical Engineering from University of Mumbai, India. He received licentiate in mechanical engineering (LME) from well-known institute- Veermata Jeejabai Technological Institute (VJTI), where he was awarded with silver medal for achieving highest aggregate marks. Sandeep worked as Scientific Officer at one of premiere research institute in India- Bhabha Atomic Research Centre (BARC). He received Group Achievement Award as Gold Medal and citation from Government of India for indigenous development of radiation shielding windows at BARC. He also represented India at technical meeting held at La Grande Motte, France by International Atomic Energy Agency (IAEA). He is also active member at American Society of Mechanical Engineers (ASME), where he is treasurer of West Texas Section. He also served as session chair (Design under uncertainty) at ASME IMECE 2016. During his stay at UTA, he was awarded for academic achievement (4.0 GPA) and innovative projects with many coveted fellowships like Krishnan Rajeshwar and Rohini Krishan Graduate Fellowship, Lockheed Martin Missiles and Fire Control Graduate Fellowship, Carizzo Oil and Gas Graduate Research Scholarship. He was designated as a judge for undergraduate poster presentation at Annual Celebration of Excellence by Students's (ACES) 2014, 2016, 2018 at UTA.

He also served as President of non-profit organization - Fine Arts Society of India, UTA, where team won best spirited organization award in April' 2014. He

also represented students of college of engineering at meeting between University of Texas Arlington and US-India Chamber of Commerce. In addition, during his stint as Co-Op Engineer at Advanced Micro Devices (AMD), Austin, he has shown his creativity by installing parallel server computation facility and modification of thermal software, which showed increase of 1825% increase in computational performance (reduction of simulation time from 73 hours to 4 hours). As a hobby project, he has also developed android application for tracking bus routes, time and successfully implemented at K.K.Wagh College of Engineering, Nasik, India. He is also in advisory board at eBharat, India, where he has imparted his Computational Fluid Dynamics, Heat transfer knowledge to successfully complete many projects. He has developed Pakshimitra brand with eBharat for assisting poultry industry. Apart from academic skills, he has also performed in innovative maiden shadow dance at UTA, which has more than 18000 views on youtube. He also come up with innovative idea of selling fast-food and collect money at UTA and help drought affected farmers in India, where team garnered more than 100,000 Indian Rupees.

His research interest includes thermal management in heat generating body (Li-ion batteries, cancer cell, nuclear fuel rod), thermal modeling, computational fluid dynamics, reliability study, machine learning, artificial intelligence, software application development (virtual reality, augmented reality, android, ios) for assisting mechanical industry to improve productivity and safety.

In future, he aspire to be technology solution provider, where he likes to bridge gap between academic research and industrial practical solution. He would love to use his multi-subject knowledge for good of human kind.